

SYNTHESIS AND ENCAPSULATION OF 1,3,5-TRIAZINE DERIVATIVES AS
ANTICANCER AGENT



A Thesis Submitted in Partial Fulfillment of the Requirements

for the Degree of Master of Science in Chemistry

Department of Chemistry

FACULTY OF SCIENCE

Chulalongkorn University

Academic Year 2020

Copyright of Chulalongkorn University

การสังเคราะห์และการกักเก็บอนุพันธ์ 1,3,5-ไตรอะซีนเพื่อเป็นสารต้านมะเร็ง



วิทยานิพนธ์นี้เป็นส่วนหนึ่งของการศึกษาตามหลักสูตรปริญญาวิทยาศาสตรมหาบัณฑิต

สาขาวิชาเคมี ภาควิชาเคมี

คณะวิทยาศาสตร์ จุฬาลงกรณ์มหาวิทยาลัย

ปีการศึกษา 2563

ลิขสิทธิ์ของจุฬาลงกรณ์มหาวิทยาลัย

มนยา เฉลิมนนท์ : การสังเคราะห์และการกักเก็บอนุพันธ์ 1,3,5-ไตรอาซีนเพื่อเป็นสารต้านมะเร็ง.
 (SYNTHESIS AND ENCAPSULATION OF 1,3,5-TRIAZINE DERIVATIVES AS
 ANTICANCER AGENT) อ.ที่ปรึกษาหลัก : ผศ. ดร.โรจน์ฤทธิ์ โรจนธเนศ, อ.ที่ปรึกษาร่วม : ผศ.
 ดร.ธนธรณ์ ขอทวีวัฒนา

การออกฤทธิ์ทางชีวภาพของโครงสร้าง 1,3,5-ไตรอาซีน มีความหลากหลาย โดยเฉพาะเมื่อใช้เป็นสารต้านมะเร็ง เนื่องจากความสามารถในการเข้าถึงเซลล์มะเร็งของโครงสร้างนี้มีข้อจำกัด ซึ่งส่งผลต่อฤทธิ์ต้านมะเร็งของโครงสร้างนี้ การศึกษาครั้งนี้จึงได้ทำการศึกษาฤทธิ์การต้านมะเร็งของอนุพันธ์ 1,3,5-ไตรอาซีน จำนวนสิบสองชนิด โดยทดสอบกับเซลล์มะเร็งลำไส้ใหญ่สองชนิด รวมถึงทดสอบระบบนำส่งยา (Drug Delivery System, DDS) โดยใช้อนุภาคนาโนของแคลเซียมซิเตรต (CaCit NPs) เป็นตัวนำส่งยา ผลจากการศึกษาฤทธิ์การต้านมะเร็งของอนุพันธ์ 1,3,5-ไตรอาซีน พบว่าสารประกอบมีฤทธิ์การต้านมะเร็งที่แตกต่างกัน สารประกอบบางชนิดมีความเป็นพิษต่อเซลล์มะเร็งในระดับเดียวกันกับยาต้านมะเร็งอ้างอิงซิสพลาติน (Cisplatin) นอกจากนี้ยังพบว่าสารประกอบ 2a และ 3d เป็นสารประกอบที่เป็นพิษต่อเซลล์มะเร็งมากที่สุด และสารประกอบ 2c และ 3c ซึ่งมีหมู่แทนที่เป็น *o*-hydroxyphenyl ที่เหมือนกันทั้งสองชนิด แสดงค่า IC_{50} ต่ำที่สุดที่ค่าประมาณ 20-27 ไมโครโมลาร์ นอกเหนือจากนี้การศึกษานี้ยังแสดงให้เห็นถึงการใช้อนุภาคนาโนของแคลเซียมซิเตรตเป็นตัวนำส่งอนุพันธ์ 1,3,5-ไตรอาซีน 2a วิธีการเตรียม 1,3,5-ไตรอาซีนร่วมกับอนุภาคนาโนแคลเซียมซิเตรต (CaCit-2a NPs) มีการปรับให้เหมาะสมโดยการเลือกระบบตัวทำละลาย แหล่งที่มาของซิเตรตไอออน และเวลาในการสังเคราะห์ เนื่องจากปัจจัยเหล่านี้มีผลต่อ รูปร่าง ขนาด และ %drug loading ของอนุภาคนาโน เมื่อใช้วิธีการที่เหมาะสมที่สุดมาสังเคราะห์ CaCit-2a NPs อนุภาคนาโนที่ได้รับ มีการกระจายตัวแบบ monodisperse มีขนาดอนุภาคที่เหมาะสมสำหรับความต้องการของ Enhanced Permeability and Retention (EPR) effect และมี %drug loading ในระดับปานกลาง ซึ่งพฤติกรรมการปลดปล่อยยาที่ควบคุมได้สามารถเกิดขึ้นได้ภายใต้สภาวะที่เป็นกรด ความรู้จากการศึกษาในครั้งนี้สามารถนำไปสู่การพัฒนาต้านมะเร็งที่ใช้ 1,3,5-ไตรอาซีน และยังเป็นพื้นฐานของการพัฒนาระบบการนำส่งยาที่ใช้อนุภาคนาโนของแคลเซียมซิเตรตเพื่อนำส่งยาชนิดอื่น ๆ ในอนาคต

สาขาวิชา เคมี
 ปริญญาโท 2563

ลายมือชื่อ นิสิต
 ลายมือชื่อ อ.ที่ปรึกษาหลัก
 ลายมือชื่อ อ.ที่ปรึกษาร่วม

6172037923 : MAJOR CHEMISTRY

KEYWORD: 135-triazine, anticancer activity, drug delivery system, calcium citrate, nanoparticles

Monnaya Chalermnon : SYNTHESIS AND ENCAPSULATION OF 1,3,5-TRIAZINE DERIVATIVES AS ANTICANCER AGENT. Advisor: Asst. Prof. Dr. ROJRIT ROJANATHANES Co-advisor: Asst. Prof. Dr. TANATORN KHOTAVIVATTANA

The 1,3,5-triazine scaffold is known for its versatile biological activities especially as an anticancer agent, but a limitation of 1,3,5-triazine is the ability to reach cancer cells thus affecting its anticancer potency. In this work, the anticancer activity of twelve 1,3,5-triazine derivatives was evaluated against two colon cancer cell lines along with an investigation of a drug delivery system (DDS) using calcium citrate nanoparticles (CaCit NPs). Results from the biological evaluation showed that there was a variation in the anticancer activity of 1,3,5-triazine derivatives which some of them exhibited comparable activity to the reference drug cisplatin. Compound 2a and 3d were the two most cytotoxic derivatives and 2c and 3c, both bearing the *o*-hydroxyphenyl substituent, exhibited the lowest IC₅₀ values around 20-27 μM. Moreover, the use of CaCit NPs as drug carrier for the selected 1,3,5-triazine derivative 2a was demonstrated. The preparation method of 1,3,5-triazine incorporated calcium citrate nanoparticles (CaCit-2a NPs) was optimised by selecting an appropriate solvent system, source of citrate ion, and synthesis time because these factors have effects on the morphology, size and %drug loading of nanoparticles. Upon using the optimised method, the obtained CaCit-2a NPs was monodispersed with particles size suitable to take advantage of the Enhanced Permeability and Retention (EPR) effect, possessed moderate %drug loading and showed controlled drug release behaviour under the acidic condition. The knowledge from this study could contribute to the future development of the 1,3,5-triazine-based anticancer drugs and provide calcium citrate nanoparticles as an emerging drug delivery platform to incorporate future drugs.

Field of Study: Chemistry

Student's Signature

Academic Year: 2020

Advisor's Signature

Co-advisor's Signature

ACKNOWLEDGEMENTS

This thesis was completed with the greatest possible success due to the numerous contributions from many individuals who provided useful and informative guidance, instrument assistance and moral supports as well as the research grant funds provided by Chulalongkorn University.

First and foremost, I would like to express my deepest gratitude to my advisor and co-advisor, Assist. Prof. Dr.Rojrit Rojanathanes and Assist. Prof. Dr.Tanatorn Khotavivattana, for allowing me to work on such a captivating research project that integrated drug discovery and drug delivery system, both of which are to my liking and interests. With your warmth, motivations, enthusiasm and advices, I was able to overcome both major and minor hurdles throughout the project. It is the greatest pleasure and honour to work under your supervisions.

I would like to express my sincere gratitude to Assist. Prof. Dr.Amornpun Sereemasapun and Nanomedicine RU for trusting me to conduct the biological studies myself and for teaching me how to analytically and logically interpret data. I would like to also acknowledge Chula MRC for providing me with access to the essential instruments. Many appreciations go to the seniors of the Nanomedicine RU lab especially Miss Slocha Cherdchom for the many useful advices about the biological data and the cheerful supports, and Miss Siwaporn Nilyai for training me the steps needed to work with cell cultures.

My greatest appreciation to Prof. Dr.Supason Wanichwecharungruang for lending me many instruments. Special thanks to Miss Parichat Tawornchat for providing me assistance with drug release study and provided me with DLS data; Mr. Wittawat Keawsongsaeng and Mr. Natchanon Rimsueb for helping me with nanoparticles preparation, FTIR and TGA.

I would like to give my deepest appreciation for the research grant funds provided by Chulalongkorn University: CU_GR_63_159_23_25, the 72nd Anniversary of His Majesty King Bhumibol Adulyadej Scholarship, and the 90th Anniversary Chulalongkorn University Fund (Ratchadapiseksomphot Endowment Fund).

Lastly, I would like to take this opportunity to thank my family for supporting me with kind words that helped me through hard times. I am very thankful to the members of TK Lab, SW Lab and YS Lab for moral supports and willingness to help throughout the project.

Monnaya Chalermnon

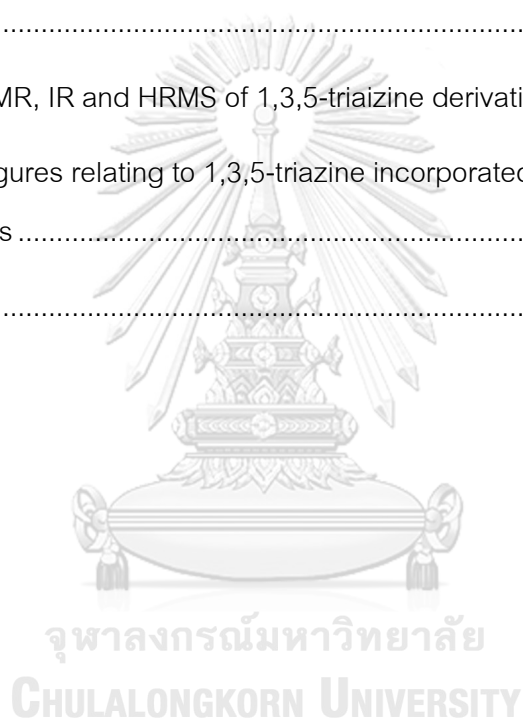


TABLE OF CONTENTS

	Page
ABSTRACT (THAI).....	iii
ABSTRACT (ENGLISH)	iv
ACKNOWLEDGEMENTS.....	v
TABLE OF CONTENTS.....	vii
LIST OF TABLES.....	x
LIST OF FIGURES	xi
ABBREVIATION LIST.....	1
CHAPTER I INTRODUCTION.....	2
1. Background and significance of research.....	2
2. Literature review	4
2.1. Modified metformin as anticancer agents	4
2.2. Metformin and biguanide-derived 1,3,5-triazine as anticancer agents	6
2.3. Other 1,3,5-triazine derivatives	9
2.4. Drug delivery system (DDS)	10
2.5. Drug delivery system using calcium salt	13
2.5.1. <i>Calcium citrate</i>	13
2.5.2. <i>Synthesis of calcium citrate</i>	14
2.5.3. <i>Application of calcium citrate</i>	15
2.5.4. <i>Calcium citrate as drug carrier</i>	16
3. Objectives.....	19
4. Scope of research	19

5. Beneficial outcomes	19
CHAPTER II EXPERIMENTALS	20
1. Experimental procedures for the synthesis of 1,3,5-triazine derivatives	20
1.1. Chemicals and instruments for 1,3,5-triazine derivatives synthesis	20
1.2. General synthetic procedures for 1,3,5-triazine derivatives	20
1.3. Synthesis of Compound 1a and 1b	22
1.4. Synthesis of Compound 2a-2f.....	23
1.5. Synthesis of Compound 3a-3f.....	26
2. Experimental procedures for anticancer evaluation	30
2.1. Materials and instruments for biological assays	30
2.2. Cell culture	30
2.3. %Inhibition and IC ₅₀ evaluation.....	30
3. Experimental procedures for the synthesis of CaCit-triazine NPs.....	31
3.1. Chemicals and instruments for nanoparticles synthesis	31
3.2. Synthesis of 1,3,5-triazine incorporated in calcium citrate nanoparticles ...	31
3.3. Synthesis of calcium citrate nanoparticles	32
3.4. <i>In vitro</i> drug release study	32
CHAPTER III RESULTS AND DISCUSSIONS.....	34
1. Synthesis and characterisation of 1,3,5-triazine derivatives	34
1.1. Synthesis of 1,3,5-triazine derivatives <i>via</i> Pathway I.....	36
1.2. Synthesis of 1,3,5-triazine derivatives <i>via</i> Pathway II.....	40
1.3. <i>In vitro</i> anticancer activities of 1,3,5-triazine derivatives	41
2. Synthesis and characterisation of CaCit-triazine NPs	45

2.1. Optimisation of reaction condition for CaCit-triazine NPs	45
2.2. Preparation of CaCit-triazine NPs using the optimised method	51
2.3. Calcium citrate nanoparticles (CaCit NPs)	55
2.4. <i>In vitro</i> drug release study	56
CHAPTER IV CONCLUSION	59
REFERENCES	60
APPENDICES	75
APPENDIX A: NMR, IR and HRMS of 1,3,5-triazine derivatives (2a-2f and 3a-3f)	76
APPENDIX B: Figures relating to 1,3,5-triazine incorporated calcium citrate nanoparticles	107
VITA	112



LIST OF TABLES

	Page
Table 1. Experimental conditions for the synthesis of CaCit-triazine NPs	32
Table 2. Optimisation of base and solvent	38
Table 3. Reactions of metformin with diethyl oxalate	39
Table 4. Reactions of phenylbiguanide with diethyl oxalate	41
Table 5. Anticancer activities of 1,3,5-triazine derivatives in 1% DMSO at 48 hours	43
Table 6. Unsuccessful methods.....	46
Table 7. Characterisation of CaCit-2a NPs by SEM and DLS	52
Table 8. Characterisation of CaCit-2a NPs by EA and TGA.....	54
Table 9. Conditions for the preparation of calcium citrate	55

LIST OF FIGURES

	Page
Figure 1. 1,3,5-Triazine scaffold.....	2
Figure 2. Chemical structure of metformin.....	5
Figure 3. Chemical structures of (A) HL156A and (B) sulfenamide derivatives of metformin.....	5
Figure 4. Metformin salts	6
Figure 5. Metformin-derived 1,3,5-triazine, HL010183	6
Figure 6. 2,4,6-trisubstituted 1,3,5-triazines	7
Figure 7. (A) Compound TZ-8 and TZ-9, (B) 4,6-diamino-1,3,5-triazine-2-carbohydrazides and -carboxamides and (C) 4,6-diamino-1,3,5-triazine-2-carbohydrazides.....	8
Figure 8. (A) Hybrid molecules of 2,4-Diamino-1,3,5-triazines with 2-iminocoumarin or coumarin and (B) 2,4-diamino-1,3,5-triazine acetonitrile derivatives.....	9
Figure 9. Various examples of 1,3,5-triazine derivatives	10
Figure 10. Diagrams illustrating (A) normal vasculature and (B) tumour vasculature ⁵¹ ...	11
Figure 11. Citrate role in the cell metabolism ⁶²	14
Figure 12. (A) calcium citrate nanosheets and (B) calcium citrate microsphere.....	15
Figure 13. SEM of (A) VAN-loaded calcium citrate particle and (B) CaCit-FITC	18
Figure 14. Schematic diagram of the reaction of biguanides with several esters. Reagents and conditions: (i) ester (1-3 equiv.), NaOMe (1-5 equiv.), anh. MeOH, reflux; (ii) NaOMe (1 equiv.), anh. MeOH, rt.; (iii) ester (1-excess equiv.) anh. MeOH	21
Figure 15. A pictorial diagram of the <i>in vitro</i> drug release study	33

Figure 16. Scheme demonstrating the synthesised 1,3,5-triazine derivatives; Blue represents compound synthesized by pathway I and Green is for pathway II.....	35
Figure 17. Proposed mechanism for the formation of 1,3,5-triazine derivatives.....	37
Figure 18. The hypothesised structure of the di-triazine compound.....	40
Figure 19. %cell inhibition at various %DMSO in 100 μ L. %inhibition was expressed as the mean values of five replicates \pm SD. The negative control was the cell culture media	42
Figure 20. Concentration-response curves of six 1,3,5-triazine derivatives against SW620 and HCT116.....	44
Figure 21. Cell viability study results of twelve 1,3,5-triazine derivatives at 100 μ M against HaCat cell line	45
Figure 22. FTIR spectrums of (a) calcium citrate nanoparticles, (b) 2a, (c) reaction using sodium citrate, and (d) reaction using citric acid with NaOH	48
Figure 23. SEM images at x10,000 magnification of product obtained with (A) sodium citrate and (B) citric acid with NaOH	49
Figure 24. SEM images of Condition C at various synthesis time between 1-24 hours at 10,000x magnification; i (1 hr), ii (2 hrs), iii (4 hrs), iv (6 hrs), v (8 hrs), vi (12 hrs), vii (16 hrs), viii (20 hrs) and ix (24 hrs)	50
Figure 25. SEM of CaCit-triazine at 2, 5 and 8 hours (Condition A-C)	52
Figure 26. DLS correlograms and size distribution graphs of Condition A and C	53
Figure 27. TGA curves of Condition A-C	54
Figure 28. SEM of Repeat A & Repeat B of Condition C	55
Figure 29. SEM of calcium citrate particles from Condition 9-1 to 9-4.....	56
Figure 30. Cumulative drug release (%) graph	58

ABBREVIATION LIST

anh.	anhydrous
DDS	Drug Delivery System
EPR	Enhanced Permeability and Retention Effect
CaCit NPs	Calcium citrate nanoparticles
CaCit-triazine NPs	1,3,5-triazine incorporated calcium citrate nanoparticles
CaCit-2a NPs	2a incorporated calcium citrate nanoparticles



CHAPTER I INTRODUCTION

1. Background and significance of research

Cancer is a major health issue resulting in a significant amount of deaths with the incident and mortality rates continuing to rise.¹ From the 2020 statistics, lung and colorectal cancer are the two types of cancer causing the greatest mortality worldwide.² Currently, chemotherapy and surgery are the conventional treatment methods of cancer, but there are several disadvantageous consequences including drug non-selectivity, resistance, and possibilities for recurrences.³ In order to overcome these issues, the development of a new anticancer drug with an efficient delivery system is necessary.⁴

1,3,5-Triazine is a heterocyclic scaffold containing nitrogen atoms in its core structure (Figure 1), and is being reported for many biological activities such as anti-inflammatory,⁵ antimicrobial,⁶ antimalarial,⁷ and anticancer activities.⁸ Numerous 1,3,5-triazine compounds possessing anticancer activities have been reported, for example, HL010183,⁹ Altretamine¹⁰ and Gedatolisib.¹¹ Substituents at the 2-, 4- and 6-position of the ring could greatly affect the activity of 1,3,5-triazine derivatives, and there are a variety of synthetic routes, for example, using cyanuric chloride (2,4,6-trichloro-1,3,5-triazine) as the starting material, three-component methods^{12, 13} or reactions between biguanides with alcohol,^{14, 15} amide¹⁶ or carboxylic acid derivatives.^{17, 18}

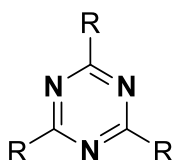


Figure 1. 1,3,5-Triazine scaffold

Without taking into consideration the exceptional antidiabetic and the recently discovered anticancer property of metformin,¹⁹⁻²¹ metformin is already a compelling biguanide to be used as the starting material for 1,3,5-triazine synthesis.^{15, 17, 22, 23} Upon a slight modification to the biguanide structure²⁴ or reacting it with organic salts,⁹ the

anticancer activity was improved. However, comparing the activity of modified metformin to 1,3,5-triazine, the latter possess greater anticancer property as seen in a research that evaluated the anticancer activity of both metformin salts and a metformin derived 1,3,5-triazine.⁹ Other biguanide-derived 1,3,5-triazines also exhibit great anticancer activity such as compounds derived from aryl-biguanides as Rad6 ubiquitin-conjugating enzymes inhibitors²⁵ and 2,4-diamino 1,3,5-triazine acetonitrile derivatives.²⁶ Therefore, it would be interesting to explore and develop new 1,3,5-triazine derivatives to further enhance the anticancer activity of this scaffold. However, a study have reported that a limitation of 1,3,5-triazine is its ability to reach the target site, thus affecting its anticancer activities.⁸ This means that a drug delivery system (DDS) is needed to solve the delivery issue.

DDS is a safe and efficient way to deliver drug while enhancing the therapeutic efficiency and reducing side effects. Many factors have impacts on the delivery of nanoparticles to the target site hence careful considerations about the drug carrier design is necessary. Nanoparticles could benefits from the Enhanced Permeability and Retention (EPR) effect, a feature seen for cancer cells because they have leaky vasculatures and an impaired lymphatic system.²⁷ In order to benefit from the EPR effect, the size should be between 30-300 nm because particles size outside of this range are prone to rapid clearance by the mononuclear phagocyte system.^{28, 29} By having the suitable particles size, the leakiness of tumour vessel could further dictate the selectivity of nanoparticles by directing them towards cancer cells. Additionally, as the environment surrounding cancer cells is relatively lower in pH values than normal cells, pH-responsive nanoparticles would further reinforce the usefulness of nanoparticles for DDS.³⁰ DDS using calcium citrate nanoparticles is of many interest especially for our research group because calcium citrate is a biocompatible material, an essential mineral for the body, and citrate is an intermediate of the tricarboxylic cycles.³¹ Citrate has been a participant in the making of many drug carriers because of its stabilising properties.³²⁻³⁴ Most recently, the use of calcium citrate particles as a drug carrier has emerged. The particles had

successfully delivered, and controlled the release of Vancomycin and FITC, which are an antibiotic drug and a fluorescent agent, respectively.^{35, 36}

In this research, the synthesis and anticancer activity of two series of biguanide derived 1,3,5-triazine were studied. Different substituents were presented on the triazine scaffold to determine a structure-activity relationship (SAR) between the hydrophobicity of the substituent with the anticancer activity. Furthermore, a selected 1,3,5-triazine derivatives was incorporated in calcium citrate nanoparticle (CaCit-triazine NPs). The preparation method and its behaviour under simulated environment were investigated. The method to prepare CaCit-triazine NPs was a simple coprecipitation to obtain nanoparticles with the size around 100-300 nm. The nanoparticle is expected to be suitable for the EPR effect and likely be selective towards cancer cells. The significance concept underlying this work were the anticancer activity study of the synthesised 1,3,5-triazine derivatives and the development of a drug delivery system for 1,3,5-triazine using calcium citrate nanoparticles. Therefore, the provided information is hoped to contribute to the future development of triazine compounds as well as introducing calcium citrate nanoparticles as an anticancer drug carrier.

2. Literature review

2.1. Modified metformin as anticancer agents

N,N-dimethylbiguanide, as known as metformin, is a biguanide derived from Galegine, the active substance of *Galega Officinalis* (Figure 2).³⁷ Nowadays, metformin is used as the first-line therapy for Type 2 Diabetes Mellitus (T2DM).¹⁹ Diabetes and cancer have several shared common factors that influence their progression. Several studies have revealed the anticancer mechanism of metformin and a commonly proposed hypothesis was that metformin exhibits either direct or indirect effects on cancer cells. The former is *via* the activation of AMPK, and the latter is an insulin-dependent method by reducing blood glucose, circulating insulin and insulin growth factor I concentration.^{38, 39}

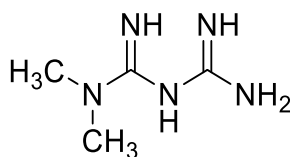


Figure 2. Chemical structure of metformin

A limitation of metformin is its hydrophilicity thus requiring organic cation transporters (OCTs) for passive uptake to occur.⁴⁰ By chemically modifying the backbone of metformin, not only that the uptake into cells was increased, but also improved the anticancer potency. HL156A, a metformin derivative, had better penetration, high bioavailability and resulted in the release of pro-apoptotic factors that ultimately caused cell death (Figure 3A).^{24,41} Modification of metformin with sulfenamide substituents could also increase the cellular uptake by having greater binding with the OCTs leading to enhance antiproliferative property compared to metformin (Figure 3B).⁴² Due to the higher binding to cells, higher antiproliferative properties was observed for the sulfenamide derivative with cyclohexyl ring having IC_{50} values at $0.72 \pm 1.31 \mu\text{M}$ against MCF-7 cell and $39.3 \pm 1.18 \mu\text{M}$ against MDA-MB-231 cell while other compounds with different alkyl length had IC_{50} values above $370 \mu\text{M}$.

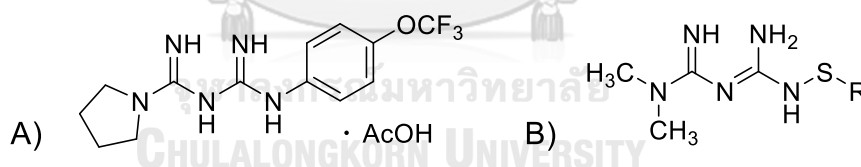


Figure 3. Chemical structures of (A) HL156A and (B) sulfenamide derivatives of metformin

Alternatively, treating metformin in the free base form with organic salts resulted in higher inhibitory effect than metformin (Figure 4).⁹ It was found that the three metformin salts modified with gamma-aminobutyric acid (GABA), pregabalin and gabapentin were more cytotoxic towards Hs578T cells exhibiting three-fold lower IC_{50} values than metformin at 4-9.1 mM. Furthermore, they inhibited the proliferation of MDA-MB-231 breast cancer cells at 16.1-41.5 mM.

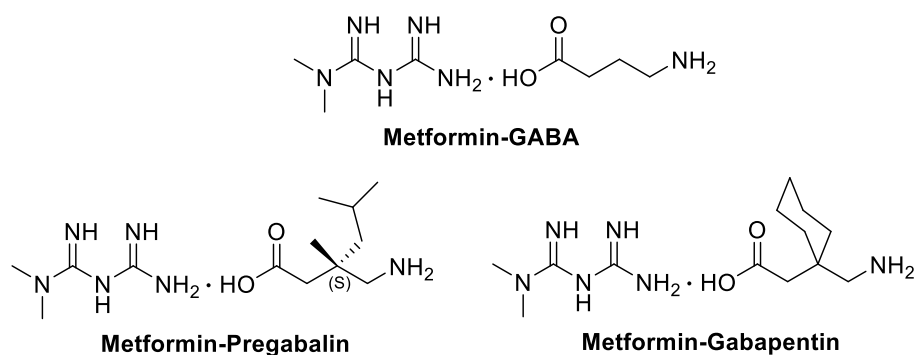


Figure 4. Metformin salts

Regardless of how the modifications to the biguanide structure led to improvements of the anticancer activity, metformin-derived 1,3,5-triazine (HL010183) reported in the same study as the three metformin salts was found to be more cytotoxic (Figure 5).⁹ HL010183 was 100 times more potent as the activator of AMPK and mTOR inhibitor than metformin. The *in vivo* evaluation additionally showed that HL010183 had more effective antitumour efficacy, and inhibitory effects on proliferation and invasion of breast cancer cells than metformin. Even though the comparison between metformin salts and 1,3,5-triazine derivative is not practical in terms of their difference in chemical structure, but it is apparent that metformin could participate in the synthesis of 1,3,5-triazine derivatives in order to achieve the ultimate goal of developing new anticancer drugs.

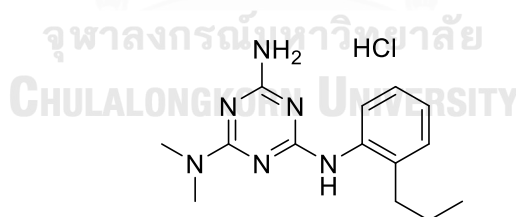


Figure 5. Metformin-derived 1,3,5-triazine, HL010183

2.2. Metformin and biguanide-derived 1,3,5-triazine as anticancer agents

In many literatures, the use of metformin and its biguanide derivatives to synthesise 1,3,5-triazine derivatives are notable. HL010183 was synthesised using *N,N*-dimethylguanide sulfate with dimethyl-*N*-cyanodithioiminocarbonate.⁹ In another work, the

synthesis of 2,4,6-trisubstituted 1,3,5-triazine acting as a histamine H₄ receptor used 4-methylpiperazin-1-yl biguanide dihydrochloride as the starting material (Figure 6).⁴³

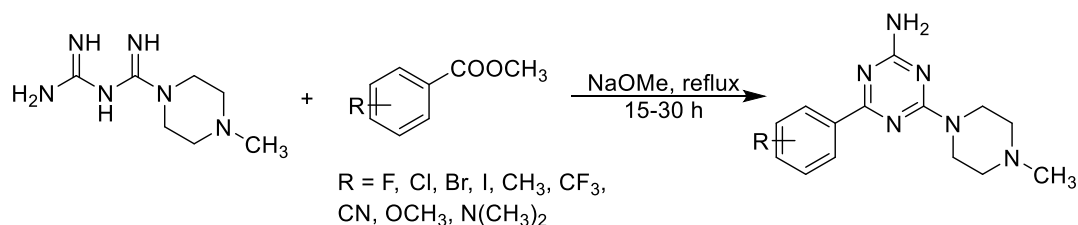


Figure 6. 2,4,6-trisubstituted 1,3,5-triazines

Since 2013, 1,3,5-triazine derivatives with the ability to inhibit Rad6 ubiquitin conjugating enzyme was synthesised with various arylbiguanide as the starting material.^{25, 44, 45} The enzyme inhibition could prevent malignant progression because it regulates the turnover of regulatory proteins found in cellular processes such as cell cycle progression, angiogenesis and cell signalling pathways.²⁵ TZ8 and TZ9 were the only two compounds that were active towards MDA-MB-231 cell line (Figure 7A). They were able to inhibit MDA-MB-231 cell proliferation with IC₅₀ values around 6 and 25 μM, respectively. As a result of the enzyme inhibition, cell progression was delayed, cell survival was inhibited as well as jeopardising the capacity of cell reproduction.⁴⁴ In the same year, Kothayer et al. introduced derivatives of TZ8 and TZ8 with an improved synthesis method by replacing the use of unprotected glycolate to an esters resulting in higher yield and less by-products (Figure 7B).⁴⁵ The activity of the new compounds were more favourable than TZ8 and TZ9 because the inhibitory effect on MBA-MD-231 were lower at 2.48-4.79 μM. In contrast to the selectivity of compound 3a-3e towards MBA-MD-231, they did not exhibit inhibitory activity towards breast epithelial cell lines. Moreover, docking studies have indicated that the triazine carbonylhydrazide derivatives was embedded inside the pocket of the Rad6B binding pocket making two key interactions. From this result, the structure was further modified by removing the phenyl(hydrazide) ring and the addition of a phenyl group onto the free amino group (Figure 7C).²⁵ The anticancer activity of the synthesised compounds was comparable and superior to the TZ9 with IC₅₀ values in the low molar concentration. For compounds of the 6a-e series, the IC₅₀ for breast cancer (MCF-7 and MDA-MB231)

was 2.5-7.2 μM , lung cancer (A549) at 6.9-14.6 μM , and colon cancer (HT-29) at 4.1-9.5 μM . The synthesised compounds were tested for Rad6 inhibitory ability and found to be better than TZ9 at the equimolar concentration of 25 nM.

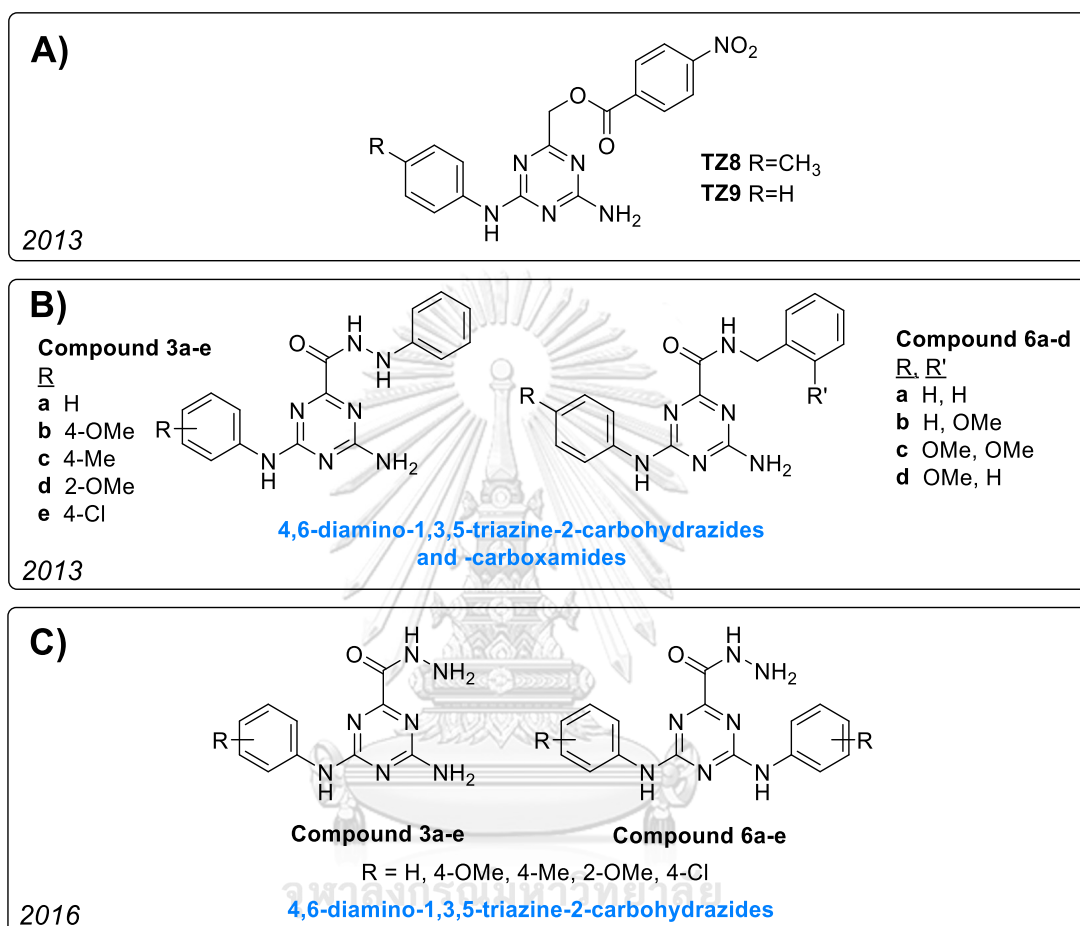


Figure 7. (A) Compound TZ-8 and TZ-9, (B) 4,6-diamino-1,3,5-triazine-2-carbohydrazides and -carboxamides and (C) 4,6-diamino-1,3,5-triazine-2-carbohydrazides

Other examples are the hybrid molecules of 2,4-diamino-1,3,5-triazines and coumarin and 2,4-diamino-1,3,5-triazine acetonitrile derivatives.^{18, 26} The most potent compound for the hybrid molecules has an electron donating diethylamino substituent at the 7 position of the iminocoumarin ring and the cytotoxic effects were in the range of 5.67-15.02 μM ("Compound 6 and 7").¹⁸ For the acetonitrile derivatives, they were synthesised from several biguanide hydrochloride with ethyl cyanoethanoate and

exhibited cytotoxic activities with IC_{50} values at 1.51-5.97 μ M against four cancer cell lines, 5637, DAN-G, MCF-7 and LCL-103H.

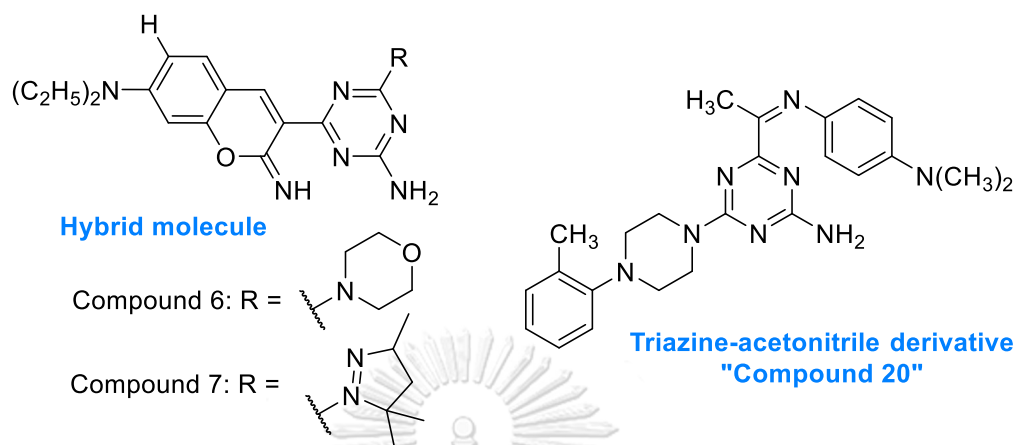


Figure 8. (A) Hybrid molecules of 2,4-Diamino-1,3,5-triazines with 2-iminocoumarin or coumarin and (B) 2,4-diamino-1,3,5-triazine acetonitrile derivatives

2.3. Other 1,3,5-triazine derivatives

In addition to the 1,3,5-triazine derivatives synthesised from biguanide, there are many other 1,3,5-triazine derivatives with great anticancer activity. From the alkenyl-1,3,5-triazine derivatives, "Compound 9" had a particularly interesting property despite its moderate anticancer activity because it was selective towards renal cancer cells whereas other compounds were cytotoxic against more than one cancer cell lines (**Figure 9**).⁴⁶ The 1,3,5-triazine core could be modified with other functional groups as well to improve its anticancer activity, for instance, phenylthiazole and benzimidazole.^{8,47} Novel 1,3,5-triazine substituted with phenylthiazole were found to have anti-cervical cancer activity.⁴⁷ The inhibition behaviour varied with the type and position of the substituent of the phenylthiazole moiety. Sixteen 1,3,5-triazine derivatives were tested against four cancer cell lines and found that the most active compound was the one bearing a para-substituted fluorine atom with IC_{50} at 2.21-28.33 μ g/mL (**Figure 9**). To emphasise on the fluorine substituent, despite of its position on the phenyl ring, they exhibited similar IC_{50} values for the anti-cervical cancer activity and they were more selective towards the cervical cancer than breast cancer.⁴⁷ Regarding the triazine-benzimidazole analogues,

the R-substituent was replaced with various secondary amine or aryl groups (Figure 9).⁸ When the compounds were tested against 60 cancer cell lines, four compounds bearing piperidine, phenyl, 4-fluorophenyl and 4-chlorophenyl exhibited the most anticancer potency with the GI₅₀ (50% of growth inhibition) in nanomolar range.

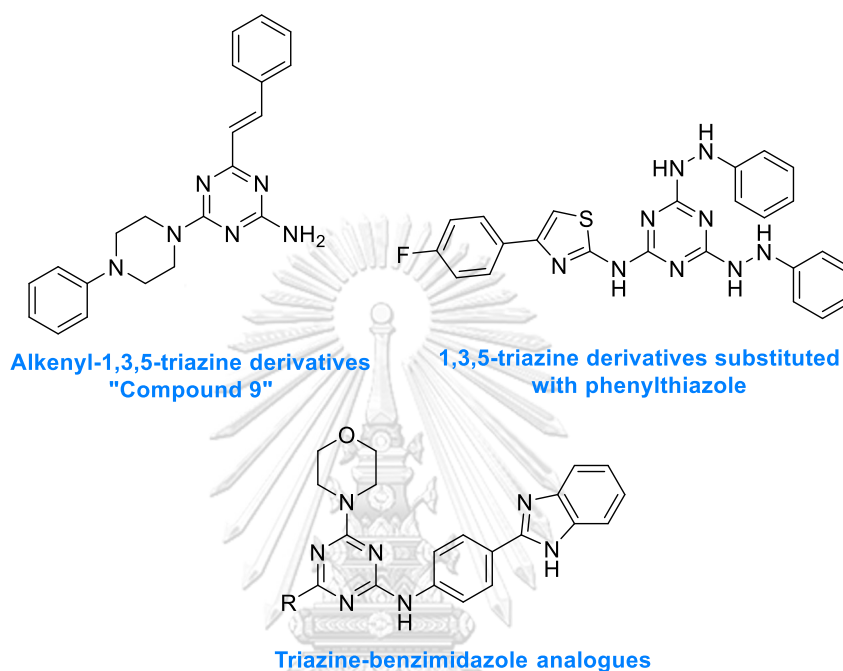


Figure 9. Various examples of 1,3,5-triazine derivatives

2.4. Drug delivery system (DDS)

Due to the rapid advancements of nanotechnology, nanomedicine is becoming an attractive option for cancer treatments. It could overcome drawbacks of conventional methods by minimising the distribution of drugs to normal cells and enhancing therapeutic efficiency with lower drug dosage.^{33, 48} DDS using nanoparticles (nano = 1-1000 nm) is able to deeply penetrated into tissues, remain in the bloodstream for a prolonged period, and favour drug bioavailability, serum stability and pharmacokinetics. Therefore, toxic or poorly water-soluble drugs could have a chance to reach the tumour cells without premature degradation or cause damages to healthy cells.^{32, 49}

The concept underlying the elevated therapeutic efficiency of nanoparticles is the EPR effect.⁴⁸ The EPR effect was first introduced by Matsumura and Maeda et al. which

they found that intravenously injected macromolecules could be retained in the tumour cells for a prolonged periods due to the hypervascularity and enhanced permeability of cancer cells.⁵⁰ Tumour vasculatures are different from normal healthy vasculatures because they are abnormal with an impaired lymphatic system. A diagram of defective tumour vessels is depicted in Figure 10B where they have irregular diameters, abnormal branching, structural irregularities, heterogeneity and leakiness.²⁷

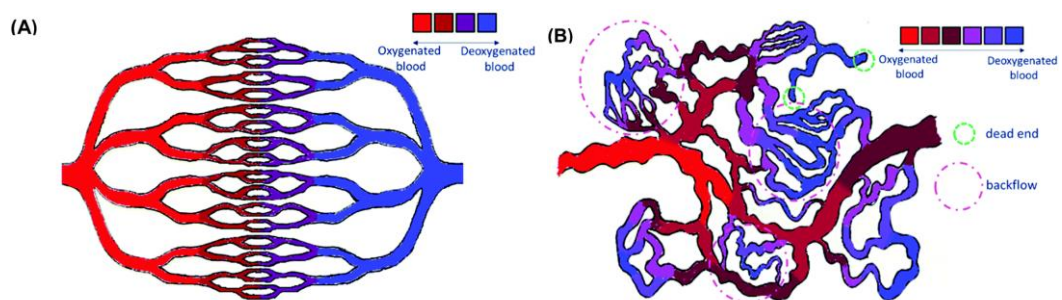


Figure 10. Diagrams illustrating (A) normal vasculature and (B) tumour vasculature⁵¹

The leakiness of tumour vessel is explained as a phenomenon resulting from the urge of survival for cancer cells. Tumour typically sized between 1-2 mm are known to be in the 'dormant' stage because they have sufficient oxygen supply and a balance of cell proliferation and apoptosis. As a tumour grows, it becomes further away from the nutritional supplies with an imbalance in the stimulatory and inhibitory factors resulting in the aberrant development of vasculatures.⁵¹ Vascular endothelial growth factor (VEGF) is a tumour angiogenic factors (TAFs) that trigger the formation of new tumorigenic blood vessels. The proliferation of endothelial cell triggered by the rapid release of angiogenic factors is 50-200 times more than normal cell thus immature vasculature could undergo formation, but with the accompany of incomplete structural remodelling. The incomplete structural remodelling would result in abnormal coverage of pericytes, thick or totally absent basal membrane, transendothelial channels and a large number of fenestrae. As a consequence of the hyperpermeability, blood flow becomes restricted, causing a hostile tumour microenvironment, such as acidity and hypoxia. This hostile environment creates a positive feedback loop where hypoxia increase VEGF production thus promoting angiogenesis.^{48, 51, 52}

The delivery of nanoparticles to cancer cells is also affected by the lymphatic system. The lymphatic system controls the intravasation and extravasation of fluids to maintain a lower interstitial pressure inside cells allowing transports of fluids/particles from the bloodstream. Unlike normal cell, cancer cells have an impaired lymphatic system, and the vascular pressure of cancer cells is higher than that of normal cells. This means that the difference of pressure could facilitate the internalisation of nanoparticles into cancer cell enhancing the EPR effect. However, under the same situation cancer cells usually have high interstitial fluid pressure (IFP) between the interior and the peripheral creating a gradient from high to low; therefore, the ability of nanoparticles to diffuse across cancer cell wall could be hindered by the elevated IFP.^{48, 51}

Another crucial aspect to consider for the EPR effect is the size of nanoparticles because tumour vessels have fenestrae and different pore sizes exist with different cancer types. The maximum reported diameter of stabilised liposome nanoparticles that penetrated from tumour vessels into the tumour interstitium was around 500 nm.⁵³ This finding correlates to the targeted range of nanoparticle size for the EPR effect of being between 30-300 nm because they are likely to exhibit lower clearance than larger particles.^{28, 29, 54} Nanoparticles could be recognised as a foreign body, making them more prone to the mononuclear phagocyte system (MPS), such as clearance by the kidney, liver or spleen.²⁸ A relationship between the hydrodynamic diameter of nanoparticles against renal clearance was established, and it was found to be inversely proportional.⁵⁵ If the nanoparticles are larger than 6 nm and 200 nm, they have the tendency to be cleared by the liver and captured by the spleen, respectively.^{28, 56} In addition, it is also evident that as the size of nanoparticles increases, they would be more selective towards the leaky tumour vessels, but this is at the expense of extravasation and diffusion efficiency.⁴⁸ By selecting the right nanoparticles size, the selectivity of nanoparticles towards cancer cells could be expected because normal healthy vasculatures are not as leaky and the pore size is at 4.5 nm or unusually large pores are 25 nm.⁵⁷

2.5. Drug delivery system using calcium salt

In the field of nanotechnology, there are many materials already investigated as the drug carrier such as polymers, metals and ionic compounds. Chitosan, alginate and liposome are polymers that are extensively studied. The advantages are availability because both chitosan and alginate are extractable from natural resources, low cost, biodegradable, biocompatible and non-toxic.⁵⁸ However, there are drawbacks to polymeric materials, such as shape and size polydispersity are limited for polymeric nanoparticles synthesised *via* emulsion, and liposome could have poor reproducibility and low drug loading capacity.³³ Gold and silver nanoparticles are also widely used in the biomedical field due to their inert nature, long stability, high surface area and electronic properties, however, their abilities are limited by the low drug loading capacity and could not effectively load hydrophilic drugs.⁵⁹ Another capable drug carrier material is calcium ionic compounds, for example, calcium carbonate (CaCO_3), calcium phosphate ($\text{Ca}(\text{H}_2\text{PO}_4)_2$), hydroxyapatite ($\text{Ca}_{10}(\text{PO}_4)_6(\text{OH})_2$) and calcium citrate ($\text{Ca}_3(\text{C}_6\text{H}_5\text{O}_7)_2$). The main features of calcium salts are biocompatibility and controlled release.⁴⁹

2.5.1. Calcium citrate

Calcium citrate is a biocompatible calcium salt with interesting properties and is expected to possess an exceptional drug delivery ability. It would be an excellent competitor of calcium carbonate and calcium phosphate. Calcium citrate is an essential chemical compound found in many parts of the body, for example, bones, teeth, blood, brain, kidney, liver and prostate.^{60,61}

Citrate-based biomaterials are known for biocompatibility, hemocompatibility and adequate immune response.⁶⁰ Citrate has many functions, such as metabolic and mineralisation regulation, anticoagulant effect and renal stone prevention.⁶⁰ It is an essential chemical compound found in many biological reactions such as glycolysis, gluconeogenesis and fatty acid synthesis. It also acts as the key metabolic intermediate in the tricarboxylic acid (TCA) cycles and a regulator of energy homeostasis of cells. (Figure 11).^{31,60} As an energy substrate, it is metabolised by ATP-citrate lyase (ACL) to

become precursors for fatty acid biosynthesis.⁶⁰ Citrate metabolism is important to cancer cells due to the reprogramming of cellular metabolism to generate sufficient biomolecules to facilitate rapid and unlimited proliferation.³¹

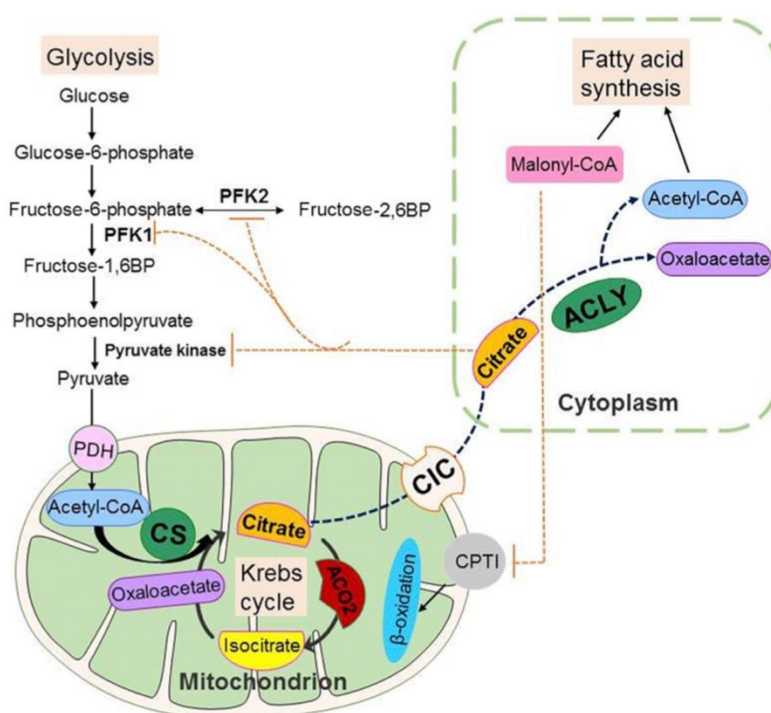


Figure 11. Citrate role in the cell metabolism⁶²

2.5.2. Synthesis of calcium citrate

There are various methods to synthesise calcium citrate particles. Some examples are a direct reaction of citric acid with calcium carbonate; citric acid reacting with calcium hydroxide through acid-base neutralisation; or using egg shells rich in calcium carbonate as the starting raw material.⁶³ Several techniques were also implemented to synthesise calcium citrate nanoparticles such as a pulsed jet mill⁶⁴ and hydrothermal method.⁶⁵ However, these techniques were complicated, time consuming and require specialised equipment rendering its applicability in industrial-scale production.⁶³ Those limitations drive the need of a more direct chemical synthesis method of calcium citrate particles. Calcium citrate nanosheets was synthesised *via* the direct chemical reaction between sodium citrate and calcium chloride in ethanol and water (Figure 12A).⁶³ The obtained calcium citrate was in the form of sheets, and the physical appearance was influenced by

ethanol:water ratio. Moreover, the self-assembly of nanosheets resulted in the formation of 3D-flowerlike calcium citrate microspheres (Figure 12B).⁶⁶ The method used to obtain the microspheres was to mix trisodium citrate with calcium chloride then stir and heat the mixed solution. From varying the heating time, the longer the heating time, the bigger and spherical shaped microparticles achieved. As a final step, both calcium citrate nanosheet and microsphere used freeze-drying to preserve the obtained final products.⁶⁶

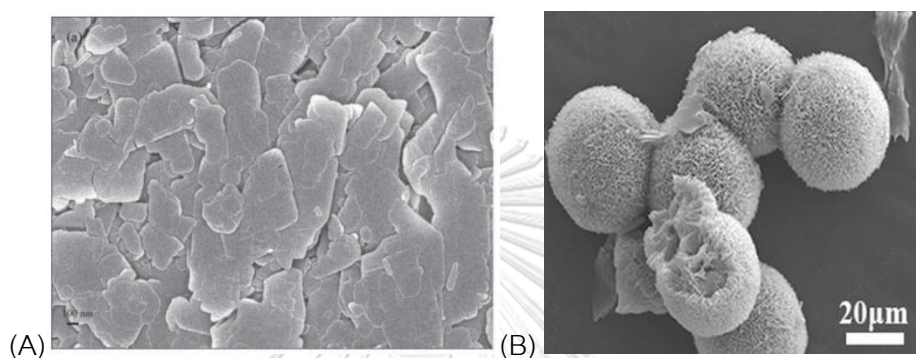


Figure 12. (A) calcium citrate nanosheets and (B) calcium citrate microsphere

2.5.3. Application of calcium citrate

The well-known application of calcium citrate is as a calcium supplement. Citrate is among the many calcium salts suitable as calcium supplements, for example, phosphate, carbonate and citrate-malate.⁶⁷ Osteoporosis is a condition of calcium deficiency causing brittle and weak bones because bones are being resorbed to maintain a stable serum calcium concentration.^{67,68} There are several factors that could influence the bioavailability of calcium ions from calcium salts, such as size, time of absorption, gastric acid⁶⁹ and dissolution of calcium salts. Nano-sized calcium salts was found to be effective at increasing both the calcium absorption and bioavailability.⁶⁷ To support the nano-size calcium salts theory, the absorption and bioavailability of nano-sized and micro-sized calcium carbonate and calcium citrate in ICR mice was studied. Micro-sized calcium supplements were not as efficient as nano-sized calcium salts due to low absorption efficiency and the higher serum calcium concentration from nano-calcium salts. Furthermore, the biocompatibility of both calcium carbonate and citrate were evaluated for acute and chronic toxicity. The acute toxicity test indicated the no-observed-adverse-

effect level (NOAEL) was 1.3 g kg^{-1} body weight for calcium carbonate and 2.3 g kg^{-1} body weight for calcium citrate. For chronic toxicological evaluation, three doses for each calcium salt were examined, and the result showed apparent symptoms of toxicity or mortality.⁶⁴

Extending from the previous application, calcium citrate is a biomaterial for bones such as bone healing and bone grafting.^{63,70} For bone healing, calcium citrate was found to be resorbed faster than calcium phosphate or hydroxyapatite. This result led to the reduction of bone defect size after four weeks of treatment.⁷⁰ In terms of bone grafting, calcium citrate nanosheets were effective at forming the new bone by filling into the defected sites. The reason for this phenomenon was due to the ability of calcium release in high concentration stimulating bone growth.⁶³

2.5.4. Calcium citrate as drug carrier

Inspired by the use of calcium citrate as calcium source and for bone-related applications, it could further expand its applicability into drug delivery system. Citrate participated as a stabilising agent in the citrate-apatite nanocarrier of Doxorubicin (DOXO).³² The nanocarriers were prepared by batch crystallisation method with calcium/citrate/phosphate/carbonate system. In aqueous condition, DOXO has NH_3^+ moiety that electrostatically adsorbed onto the negative surface of nanocrystal bearing the citrate and carbonate functional groups. Two assemblies of nanocarrier with and without sodium carbonate functionalisation had a slightly different adsorption strength and different drug release. Nevertheless, both exhibited pH-responsive release and efficient internalisation and release of DOXO into tumour cells.³² Similarly, citrate- and succinate-modified carbonate apatite (CA) nanoparticles loaded with Doxorubicin was reported.³³ The CMCA NPs (citrate modified) and SMCA NPs (succinate modified) were synthesised using a supersaturated solution of calcium, phosphate and carbonate ions along with exogenous calcium ions and citrate or succinate. The synthesised CMCA nanoparticles were smaller than the unmodified CA nanoparticles because citrate stabilised and prevented particle aggregation. For the cytotoxicity evaluation, the DOX-loaded CMCA nanoparticles showed greater cytotoxicity than DOX-loaded CA and DOX-loaded SMCA

nanoparticles. The DOX-loaded CMCA NPs were further able to significantly release its payload in the weakly acidic environment of pH 5, which is similar to the environment of the endosome of cancer cells.³³ The application of citrate as a stabiliser extends to calcium phosphate nanoparticles for the delivery of miRNA for cardiovascular diseases.³⁴ Alike the results in the previous two publications, with the addition of citrate in the synthesis process, the growth of CaP NPs was limited to a size between 20-50 nm. Also, the colloid stability was enhanced, and the nanoparticles had negatively charged surface. The negatively charged surface resulted in it to be a suitable material for cardiac-related application because the negative charge leads to nanoparticles selectivity towards polarised cells.³⁴

Most recently, the use of calcium citrate particles as drug carrier has emerged. An antibiotic drug for bone spacer and a fluorescent agent were successfully encapsulated in calcium citrate particles.^{35, 36} To prevent infection from occurring with bone spacer, antibiotic agents is needed to be contained within the bone spacer material. Calcium citrate was one of the material chosen to encapsulate Vancomycin, an antibiotic drug.³⁵ The synthesised Vancomycin encapsulated calcium citrate particles (VAN-CC) were 554.4 ± 220.3 nm in size with VAN loading content of $4.9 \pm 3.2\%$ and encapsulation efficiency of $27.9 \pm 18.3\%$ (Figure 13A). These VAN-CC have then embedded inside PMMA (VAN-CC-PMMA) composite matrix which 40.8% (by %wt) was VAN-CC. The calcium citrate was a capable drug carrier of Vancomycin proven by the release study over 42-days period showing a high VAN release for the whole experimental period. Overall, compared to other encapsulation formulations using natural rice granule, ethyl cellulose and PLGA, VAN-CC-PMMA had excellent drug release behaviour, and there was no change in compressive strength even after drug release. The results indicated that only the antibiotic drug was eluted out of the material thus serving its purpose as biocompatible bone spacer material with a continuous antibiotic release.³⁵ Later in 2020, FITC encapsulated calcium citrate nanoparticles (CaCit-FITC) were synthesised *via* a bottom-up coprecipitation method (Figure 13B).³⁶ The ratio and concentration of calcium and citrate ions were optimised and was later used in the synthesis of CaCit-FITC. The

presence of FITC was confirmed by thermogravimetric analysis indicating its existence at 3.5%. Reassuring the biocompatibility of calcium citrate, CaCit was tested for cytotoxicity and found that there was no statistically difference to the untreated cells. Furthermore, CaCit-FITC could internalise into the cytosol of human keratinocytes efficiently and the detected fluorescence emission intensified after 48 hours of cell treatment demonstrating their slow-release behaviour and stability CaCit-FITC outside the cells.³⁶

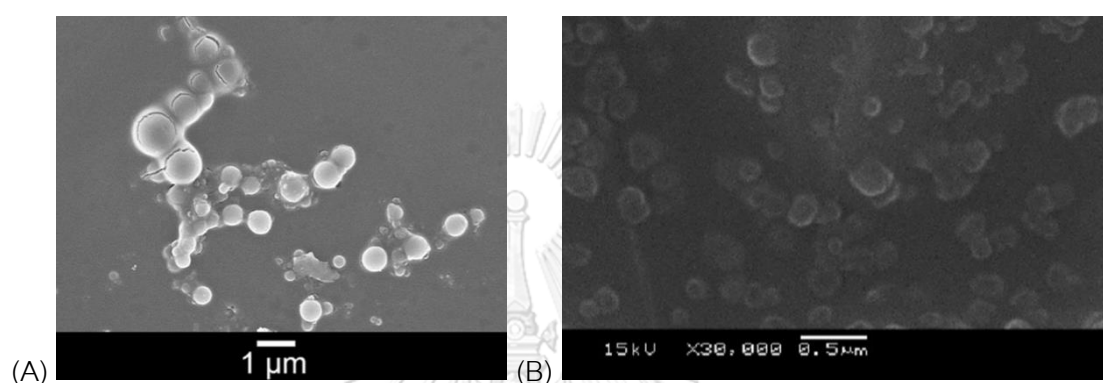


Figure 13. SEM of (A) VAN-loaded calcium citrate particle and (B) CaCit-FITC

Surprisingly, the incorporation of 1,3,5-triazine derivatives in calcium citrate nanoparticles has not been established. The initiation of using calcium citrate particles to deliver an antibiotic drug or a fluorescent agent is a good indication that calcium citrate is emerging as an interesting and practical alternative to calcium carbonate or calcium phosphate as drug carriers.

3. Objectives

1. To synthesise and characterise two series of 1,3,5-triazine derivatives using Metformin or phenylbiguanide as starting materials
2. To synthesise and characterise 1,3,5-triazine encapsulated calcium citrate nanoparticles
3. To evaluate the *in vitro* anticancer activity of 1,3,5-triazine derivatives and 1,3,5-triazine encapsulated calcium citrate nanoparticles against cancer cell lines

4. Scope of research

1. Synthesis and characterisation of 1,3,5-triazine derivatives from Metformin or phenylbiguanide
2. Synthesis and characterisation of 1,3,5-triazine encapsulated calcium citrate nanoparticles
3. Evaluation for *in-vitro* anticancer activity of 1,3,5-triazine derivatives and 1,3,5-triazine encapsulated calcium citrate nanoparticles

5. Beneficial outcomes

Novel 1,3,5-triazine derivatives synthesised from Metformin or phenylbiguanide and 1,3,5-triazine encapsulated calcium citrate nanoparticles with better anticancer activity will be obtained.

CHAPTER II

EXPERIMENTALS

1. Experimental procedures for the synthesis of 1,3,5-triazine derivatives

1.1. Chemicals and instruments for 1,3,5-triazine derivatives synthesis

Starting materials, reagents and solvents were purchased from Sigma Aldrich (St. Louis, MO, USA), TCI Chemicals (Tokyo, Japan), Fluorochem (Hadfield, Derbyshire, UK), Merck (Darmstadt, Germany) and RCI Labscan (Samutsakorn, Thailand). Aluminium Merck TLC plates coated with silica gel 60 F₂₅₄ was used for Thin Layer Chromatography (TLC) to monitor reaction progression. Purification of synthesised compounds were performed with normal phase column chromatography techniques using silica gel 60 (0.063-0.200 mm, 70-230 mesh ASTM, Merck, Darmstadt, Germany)

All of the synthesised 1,3,5-triazine derivatives were characterised by proton (¹H) and carbon (¹³C) nuclear magnetic spectroscopy using Bruker Nuclear Magnetic Resonance machine (400 MHz) and JEOL Nuclear Magnetic Resonance machine (500 MHz); high-resolution mass spectrometer using micrOTOF-Q II mass spectrometer (Bruker Daltonics) with electrospray ionization; IR spectra recorded with Thermo Scientific™ Nicolet 6700 FT-IR Spectrometer with ATR mode (32 scans); and melting point measured with Stuart SMP20 melting point apparatus.

1.2. General synthetic procedures for 1,3,5-triazine derivatives

The synthesis of 1,3,5-triazine derivatives was divided into pathway I and II (Figure 14). In general, compound **2a-2f** and **3a-3f** were synthesized *via* nucleophilic substitution between metformin hydrochloride (Met HCl) or phenylbiguanide hydrochloride (**1a**) with several esters. Five esters involved in this work were isopropyl palmitate (R³ = -C₁₅H₃₁), methyl benzoate (R³ = Ph), methyl salicylate (R³ = Ph-*o*-OH), methyl cinnamate (R³ = C=CH-Ph) and diethyl oxalate (R³ = COOC₂H₅). Upon the completion of reaction as monitored by TLC, crude was extracted with EtOAc/H₂O system. The organic layer was dried over anhydrous Na₂SO₄, filtered, and then concentrated *in vacuo* to give the final

product. Column chromatography was necessary for some reactions where extraction alone could not purify the desired products.

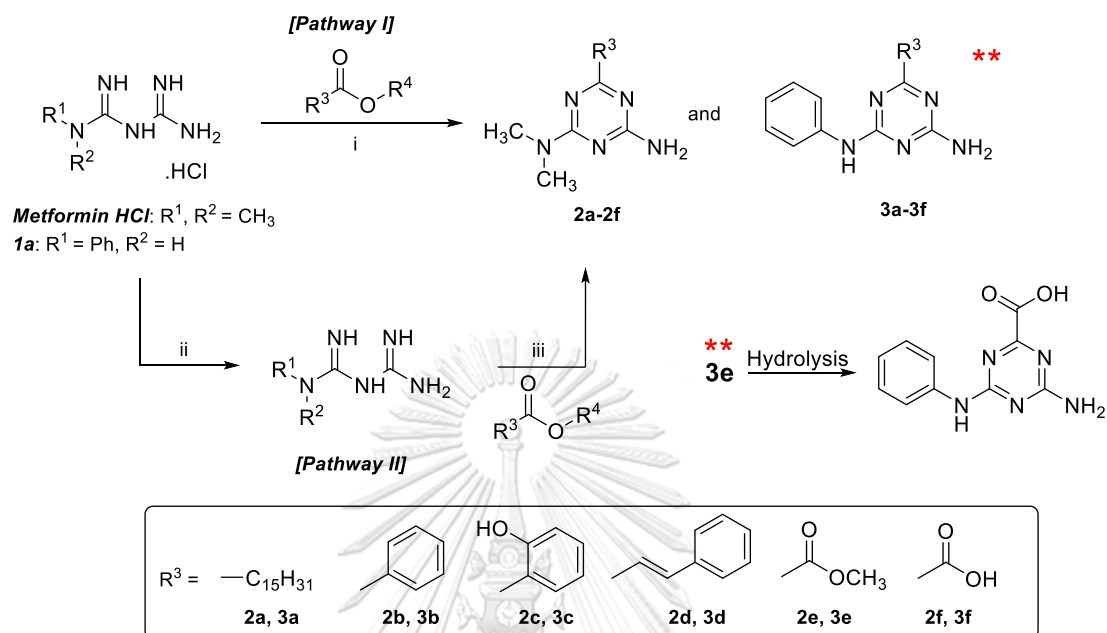


Figure 14. Schematic diagram of the reaction of biguanides with several esters. Reagents and conditions: (i) ester (1-3 equiv.), NaOMe (1-5 equiv.), anh. MeOH, reflux; (ii) NaOMe (1 equiv.), anh. MeOH, rt.; (iii) ester (1-excess equiv.) anh. MeOH

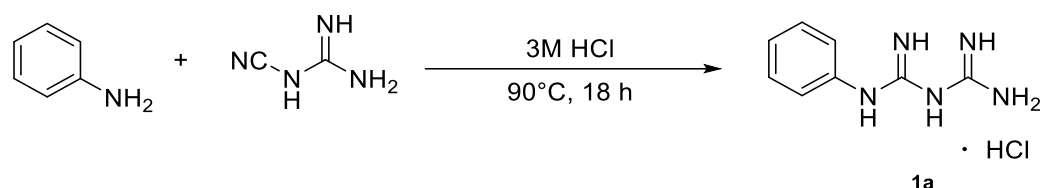
Pathway I: Compound **2a**, **2b**, **2d**, **2f** and **3a** were synthesised using modified procedures.^{17,25} A biguanide hydrochloride with sodium methoxide (NaOMe) dissolved in anh. MeOH were stirred at room temperature for about ten minutes. An ester was added into the mixture and stirred under reflux. The time to complete each reaction varied depending on each reaction.

Pathway II: Compound **2c**, **2e** and **3b-3f** were synthesised using modified procedures and the synthesis was divided into two consecutive parts.^{25,71} First, the free base of either metformin or phenylbiguanide hydrochloride was isolated by reacting with NaOMe in anh. MeOH. The mixture was stirred for 3 hours at room temperature. The filtrate was collected by vacuum filtration and concentrated *in vacuo*. The crude was redissolved in hot EtOH, filtered and the filtrate was again concentrated *in vacuo* to give the final products as metformin or phenylbiguanide (**1b**). For monoesters, they were directly added into

metformin or **1b**. However, for diethyl oxalate, free base biguanide was added dropwise into the methanolic solution of diethyl oxalate.

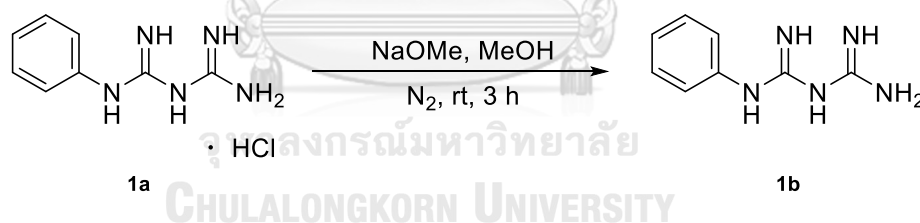
1.3. Synthesis of Compound **1a** and **1b**

Phenylbiguanide hydrochloride (**1a**)⁷¹

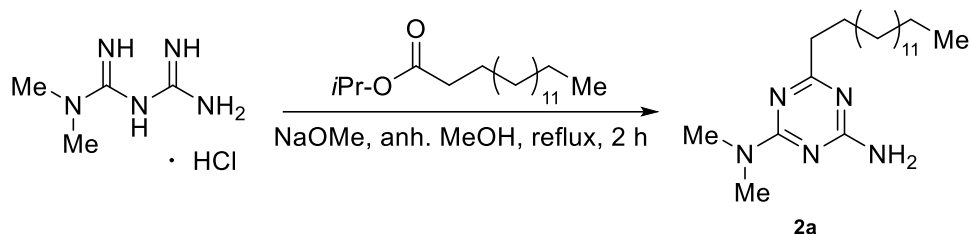


Aniline (1.826 g, 20 mmol, 1 equiv.), dicyandiamide (1.682 g, 20 mmol, 1 equiv.) and 3M HCl (6.7 mL, 20 mmol, 1 equiv.) were mixed and heated at 90 °C for 18 hours. The mixture was filtered under vacuum, and the precipitate was washed with cold DI water to obtain **1a** as a yellow solid (3.469 g, 81% yield). ¹H-NMR (400 MHz, DMSO) δ 9.75 (s, 1H), 7.41 – 7.24 (m, 8H), 7.13 – 6.97 (m, 3H); ¹³C-NMR (101 MHz, DMSO) δ 161.14, 155.31, 138.61, 128.65, 123.39, 120.96. Data is consistent with literature values.⁷²

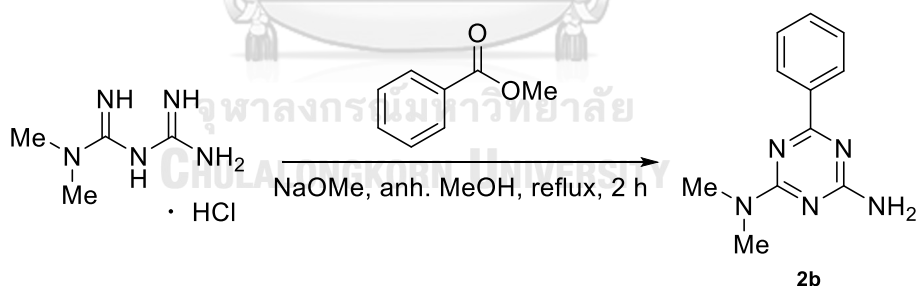
Phenylbiguanide (**1b**)



NaOMe (1.4 mL, 7 mmol, 1 equiv.) was added to **1a** (1.496 g, 7 mmol, 1 equiv.) in MeOH (3 mL). The mixture was stirred at room temperature for 3 hours. The precipitate was filtered under vacuum, washed with MeOH, and the filtrate was evaporated *in vacuo*. The crude was redissolved in hot EtOH and filtered. The filtrate was evaporated *in vacuo* to obtain **1b** as a pale-yellow solid (1.372 g, quant.). ¹H-NMR (400 MHz, DMSO) δ 7.20 (t, J = 7.6 Hz, 2H), 6.93 – 6.75 (m, 3H); ¹³C-NMR (101 MHz, DMSO) δ 159.69, 157.86, 150.16, 129.15, 122.97, 121.11. Data is consistent with literature values.⁷³

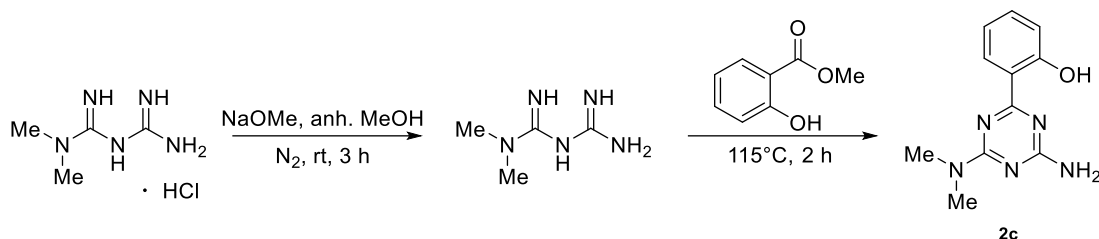
1.4. Synthesis of Compound **2a-2f***N*²,*N*²-dimethyl-6-pentadecyl-1,3,5-triazine-2,4-diamine (**2a**)

[Pathway I] metformin hydrochloride (**1a**) (497 mg, 3 mmol, 3 equiv.), NaOMe (1 mL, 5 mmol, 5 equiv.) and isopropyl palmitate (350 μ L, 1 mmol, 1 equiv.) in anhydrous MeOH (4 mL) were stirred under reflux for 2 hours. Purification *via* extraction with EtOAc/H₂O system and silica gel column chromatography (eluent: 1:3 EtOAc:hexane) yielded **2a** as a white solid (225 mg, 64% yield). ¹H-NMR (400 MHz, CDCl₃) δ 5.17 (brs, 2H), 3.15 (brs, 3H), 3.11 (brs, 3H), 2.49 (t, *J* = 7.7 Hz, 3H), 1.78–1.64 (m, 2H), 1.32–1.19 (m, 24H), 0.87 (t, *J* = 6.7 Hz, 3H); ¹³C-NMR (101 MHz, CDCl₃) δ 178.1, 166.3, 165.6, 38.8, 36.3, 32.1, 29.8, 27.7, 22.8, 14.2. Data is consistent with literature value.⁷⁴

*N*²,*N*²-dimethyl-6-phenyl-1,3,5-triazine-2,4-diamine (**2b**)

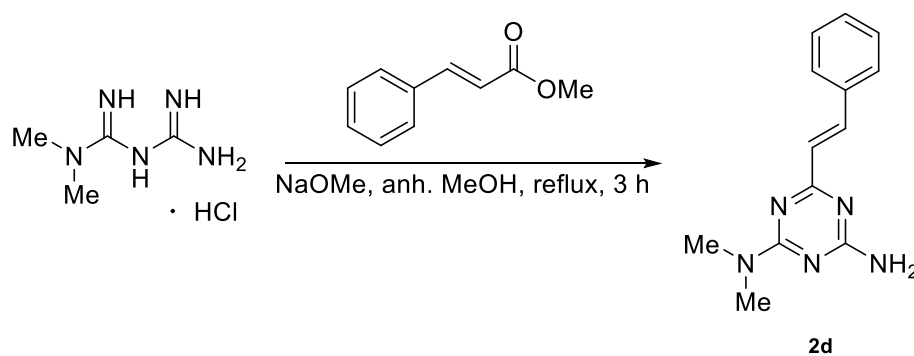
[Pathway I] metformin hydrochloride (497 mg, 3 mmol, 3 equiv.), NaOMe (1 mL, 5 mmol, 5 equiv.) and methyl benzoate (126 μ L, 1 mmol, 1 equiv.) in anhydrous MeOH (4 mL) were stirred under reflux for 2 hours. The crude mixture purified by silica gel column chromatography (eluent: 1:2 EtOAc:hexane) yielded **2b** as a white-yellow solid. (112 mg, 52% yield). ¹H-NMR (400 MHz, CDCl₃) δ 8.37 (d, *J* = 7.5 Hz, 2H), 7.53–7.38 (m, 3H), 5.26 (brs, 2H), 3.30 (brs, 3H), 3.17 (brs, 3H); ¹³C-NMR (101 MHz, CDCl₃) δ 171.0, 167.4, 166.0, 131.4, 130.1, 128.5, 128.3, 36.4. Data is consistent with literature values.¹⁴

2-(4-amino-6-(dimethylamino)-1,3,5-triazin-2-yl)phenol (**2c**)⁷⁵



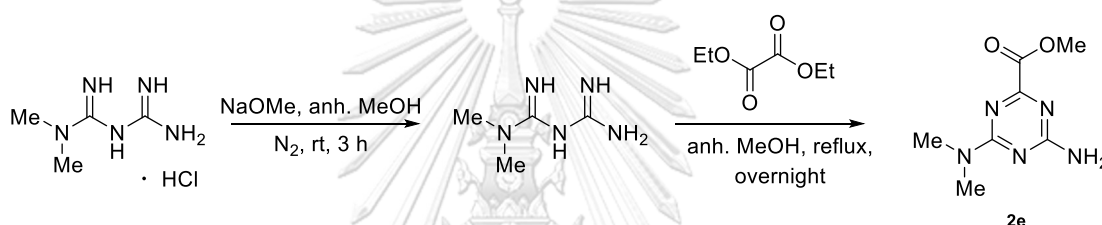
[Pathway II] metformin in the free base form was prepared with the same protocol as **1b** using metformin hydrochloride (3.313 g, 20 mmol, 1 equiv.) and NaOMe (4 mL, 20 mmol, 1 equiv.) in 15 mL of anh. MeOH. Next, excess amount of methyl salicylate (5 mL) was added into the mixture and heated at 115°C for 2 hours with a notable formation of basic fume. Upon the completion of reaction, the crude mixture was acidified with saturated NH_4Cl to neutral pH then purified by extraction with EtOAc/ H_2O system and silica gel column chromatography (eluent: 1:3 and 1:2 EtOAc:hexane). The product was further purified by recrystallisation using EtOAc and hexane which yielded **2c** as a greenish yellow solid. (2.153 g, 47% yield). $^1\text{H-NMR}$ (400 MHz, CDCl_3) δ 8.33 (d, $J = 7.9$ Hz, 1H), 7.37 (t, $J = 7.8$ Hz, 1H), 6.95 (d, $J = 8.3$ Hz, 1H), 6.89 (t, $J = 7.5$ Hz, 1H), 5.21 (brs, 2H), 3.22 (s, 3H), 3.17 (s, 3H); $^{13}\text{C-NMR}$ (101 MHz, CDCl_3) δ 171.3, 165.8, 164.4, 162.2, 134.1, 129.7, 119.1, 118.4, 118.1, 36.9, 36.7; IR (neat): 3390, 3324, 3200, 2926, 1652, 1566, 1499, 1031, 746; HRMS (ESI+): m/z calcd for $\text{C}_{11}\text{H}_{13}\text{N}_5\text{O}$ $[\text{M}+\text{H}]^+$ 232.1198, found 232.1191; Mp: 194-197°C.

(*E*)- N^2,N^2 -dimethyl-6-styryl-1,3,5-triazine-2,4-diamine (**2d**)

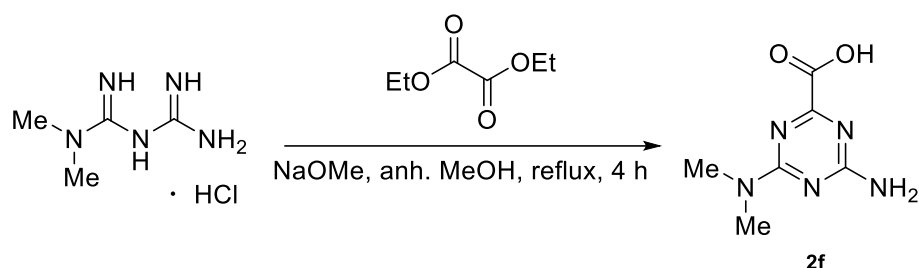


[Pathway I] metformin hydrochloride (331 mg, 2 mmol, 1 equiv.), NaOMe (800 μ L, 4 mmol, 2 equiv.), and methyl cinnamate (446 μ L, 3 mmol, 1.5 equiv.) in anh. MeOH (4 mL) were stirred under reflux for 3 hours. The crude mixture purified by extraction using EtOAc/hexane system yielded **2d** as a yellow solid (302 mg, quant.). $^1\text{H-NMR}$ (400 MHz, CDCl_3) δ 7.95 (d, J = 15.9 Hz, 1H), 7.58 (d, J = 7.0 Hz, 2H), 7.43–7.30 (m, 3H), 6.83 (d, J = 15.9 Hz, 1H), 5.28 (brs, 2H), 3.22 (brs, 3H), 3.15 (brs, 3H); $^{13}\text{C-NMR}$ (101 MHz, CDCl_3) δ 171.0, 167.2, 166.1, 139.7, 136.3, 129.6, 129.2, 128.3, 127.5, 36.7. Data is consistent with literature values.¹⁵

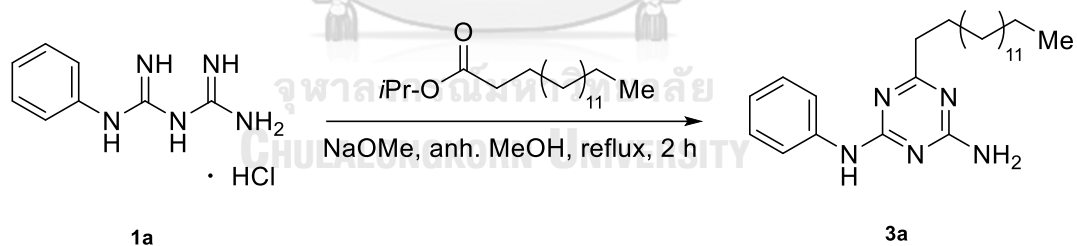
Methyl 4-amino-6-(dimethylamino)-1,3,5-triazine-2-carboxylate (**2e**)



[Pathway II] metformin in the free base form was prepared with the same protocol as **1b** using metformin hydrochloride (497 mg, 3 mmol, 1.5 equiv.) and NaOMe (400 μ L, 2 mmol, 1 equiv.) in 6 mL of anh. MeOH. Metformin dissolved in anh. MeOH (7.5 mL) was added dropwise into diethyl oxalate (1218 μ L, 9 mmol, 3 equiv.) also dissolved in anh. MeOH (7.5 mL) with constant stirring motion at room temperature. Subsequently, the mixture was heated at reflux overnight (around 18 hours). The mixture was purified by silica gel column chromatography (eluent: 3:5, 7:10 EtOAc:hexane) which yielded **2e** as a yellow solid (27 mg, 7% yield). $^1\text{H-NMR}$ (400 MHz, CDCl_3) δ 5.68 (brs, 2H), 3.95 (s, 3H), 3.23 (s, 3H), 3.13 (s, 3H); $^{13}\text{C-NMR}$ (101 MHz, CDCl_3) δ 166.5, 165.4, 164.0, 163.1, 53.1, 36.4, 36.2; IR (neat): 3426, 3303, 3170, 2953, 1732, 1640, 1566, 1439, 1247, 1209, 1011, 793; HRMS (ESI+): m/z calcd for $\text{C}_7\text{H}_{11}\text{N}_5\text{O}_2$ $[\text{M}+\text{Na}]^+$ 220.0810, found 220.0815; Mp: 219–221°C.

4-amino-6-(dimethylamino)-1,3,5-triazine-2-carboxylic acid (**2f**)

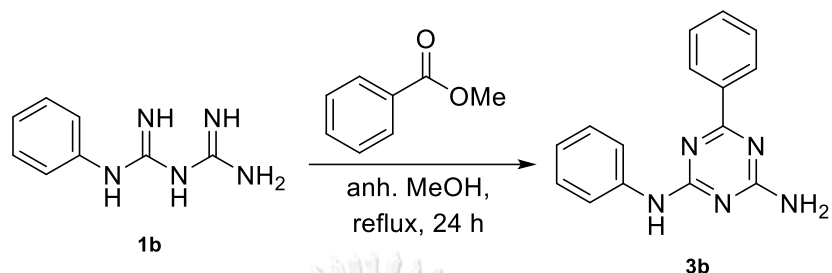
[Pathway I] metformin hydrochloride (167 mg, 1 mmol, 1 equiv.), NaOMe (400 μ L, 2 mmol, 2 equiv.) and diethyl oxalate (2975 μ L, 22 mmol, 22 equiv.) in anh. MeOH (5 mL) were stirred under reflux for 4 hours. The white precipitate was filtered, washed with MeOH, and dried by vacuum to yield **2f** as a white-yellow solid (118 mg, 65% yield). $^1\text{H-NMR}$ (400 MHz, DMSO) δ 11.08 (s, 1H), 9.01 (brs, 1H), 8.02 (brs, 1H), 3.11 (s, 3H), 3.02 (s, 3H); $^{13}\text{C-NMR}$ (101 MHz, DMSO) δ 171.2, 169.9, 163.8, 160.4, 37.9, 37.2; IR (neat): 3304, 3168, 1763, 1708, 1563, 1479, 1324, 1040, 819; HRMS (ESI+): m/z calcd for $\text{C}_6\text{H}_9\text{N}_5\text{O}_2$ $[\text{M}+\text{Na}]^+$ 206.0654, found 206.0645; Mp: $>300^\circ\text{C}$.

1.5. Synthesis of Compound **3a-3f**6-pentadecyl- N^2 -phenyl-1,3,5-triazine-2,4-diamine (**3a**)

[Pathway I] **1a** (6.410 g, 30 mmol, 3 equiv.), NaOMe (10 mL, 50 mmol, 5 equiv.) and isopropyl palmitate (10.511 mL, 30 mmol, 3 equiv.) were stirred under reflux for 2 hours. Purification *via* extraction with EtOAc/ H_2O system and silica gel column chromatography (eluent: 1:3, 1:2 EtOAc:hexane) yielded **3a** as a white solid (5.0 g, 42% yield). $^1\text{H-NMR}$ (400 MHz, DMSO) δ 9.38 (s, 1H), 7.77 (d, $J = 7.9$ Hz, 2H), 7.24 (t, $J = 7.9$ Hz, 2H), 6.94 (t, $J = 7.2$ Hz, 3H), 2.41 (t, $J = 7.6$ Hz, 2H), 1.73–1.60 (m, 2H), 1.29–1.20 (m, 23H), 0.84 (t, $J = 6.7$ Hz, 3H); $^{13}\text{C-NMR}$ (101 MHz, DMSO) δ 177.8, 166.6, 164.2, 140.0, 128.3, 121.7, 119.7, 37.9, 31.2, 29.0, 26.9, 22.0, 13.9; IR (neat): 3462, 3311, 3106, 2913, 2848, 1655,

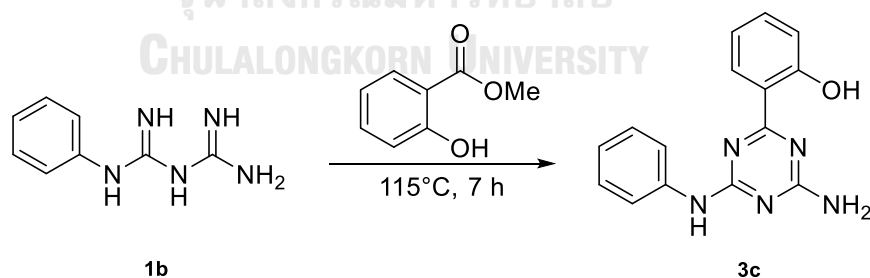
1626, 1528, 1470, 1429, 1385, 1028, 815, 747, 720, 699; HRMS (ESI⁺): *m/z* calcd for C₂₄H₃₉N₅ [M+H]⁺ 398.3284, found 398.3291; Mp: 118-121°C.

*N*²,6-diphenyl-1,3,5-triazine-2,4-diamine (**3b**)



[Pathway II] **1b** was used without further purification. Methyl benzoate (792 μ L, 6 mmol, 2 equiv.) was added into **1b** (532 mg, 3 mmol, 1 equiv.) dissolved in anh. MeOH (4 mL). The mixture was stirred under reflux for 24 hours. Purified by silica gel column chromatography (eluent: 1:3 EtOAc:hexane) yielded **3b** as a yellow solid (54 mg, 7% yield). ¹H-NMR (400 MHz, DMSO) δ 9.52 (s, 1H), 8.31 (d, *J* = 6.8 Hz, 2H), 7.84 (d, *J* = 8.0 Hz, 2H), 7.58–7.44 (m, 3H), 7.31 (t, *J* = 7.8 Hz, 2H), 7.12 (brs, 2H), 6.99 (t, *J* = 7.3 Hz, 1H); ¹³C-NMR (101 MHz, DMSO) δ 170.7, 167.6, 165.1, 140.3, 137.2, 131.8, 128.9, 128.7, 128.2, 122.5, 120.4. Data is consistent with literature values.⁷⁶

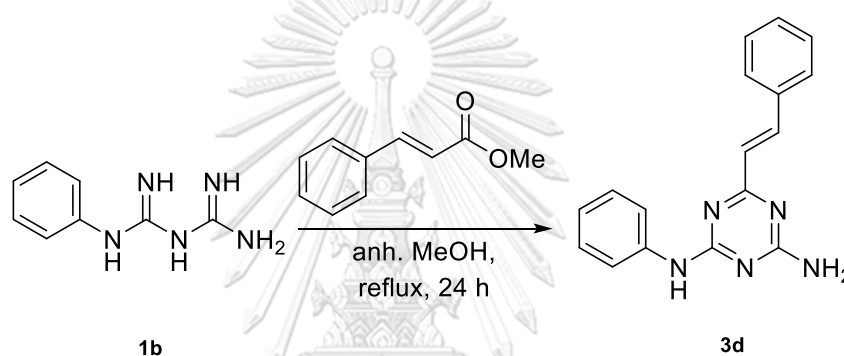
2-(4-amino-6-(phenylamino)-1,3,5-triazin-2-yl)phenol (**3c**)⁷⁵



[Pathway II] **1b** was used without further purification. A mixture of **1b** (355 mg, 2 mmol, 1 equiv.) and an excess amount of methyl salicylate (500 μ L) were stirred and heated at 115°C for 7 hours with a notable formation of basic fume. The crude mixture was acidified with NH₄Cl to neutral pH then purified by extraction with EtOAc/H₂O system and silica gel column chromatography (eluent: 1:4 – 1:2 EtOAc:hexane). The product was further purified by recrystallisation using EtOAc and hexane which yielded **3c** as a

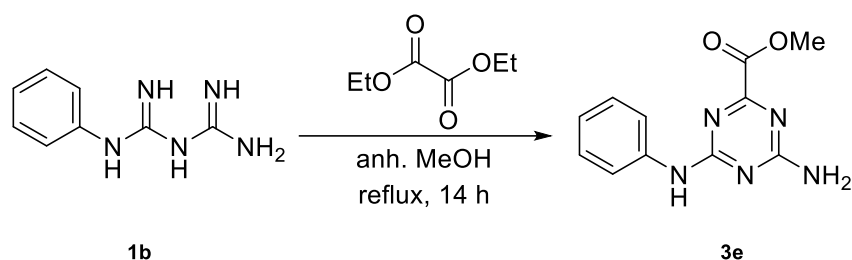
greenish yellow solid (220 mg, 39% yield). $^1\text{H-NMR}$ (400 MHz, DMSO) δ 13.49 (s, 1H), 9.77 (brs, 1H), 8.26 (d, $J = 7.3$ Hz, 1H), 7.76 (brs, 2H), 7.55 (brs, 1H), 7.44–7.35 (m, 2H), 7.33 (t, $J = 7.2$ Hz, 2H), 7.04 (t, $J = 7.5$ Hz, 1H), 6.90 (t, $J = 8.0$ Hz, 2H); $^{13}\text{C-NMR}$ (101 MHz, DMSO) δ 169.9, 164.7, 160.8, 138.8, 133.2, 128.3, 128.1, 122.3, 120.2, 117.9, 117.2, 117.1; IR (neat): 3475, 3302, 3181, 1667, 1595, 1533, 1443 1429, 1031, 811, 752, 691; HRMS (ESI+): m/z calcd for $\text{C}_{15}\text{H}_{13}\text{N}_5\text{O}$ $[\text{M}+\text{H}]^+$ 280.1198, found 280.1205; Mp: 222–224°C.

(*E*)-*N*²-phenyl-6-styryl-1,3,5-triazine-2,4-diamine (**3d**)



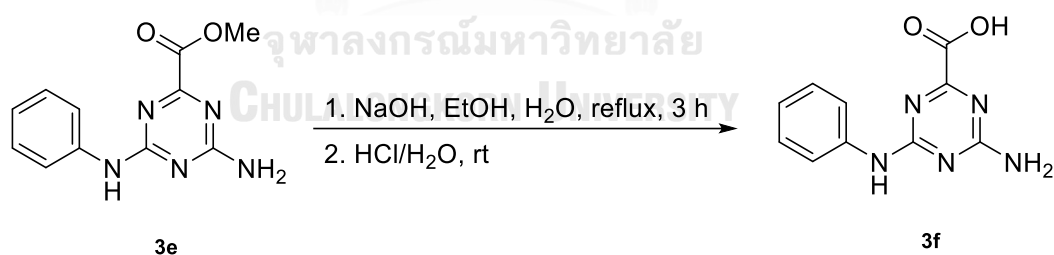
[Pathway II] **1b** was used without further purification. Methyl cinnamate (447 μL , 3 mmol, 1 equiv.) was added into **1b** (709 mg, 4 mmol, 1.33 equiv.) dissolved in anh. MeOH (4 mL). The mixture was stirred under reflux for 24 hours. Purification by silica gel column chromatography (eluent: 1:2, 1:1 EtOAc:hexane) yielded **3d** as a yellow solid (154 mg, 17% yield). $^1\text{H-NMR}$ (500 MHz,) δ 9.47 (s, 1H), 7.87 (d, $J = 15.9$ Hz, 1H), 7.81 (dd, $J = 8.7, 1.2$ Hz, 2H), 7.66 (d, $J = 7.5$ Hz, 2H), 7.46–7.36 (m, 3H), 7.28 (t, $J = 7.6$ Hz, 2H), 7.03 (brs, 2H), 6.97 (tt, $J = 7.3, 1.2$ Hz, 1H), 6.82 (d, $J = 16.0$ Hz, 1H); $^{13}\text{C-NMR}$ (101 MHz, CDCl_3) δ 171.0, 166.6, 164.3, 141.2, 138.3, 135.5, 129.9, 129.1, 129.0, 128.2, 125.5, 124.0, 121.0; IR (neat): 3462, 3276, 3058, 1638, 1574, 1526, 1490, 1442, 970, 735, 691; HRMS (ESI+): m/z calcd for $\text{C}_{17}\text{H}_{15}\text{N}_5$ $[\text{M}+\text{H}]^+$ 290.1406, found 290.1409; Mp: 186–189°C.

Methyl 4-amino-6-(phenylamino)-1,3,5-triazine-2-carboxylate (**3e**)



[Pathway II] **1b** was used without further purification. **1b** (4.430 g, 25 mmol, 1 equiv.) dissolved in anh. MeOH (62.5 mL) was added dropwise into diethyl oxalate (10.15 mL, 75 mmol, 3 equiv.) also dissolved in anh. MeOH (62.5 mL) with constant stirring motion at room temperature. Subsequently, the mixture was stirred under reflux for 14 hours. Purification by silica gel column chromatography (eluent: 1:1 EtOAc/hexane to 5% EtOAc/MeOH) yielded **3e** as a yellow solid (2.428 g, 40% yield). $^1\text{H-NMR}$ (400 MHz, DMSO) δ 9.93 (brs, 1H), 7.78 (d, $J = 7.9$ Hz, 2H), 7.56 (brs, 1H), 7.43 (brs, 1H), 7.28 (t, $J = 6.8$ Hz, 2H), 7.01 (t, $J = 7.9$ Hz, 1H), 3.83 (s, 3H); $^{13}\text{C-NMR}$ (101 MHz, DMSO) δ 167.3, 164.5, 164.2, 164.1, 139.5, 128.7, 122.7, 120.3, 52.6. Data is consistent with literature values.⁴⁵

4-amino-6-(phenylamino)-1,3,5-triazine-2-carboxylic acid (**3f**)⁷⁷



NaOH (aq.) (50 mL, 1 M) was added to a solution of **3e** (2.023 g, 8.25 mmol) dissolved in EtOH (100 mL). The mixture was stirred under reflux for 3 hours, then cooled to room temperature followed by the addition of HCl (aq.) (50 mL, 1M). The resulting precipitate was filtered, washed with DI water, and dried under vacuum to yield **3f** as a pale-yellow solid (2.416 g, quant.). $^1\text{H-NMR}$ (400 MHz, DMSO) δ 9.89 (brs, 1H), 7.78 (d, $J = 8.1$ Hz, 2H), 7.47 (brs, 2H), 7.28 (t, $J = 7.3$ Hz, 2H), 7.00 (t, $J = 7.5, 6.7$ Hz, 1H); $^{13}\text{C-NMR}$ (101 MHz, DMSO) δ 166.9, 165.4, 165.0, 164.3, 139.4, 128.5, 122.6, 120.2; IR

(neat): 3319, 3129, 1675, 1622, 1594, 1568, 1489, 1451, 1005, 788, 761, 691; HRMS (ESI+): m/z calcd for $C_{10}H_9N_5O_2 [M+2Na-H]^+$ 276.0473, found 276.0473; Mp: 248-249°C.

2. Experimental procedures for anticancer evaluation

2.1. Materials and instruments for biological assays

HCT116 (Human colorectal carcinoma) and SW620 (Human colorectal adenocarcinoma) cell lines were obtained from Nanomedicine RU, Faculty of Medicine, Chulalongkorn University. DMEM (Dulbecco's Modified Eagle Medium), RPMI, fetal bovine serum (FBS), antibiotics, trypsin-EDTA, PBS (Phosphate Buffered Saline) (1X, pH 7.4), and PrestobluTM cell viability reagent were purchased from Thermo Fisher Scientific (Waltham, MA, USA). Cisplatin was purchased from Sigma Aldrich (St. Louis, MO, USA), and dialysis bag Spectra/Por membranes (MWCO = 12-14 kDa) was purchased from Spectrum Laboratories, Inc. (Rancho Dominguez, CA, USA).

2.2. Cell culture

HCT116 cell line was cultured in a growth medium of RPMI supplemented with 10% FBS and 1% antibiotic. For SW620 cell line, DMEM was used as the growth medium and also supplemented with 10% FBS and 1% antibiotic. Both cell lines were maintained in an incubator at 37°C in a humidified atmosphere of 5% CO₂.

2.3. %Inhibition and IC₅₀ evaluation

HCT116 and SW620 were seeded in 96 well plates at a density of 1×10^4 per well in cell culture medium and incubated for 24 hours to allow cell adherence. The concentration used for %cytotoxicity study was at one concentration of 100 μM and IC₅₀ evaluations was between 0-100 μM. Following the 48 hours of incubation, 10 μL PrestoBlueTM solution was added to each well, and then plates were placed back into the incubator for a further 30 minutes incubation.⁷⁸ Fluorescence were measured using a microplate reader at 560 nm excitation and 590 nm emission (Thermo, Varioskan Flash, England). The results were

analysed by one-way ANOVA and Tukey post-test using GraphPad Prism 5.0 (Graph-Pad Software Inc., San Diego, CA, USA).

$$\% \text{cell viability} = \frac{\text{avg}(\text{absorbance of compound})}{\text{avg}(\text{absorbance of control})} \times 100$$

$$\% \text{cytotoxicity} = 100 - \% \text{cell viability}$$

3. Experimental procedures for the synthesis of CaCit-triazine NPs

3.1. Chemicals and instruments for nanoparticles synthesis

Calcium chloride dihydrate and trisodium citrate dihydrate were purchased from Merck (Darmstadt, Germany). Citric acid anhydrous was purchased from Loba Chemie PVT. LTD (Mumbai, India). All of the solvents used were analytical grade.

Size and morphology of the synthesised particles were recorded with JEOL JSM-6480LV scanning electron microscope at 15kV; hydrodynamic size and zeta potential were measured with the Malvern Zetasizer (material IR of 1.660); functional groups were analysed by Thermo Scientific™ Nicolet 6700 FT-IR Spectrometer (ATR mode, 16 and 32 scans); chemical changes or decomposition temperature by Pyris™ 1 TGA Thermogravimetric Analyzer; elemental analysis by Thermo Flash 2000 CHNS/O analyser; and %cumulative drug release study was measured by UV/Vis spectrometer (Hewlett Packard 8453, Agilent Technology, Santa Clara, CA, USA).

3.2. Synthesis of 1,3,5-triazine incorporated in calcium citrate nanoparticles

The synthesis of drug incorporated calcium citrate nanoparticles used the modified methods.^{36, 63, 79, 80} Table 1 summarise all reaction conditions in this work and condition 1-6 was the most optimised condition for the incorporation of **2a** into calcium citrate nanoparticles. Citrate ions was prepared by dissolving citric acid in 0.5 mL of DI water, followed by the addition of 1M NaOH until pH of solution reached pH 6.0 then the volume was adjusted to 5 mL with EtOH. **2a** was dissolved in 5 mL EtOH while heating at 50-60°C, and CaCl₂ was also dissolved in 5 mL EtOH. Citrate ions was added into the solution of **2a** which turned cloudy straightaway. EtOH and DI water were added to the mixture to

obtain a clear solution. The Ca^{2+} solution was added dropwise into the mixture with vigorous stirring for 8 hours at room temperature. The white suspension was centrifuged, washed with EtOH/water and freeze dried for 24 hours.

Table 1. Experimental conditions for the synthesis of CaCit-triazine NPs

		Condition	CaCl_2	Na_3Cit	Citric Acid	2a	Additional EtOH:water	Reaction Time
Reaction Optimisation	Vary citrate ion	1-1	0.15M EtOH 5 mL	0.195M EtOH/water 5 mL	-	0.20M EtOH 5 mL	29:15 mL	16-18 hours
		1-2	0.15M EtOH 5 mL	-	0.195M EtOH/water 5 mL	0.20M EtOH 5 mL	29:15 mL	
	Vary reaction time	1-3	0.15M EtOH 5 mL	-	0.195M EtOH/water 5 mL	0.20M EtOH 5 mL	29:15 mL	1-24 hours
Reaction Verification		1-4	0.15M	-	0.195M	0.20M	29:15 mL	2 hours
		1-5	EtOH 5 mL	-	EtOH/water 5 mL	EtOH 5 mL		5 hours
		1-6		-				8 hours

3.3. Synthesis of calcium citrate nanoparticles

A solution of CaCl_2 and a solution of Na_3Cit or citric acid were mixed and magnetically stirred at room temperature for an indicated time. The mixture changed from clear colourless to become white suspension which was centrifuged at 5000 rpm for 8 minutes. The white solid was washed with DI water three times and freeze dried for 24 hours.

3.4. *In vitro* drug release study

The drug release profile of the synthesised nanoparticles was determined by the dialysis method carried out at 37°C and stirring speed of 100 rpm (Figure 15). 30% (v/v) EtOH in PBS at pH 3.0, 5.0 and 7.4 were used as the release medium.⁸¹ Nanoparticles

(weight equivalent to 1 mg of **2a**) were dispersed in 10 mL 30% (v/v) EtOH/PBS at pH 3.0, 5.0 and 7.4. The dialysis bag was immersed into 190 mL of release medium. At predetermined time, the dialysis bag was moved into another container with 190 mL of fresh release medium.³⁵ To extract **2a** out of the release medium, the solution was evaporated under vacuum to remove EtOH and extracted with DCM.⁸² For the UV-Vis spectroscopy measurement, 10 mL of 60% (v/v) EtOH/PBS acidified with HCl to pH 3.0, 5.0 and 7.4 was added to each sample and measure at 200-320 nm. The calibration curve was drawn using standards which was **2a** dissolved in 60% (v/v) EtOH/PBS at various concentrations.

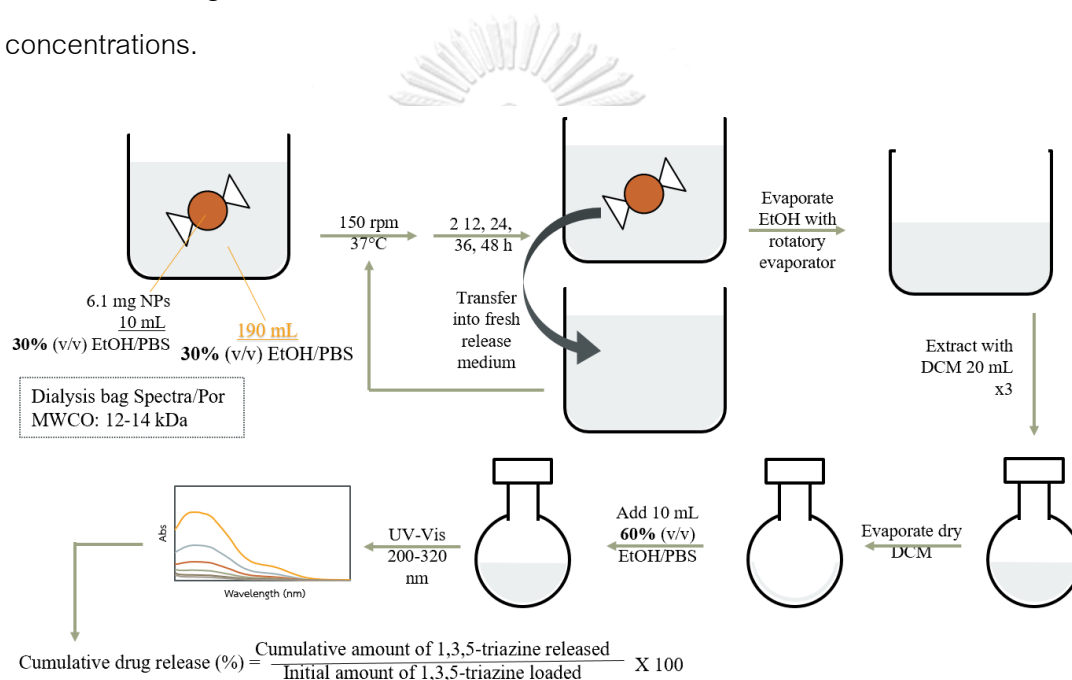


Figure 15. A pictorial diagram of the *in vitro* drug release study

CHAPTER III

RESULTS AND DISCUSSIONS

1. Synthesis and characterisation of 1,3,5-triazine derivatives

As shown in the literature reviews earlier about 1,3,5-triazine derivatives, the substituent on the 1,3,5-triazine scaffold had diverse effects on the anticancer activity. In 2011, it was found that the lipophilicity or hydrophobicity of the overall compound could affect the physicochemical and pharmacokinetic properties of the drug.⁸³ Therefore, the substituents modified onto the 1,3,5-triazine scaffold in this work were selected from compounds exhibiting anticancer activity by itself and could improve the hydrophobicity of the compound, such as cinnamic acid, salicylic acid and long alkyl chain.

Aspirin as known as acetylsalicylic acid has been reported to possess anticancer activity and many possible routes were elucidated, for example, inducing apoptosis and inhibit essential proteins relating to cancer cell growth.⁸⁴ Not only that aspirin was the active anticancer agent, but salicylate salt which is the metabolite form of aspirin could also exhibit cell growth in the same range of concentration between 2.5-10 mM. When salicylic acid was combined with β -carboline, the salicylic acid- β -carboline derivatives showed greater cell inhibition than the acetamide or benzamide derivatives of β -carboline derivatives or salicylic acid alone.⁸⁵ The salicylic acid- β -carboline derivatives displayed antiproliferative activity in the low micromolar range and they were more selective towards tumour cells.

Cinnamic acid and its derivatives also have versatile biological roles, for example, antioxidant,^{86, 87} antimicrobial^{88, 89} and antitumour activities.⁹⁰ From a study about the long alkyl chain esters of hydroxycinnamic acid as anticancer agents, derivatives containing the *p*-coumaric acid moiety resulted in the best anticancer activity, followed by caffeate, ferulate and sinapate.⁹¹ As *p*-coumaric acid, caffeic acid, ferulic acid and sinapic acid have different hydroxy groups on the phenyl ring, it was found that the number of the hydroxy group had influences on the cytotoxic activity. In the same study, different length of the long alkyl chain modified onto the carboxylic acid moiety of cinnamic acid

derivatives had different effects on the anticancer activity. Tetradecyl ester was the most active derivatives because the compound possesses optimal chain length for physicochemical requirements, such as lipophilicity for cellular uptake and intracellular accumulation.⁹¹ Therefore, the lipophilicity of compound was improved hence the anticancer activity.

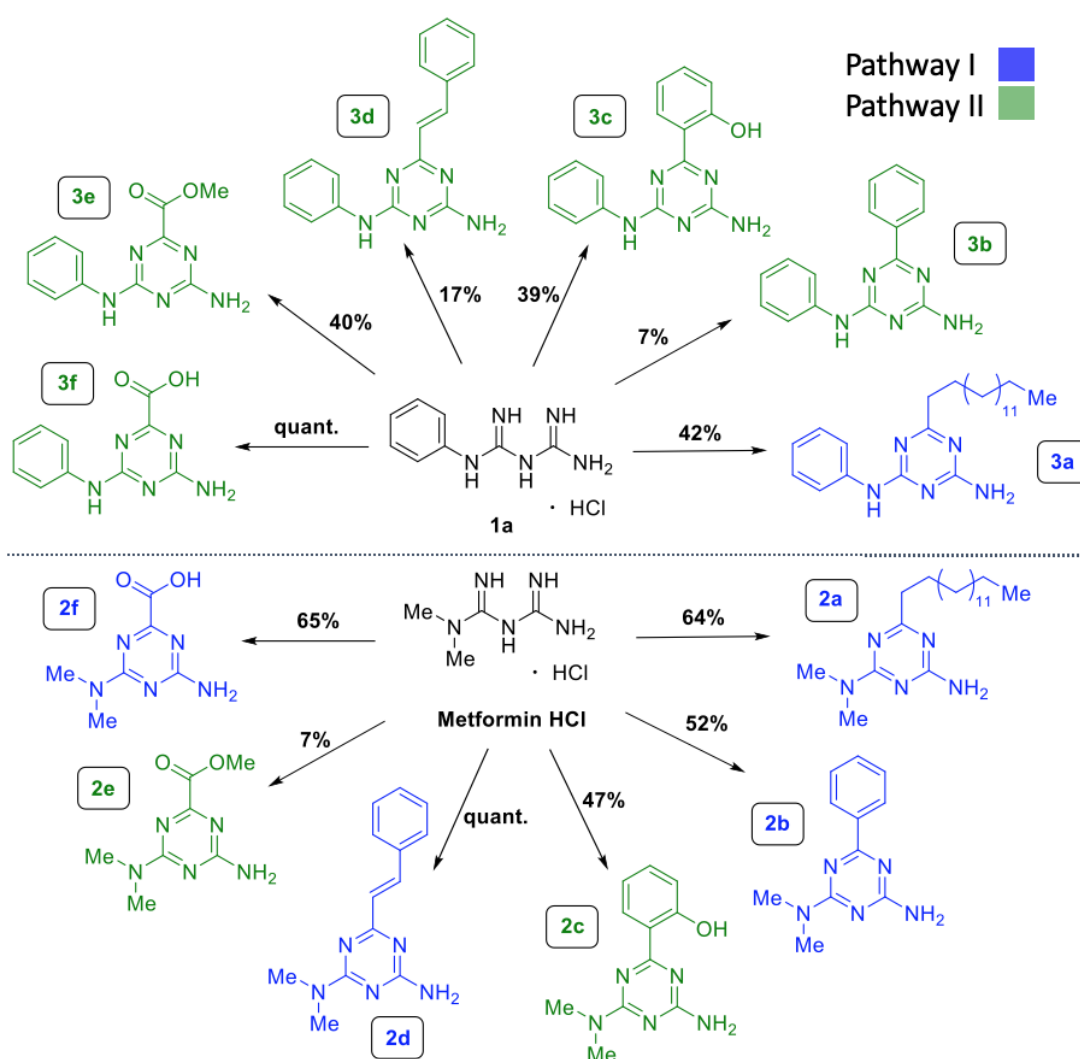


Figure 16. Scheme demonstrating the synthesised 1,3,5-triazine derivatives; Blue represents compound synthesized by pathway I and Green is for pathway II

Both 1,3,5-triazine bearing salicylic acid and cinnamic acid moiety had been synthesised but have not been evaluated for anticancer activity.^{15, 75} Therefore, it would be interesting to study the effect of these substituents on the anticancer activity of the

1,3,5-triazine scaffold. As seen with long alkyl chain ester of hydroxycinnamic acid, long alkyl chain substituent is also interesting because it could modify the lipophilicity of compound as reported for dodecanoyl amide derivative of DOX.⁸³

In this work, metformin and phenylbiguanide hydrochloride were used as the starting materials, and each yielded six 1,3,5-triazine derivatives with low to moderate yields. The synthesis of 1,3,5-triazine derivatives had two pathways, pathway I and II. In total, 12 1,3,5-triazine derivatives were synthesised of which four compounds were novel; three compounds were known, but not fully characterised (“partially known”); and five derivatives were known (Figure 16). The partially known and novel compounds were further characterised for IR spectra, mass spectra and melting points.

1.1. Synthesis of 1,3,5-triazine derivatives *via* Pathway I

Pathway I was a one-pot reaction containing a biguanide hydrochloride, NaOMe and an ester.^{17, 25} NaOMe acted as the base to neutralise the hydrochloride salt enabling the nucleophilic substitution between the nucleophilic NH with the electrophilic carbonyl group (Figure 17). However, a complication occurred with the one-pot reaction such that a by-product was detected even though anhydrous solvent and inert atmosphere were used. The by-product was found to be the carboxylic acid of the ester reactant. This was possible due to the hydrolysis of the ester moiety as both base and water were presented in the reaction mixture. In order to overcome this issue, the neutralisation reaction that required base was completed in a separate step. Then, the biguanide in the free base form reacted with the ester (pathway II).^{17, 25, 71, 75} All the reactions were attempted with the one-pot reaction, but if the %yield was low, the synthesis method *via* pathway II was substituted.

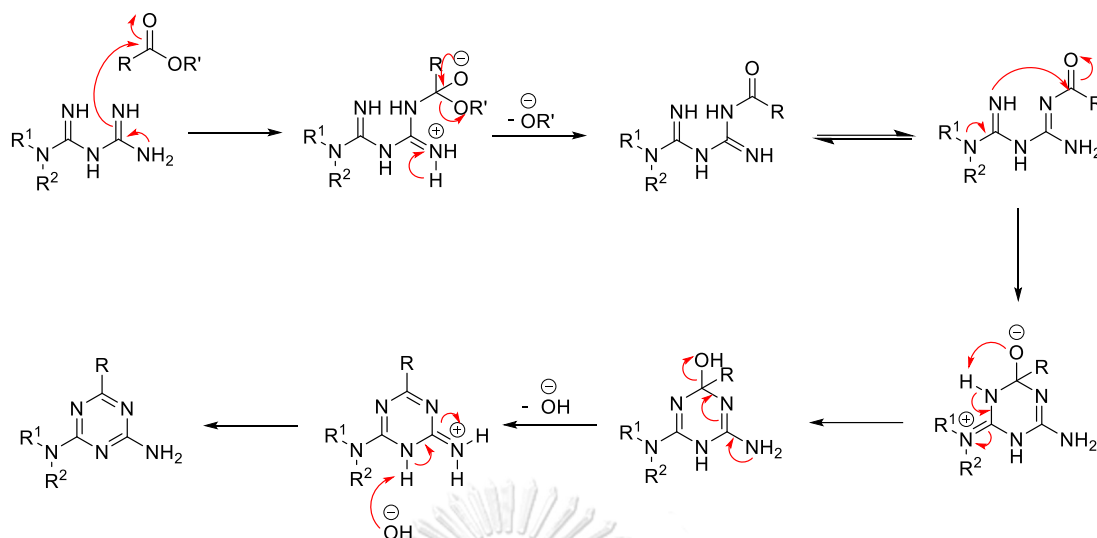


Figure 17. Proposed mechanism for the formation of 1,3,5-triazine derivatives

Compound **2a**, **2b**, **2d**, **2f** and **3a**, were successfully synthesised *via* pathway I with moderate to quantitative yield (Figure 16). In the initial stage, reaction conditions were optimised by using various bases and solvents. The four bases were sodium hydroxide, potassium carbonate (K_2CO_3), sodium hydride and NaOMe. Using the reaction between metformin hydrochloride and methyl benzoate as reference, NaOMe resulted in a product with the highest %yield whereas the reaction with sodium hydroxide was not successful according to TLC and NMR (Entry 2-3 to 2-5). Next, four solvents were compared, and it was found that dry toluene gave the highest %NMR yield at 88% (Entry 2-1), followed by anh. MeOH (Entry 2-3), and no reaction was observed for THF and ACN because the reactants were not soluble in either solvent (Entry 2-6 and 2-7). When the reaction was repeated and carried out at a larger scale, %yield for dry toluene was 53% (Entry 2-2). Interestingly, even though the %NMR yield of anh. MeOH was not as high as the dry toluene, the reaction using anh. MeOH resulted in 52% yield (Entry 2-3). To further confirm the results, another reaction between metformin hydrochloride and methyl cinnamate was conducted. In agreement with the previous reaction, NaOMe resulted in higher %NMR yield than K_2CO_3 , and anh. MeOH was the most suitable solvent for the reaction (Entry 2-8 to 2-13). Moreover, anhydrous solvent was favoured over the conventional ones. Therefore, NaOMe and anh. MeOH were selected as the base and solvent, respectively, for future reactions.

Table 2. Optimisation of base and solvent

	Entry	Metformin (mmol)	Ester (mmol)	Base (mmol)	Solvent (mL)	Yield (%)
Methyl Benzoate	2-1	0.3	0.1	NaOMe (0.5)	Dry Tol	88%*
	2-2	3	1	NaOMe (5)	Dry Tol	53%
	2-3	3	1	NaOMe (5)	anh. MeOH	52%
	2-4	0.3	0.1	NaH (0.3)	anh. MeOH	10%*
	2-5	0.3	0.1	K ₂ CO ₃ (0.3)	anh. MeOH	5%*
	2-6	0.3	0.1	K ₂ CO ₃ (0.3)	ACN	NR
	2-7	0.3	0.1	K ₂ CO ₃ (0.3)	THF	NR
Methyl Cinnamate	2-8	0.1	0.15	NaOMe (0.2)	anh. MeOH	51.0%*
	2-9	0.1	0.15	NaOMe (0.2)	anh. ACN	15.4%*
	2-10	0.1	0.15	NaOMe (0.2)	Dry Tol	23.2%*
	2-11	0.1	0.15	NaOMe (0.2)	MeOH	44.6%*
	2-12	0.1	0.15	NaOMe (0.2)	ACN	11.4%*
	2-13	0.1	0.15	K ₂ CO ₃ (0.2)	anh. MeOH	25.3%*

* = %yield calculated from NMR; NR = No reaction

The reactions involving isopropyl palmitate used the optimised reaction condition resulting in two 1,3,5-triazine derivatives with moderate yield of 64% for **2a** and 42% for **3a**. Compound **2d** was synthesised by using the mmol equivalent similar to those reported by Kothayer et al. which was 2:3 metformin hydrochloride to methyl cinnamate.²⁵ Surprisingly, from this reaction the product obtained had quantitative yield, and its purity was confirmed by NMR spectroscopy. Another unexpected result was the synthesis of **2f**. Initially, compound **2e** was the expected product from the reaction between metformin and diethyl oxalate because Kothayer et al. had reported a similar reaction, but used dimethyl oxalate instead and the product was 1,3,5-triazine with a carboxylate substituent.²⁵ Several reaction conditions between metformin and diethyl oxalate were attempted as shown in Table 3, the optimised condition yielded no product and despite

increasing the amount of diethyl oxalate, a di-triazine product was obtained instead (Figure 18). The hypothesised structure of the di-triazine product was confirmed by MALDI-TOF mass spectrometer and NMR (data not shown). However, when the reaction condition was carried out at the ratio of 1:2:22 metformin:NaOMe:diethyl oxalate (Entry 3-4), **2f** was synthesised with moderate yield. It was apparent that the product did not have a carboxylate group because the product was not soluble in alcohol which was used as solvent. In addition to the characterisation of **2f** by NMR, HRMS verified the molecular weight of the product to be in consistent with the triazine derivative bearing a carboxylic acid substituent, and FTIR spectrum indicated that **2f** might exist in dimer hence the absence of O-H stretching peak. The formation of **2f** instead of **2e** was not only unexpected, but it was also hypothesised that **2e** might have been formed then got hydrolysed due to the presence of base (NaOMe) and water in the reaction mixture. Despite the use of anhydrous solvent, the reaction was not dried enough to prevent subsequent hydrolysis reaction. In order to prevent the hydrolysis from happening, the solvent must truly be anhydrous and molecular sieve could be added into the reaction.

Table 3. Reactions of metformin with diethyl oxalate

Entry	Metformin (mmol)	NaOMe (mmol)	Diethyl oxalate (mmol)	Solvent (mL)	Reaction Temperature / Time	Yield (%)
3-1	3	5	1	Dry Tol (4)	Reflux / 4 h	NP
3-2	2	4	4	anh. MeOH (4)	Reflux / 4 h	NP
3-3	2	4	20	anh. MeOH (4)	Reflux / 4 h	NP
3-4	1	2	22	anh. MeOH (5)	Reflux / 2 h	65%

NP = no desired product was obtained from the reaction

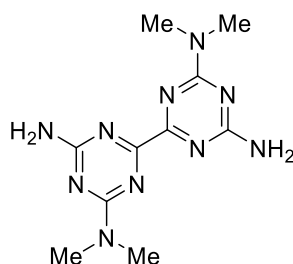


Figure 18. The hypothesised structure of the di-triazine compound

1.2. Synthesis of 1,3,5-triazine derivatives *via* Pathway II

Seven 1,3,5-triazine derivatives, **2c**, **2e**, **3b-3f** were obtained using this pathway, and the %yield are as shown in Figure 16. Both reactions of metformin or phenylbiguanide with methyl salicylate initially used the protocol of pathway I, but the %yield was low at around 15%. A new method was adapted involving the use of methyl salicylate in excess amount.⁷⁵ At the expense of using a greater amount of reagent and higher temperature, the reaction time was shortened and significantly increased %yield of products. Compound **3c** had a slightly lower %yield at 39% than **2c** at 47%.

The synthesis of **2e** and **3e** required a more careful consideration due to the di-ester nature of diethyl oxalate. As mentioned earlier that the one-pot reaction for diethyl oxalate resulted in the formation of the undesired di-triazine compound. Three methods of reactant addition and reaction temperature were experimented (Table 4). The first approach (Entry 4-1) was adding the mixture of phenylbiguanide hydrochloride with NaOMe in anh. MeOH into a solution of diethyl oxalate in anh. MeOH. The mixture was stirred at room temperature for 2 hours then 4 hours under reflux. For entry 4-2, phenylbiguanide hydrochloride was neutralised and isolated, followed by the addition of phenylbiguanide into diethyl oxalate in a dropwise manner to prevent local concentration of biguanide. Lastly, entry 4-3 was similar to entry 4-2, but reaction occurred at room temperature for six hours. The %yield were 24%, 27% and 8%, respectively, hence the best reaction condition for diethyl oxalate was entry 4-2. When the reaction was conducted at a larger scale, the %yield of **3e** increased to near 40%. In contrast to the moderate yield of **3e**, the %yield of **2e** was significantly lower at 7%. The very low %yield was hypothesised to be due to the incomplete neutralisation of metformin, as well as the

point discussed earlier that the reaction with diethyl oxalate might require dry reaction condition to drive the reaction forward thus increasing %yield. Unfortunately, the synthesis of **2e** has not been repeated because the amount of product obtained was sufficient for characterisation and anticancer activity evaluation.

Table 4. Reactions of phenylbiguanide with diethyl oxalate

Entry	phenylbiguanide (mmol)	Diethyl oxalate (mmol)	Solvent (mL)	Reaction Temp. / Time	Yield (%)
4-1	1	3.3	anh. MeOH (3)	Reflux / 4 h	24%
4-2	1	3.3	anh. MeOH (3)	Reflux / 4 h	27%
4-3	1	3.3	anh. MeOH (5)	r.t. / 6 h	8%

For compound **3f**, it was synthesised *via* neither pathway I nor II and the reaction condition that yielded **2f** was not attempted because the synthesis of **2f** was unexpected and di-triazine by-product could be obtained. Furthermore, from doing multiple repeats on the reaction between phenylbiguanide and diethyl oxalate, only **3e** was synthesised hence a new method to synthesise 1,3,5-triazine with a carboxylic acid substituent was carried out. Hydrolysis of a triazine derivative with similar structure **3e** has been reported and the protocol was followed yielding **3f** with quantitative yield.⁷⁷

1.3. *In vitro* anticancer activities of 1,3,5-triazine derivatives

The anticancer activities of 1,3,5-triazine derivatives were evaluated against two colon cancer cell lines, HCT116 and SW620 using Prestobblue™ as the cell viability reagent. HCT116 and SW620 differs in their isolation location and the malignancy potential which HCT116 is fast growing and SW620 has metastatic potentials.⁹² It was interesting to look into whether different effects or selectivity were to be observed. In this work, cisplatin was chosen as the reference drug and both the %cytotoxicity and IC₅₀ of cisplatin were also measured. The values were in agreement with the reported literature values.⁹³

As the synthesised compounds cannot be dissolved directly into the cell culture medium, they had to first be dissolved in DMSO. However, 100% DMSO is toxic to cells

thus hindering the measurement of the actual performance of the synthesised compounds. In order to select a suitable amount of DMSO to dissolve the triazine with minimum toxicity, the percentage of DMSO was varied between 0-5%. Not only that the %DMSO was varied, but the time to incubate cells was conducted at 24 and 48 hours. The bar graph in Figure 19 shows that the %cell viability decreased with increasing %DMSO. 1% and 3% DMSO resulted in %cell viability at around 87% and 65%, respectively. Furthermore, no changes to the %cell viability was caused with longer incubation time. Since, 1% DMSO resulted in the more stable cell inhibition and this amount of DMSO could dissolve the 1,3,5-triazine derivatives hence 1% DMSO was selected for further experiments. Before cell treatments, stock solutions of the triazine in DMSO had to be prepared then they were diluted by serial dilution with cell culture media.⁹⁴⁻⁹⁶

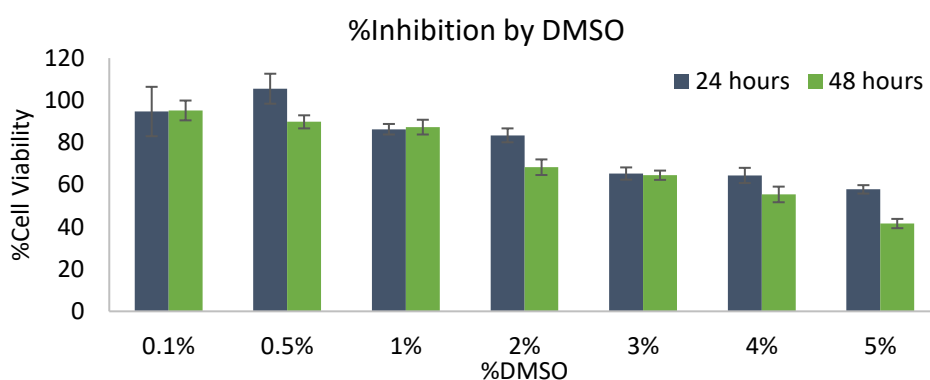


Figure 19. %cell inhibition at various %DMSO in 100 μ L. %inhibition was expressed as the mean values of five replicates \pm SD. The negative control was the cell culture media

All 12 1,3,5-triazine derivatives were preliminary screened for %cytotoxicity at a concentration of 100 μ M. Overall, it was found that metformin and phenylbiguanide were inactive towards both HCT116 and SW620 cell lines at the specified concentration (Data not shown). On the other hand, the synthesised compounds exhibited anticancer activity at varied abilities which some compounds possessed %cytotoxicity comparable to cisplatin. From the data in Table 5, higher number of 1,3,5-triazine derived from phenylbiguanide were more cytotoxic than the metformin-derived ones. This trend

demonstrates that the hydrophobicity of substituent had influences on the anticancer activities. This relationship was also reflected by the two most cytotoxic compounds, **2a** bearing the long alkyl chain with %cytotoxicity of $67.43 \pm 1.82\%$ (SW620) and $96.02 \pm 0.06\%$ (HCT116), and **3d** bearing the aryl substituent with %cytotoxicity of $92.27 \pm 0.04\%$ (SW620) and 87.47 ± 1.54 (HCT116). In contrast, compounds with hydrophilic substituents including **2e/3e** bearing the ester group and **2f/3f** bearing the carboxylic acid group had very low %cytotoxicity in the range of 5-20%. Moreover, it was observed that the synthesised compounds were selective to neither cell lines. From this screening, **2a** was selected for the latter part of this study, to be incorporated into calcium citrate nanoparticles.

Table 5. Anticancer activities of 1,3,5-triazine derivatives in 1% DMSO at 48 hours

	%Cytotoxicity		IC ₅₀ (μM) ^b	
	SW620	HCT116	SW620	HCT116
2a	96.02±0.06	67.43±1.82	59.13±1.46	59.35±1.66
2b	15.86±1.91	19.23±5.94	n.d. ^d	n.d. ^d
2c	53.85±1.40	50.77±1.83	25.25±1.12	26.29±1.07
2d	27.39±4.16	26.52±3.77	n.d. ^d	n.d. ^d
2e	11.41±3.52	7.16±2.11	n.d. ^d	n.d. ^d
2f	5.64±1.51	11.59±4.03	n.d. ^d	n.d. ^d
3a	54.96±1.46	66.56±2.58	54.55±1.09	59.17±1.48
3b	52.60±4.06	54.42±8.48	38.37±1.05	26.92±1.31
3c	56.85±3.18	65.46±1.07	22.80±1.06	20.79±1.07
3d	87.47±1.54	92.27±0.04	54.10±1.05	55.02±1.04
3e	12.14±3.40	5.54±3.65	n.d. ^d	n.d. ^d
3f	15.36±1.15	14.22±2.81	n.d. ^d	n.d. ^d
Cisplatin	62.14±5.05	78.20±0.96	31.67±1.13	19.18±1.06

^a Results expressed in percentage taken as a mean of triplicates ± standard deviation (SD); ^b Results expressed in μmol/L (μM), taken as a mean value of triplicates ± standard deviation (SD); ^c not active at the specified; ^d not determined; The negative control was the cell culture media and the positive control was 2mM H₂O₂

Six 1,3,5-triazine derivatives with %cytotoxicity at 50% or higher were further evaluated for 50% growth-inhibition (IC_{50}) value. The IC_{50} values were calculated from the concentration-response curve (Figure 20) and the values are tabulated in Table 5. Interestingly, the compounds with high %cytotoxicity did not exhibit as great anticancer activities as the compounds with mid-range %cytotoxicity. The most potent anticancer agents were **2c** and **3c** bearing the *o*-hydroxyphenyl substituent. Their IC_{50} for SW620 were $25.25 \pm 1.12 \mu\text{M}$ and $22.80 \pm 1.06 \mu\text{M}$, and HCT116 were $26.29 \pm 1.07 \mu\text{M}$ and $20.79 \pm 1.07 \mu\text{M}$, respectively. These values were comparable to the IC_{50} values of cisplatin at $31.67 \pm 1.13 \mu\text{M}$ (SW620) and $19.18 \pm 1.06 \mu\text{M}$ (HCT116). **3b** exhibited slightly higher IC_{50} values at 26–38 μM , and the activity of **2a**, **3a** and **3d** were two-fold lower than **2c/3c** having IC_{50} in the same range of 50–60 μM . In 2020, Junaid et al. reported the anticancer activity of a series of 6, N^2 -Diaryl-1,3,5-triazine-2,4-diamines and the activity of **3b** against breast cancer cell was also included.^{12,97} They found that an electron donating group at the para or meta position on the phenyl ring (the R_3 position in this work) was required to cause antiproliferative activity. As **3c** has an *o*-hydroxy group attached to the phenyl ring, this could partially be the reason behind its higher anticancer activity than **3b**. However, in order to draw a fully rational relationship between the structure and activity of the synthesised 1,3,5-triazine derivatives, a deeper investigation is needed.

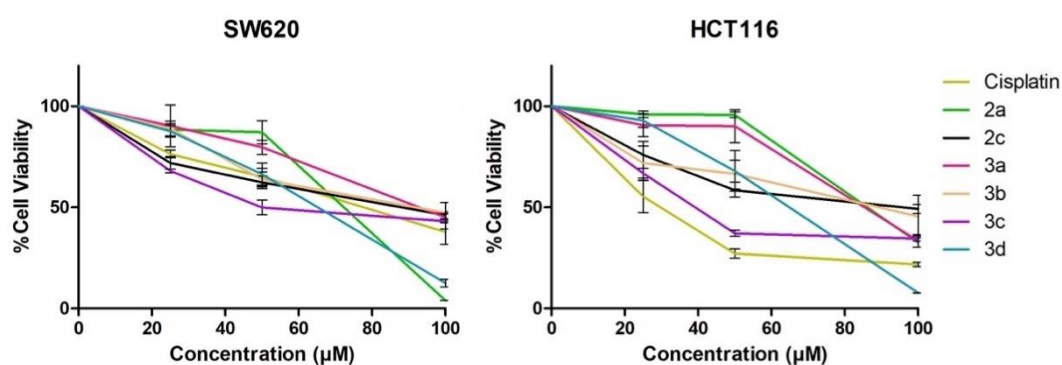


Figure 20. Concentration-response curves of six 1,3,5-triazine derivatives against SW620 and HCT116

In addition to the anticancer activity against HCT116 and SW620, all 12 1,3,5-triazine derivatives were tested against human keratinocyte cell line, HaCat (Figure 21). Unfortunately, the six compounds that displayed high %cytotoxicity towards cancer cells were also cytotoxic towards normal cells. On the other hands, the less cytotoxic compounds were not as toxic towards normal cell. Some compounds led to %cell viability over 100% indicating that there was more cell growth.

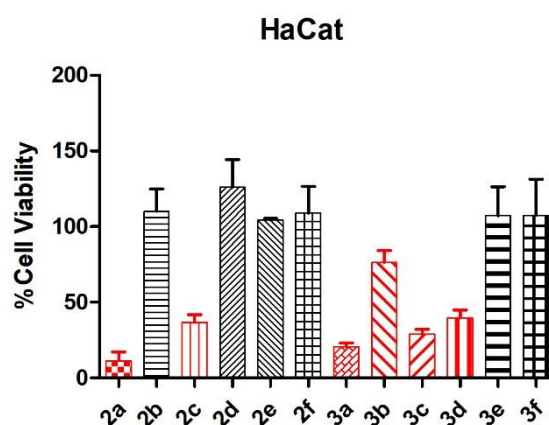


Figure 21. Cell viability study results of twelve 1,3,5-triazine derivatives at 100 μ M against HaCat cell line

2. Synthesis and characterisation of CaCit-triazine NPs

The preparation of CaCit-triazine NPs was studied and optimised. Due to the limited data for the anticancer activity at the time, **2a** was selected to be incorporated into calcium citrate nanoparticles because it exhibited the highest %cytotoxicity. **3d** was also an interesting choice because it also exhibited high %cytotoxicity, but the yield was significantly lower than **2a**.

2.1. Optimisation of reaction condition for CaCit-triazine NPs

The previously reported method that successfully encapsulated FITC in calcium citrate nanoparticles was deemed to be an appropriate preparation of CaCit-triazine NPs,³⁶ but a limitation of **2a** was its hydrophobic nature hence it does not dissolve in water. Therefore, the method was first optimised by using a binary solvent system consisting of

EtOH and DI water. The binary solvent system was reported for the preparation of etoposide encapsulated calcium carbonate particles, and calcium citrate nanosheet was prepared using EtOH and DI water at 1:2 ratio.^{63, 79} Three conditions as shown in Table 6 were attempted and they did not result in a successful drug incorporation. Even though white powder products were obtained from condition 6-1 and 6-2, 1,3,5-triazine was not presented as characterised by elemental analysis. Elemental analysis was chosen as a characterisation method to detect 1,3,5-triazine derivatives because they are the only component containing nitrogen atoms, so the percentage of nitrogen would directly refer to the amount of 1,3,5-triazine present. Unlike the previous two conditions, white powder product with particle size in the nanometre scale was obtained from condition 6-3 (Figure B-1, Appendix B). Traces of 1,3,5-triazine was observed in the FTIR spectrum, but we hypothesised that due to the very small amount of 1,3,5-triazine presented, the TGA curve showed a graph that looked similar to calcium citrate (Figure B-2 and B-3, Appendix B).

Table 6. Unsuccessful methods

Condition	CaCl ₂	Sodium citrate	1,3,5-triazine	Additional solvents	Outcomes
6-1	1.5M water 2 mL	1.95 M water 2 mL	0.02M MeOH 12 mL	-	EA: 27.17% C, 1.97% H, 0.00% N
	0.1M water 10 mL	0.1 M water 10 mL	0.0075M EtOH 20 mL	25 EtOH + 10 water	EA: 26.67% C, 2.90% H, 0.24% N
6-2 ⁷⁹	1.9 M water 2.5 mL	1 M water 1.625 mL	0.02M EtOH+water 5+2 mL	30 EtOH + 18 water	see Appendix B

Since the use of binary solvent system enabled the preparation of calcium citrate nanoparticles, the next optimisation was the source of citrate ion. The methods to synthesise nanosheet,⁶³ microsphere⁶⁶ or nanoparticles³⁶ of calcium citrate is known. The

common reactants among these methodologies are CaCl_2 and sodium citrate. Calcium citrate nanosheet and flowerlike-calcium citrate microspheres were obtained using 3:2 ratio of CaCl_2 to sodium citrate while the most suitable condition for nanoparticles was 1.3:1.^{36, 63, 66} In this work, the ratio of calcium cation to citrate ion was adapted and modified to be 1:1.3 calcium cation to citrate anion. The excess amount of citrate ion could be beneficial by stabilising and preventing particles aggregation. The surface charge would become more negative hence repel each other as seen for the citrate-encapsulated calcium phosphate nanoparticles.³⁴ The significance of Cit:Ca ratio has been studied in hydroxyapatite particles.⁹⁸ Citrate ions had the role to tailor the morphology of particles and it was found that increases in citrate ion resulted in larger size which nanorods were obtained at 3:1 (Cit:Ca) and bundled sheet-like particles at 7:1.

From the experiments, condition 1-1 (**Table 1**) used sodium citrate as the source of citrate ion and it was revealed by IR spectroscopy and SEM that the product was large microparticles of **2a**. The FTIR spectrum shows peaks consistent with the peaks of **2a** and lacked characteristic peaks of calcium citrate noticeably in the O-H stretching region and the C=O stretching (**Figure 22C**). The FTIR spectra of both calcium citrate and **2a** are also presented for comparison purpose (**Figure 22A** and **22B**). For calcium citrate, the band at 3400 cm^{-1} corresponds to the O-H stretching of water molecules in the crystal structure, and $1540\text{--}1430\text{ cm}^{-1}$ are the stretching of C=O bond of carboxylate groups (**Figure 22A**).⁶³ For **2a**, the peaks at $3491, 3293, 3094\text{ cm}^{-1}$ belong to the NH stretching; 2919 and 2849 cm^{-1} are the C-H stretching; the region between 1568 cm^{-1} to 817 cm^{-1} are characteristics to the 1,3,5-triazine ring; and 720 cm^{-1} confirms the existence of long alkyl chain (**Figure 22B**). The reason behind the unsuccessful reaction was hypothesised to be due to the basicity developed from having both **2a** and sodium citrate presented in the solution mixture.⁹⁹ In the case when the solution mixture is alkali and both citrate and hydroxide anions are present, calcium ions would have more affinity towards the hydroxide anions than citrate anion, thus forming precipitates of calcium hydroxide instead of calcium citrate.¹⁰⁰ The less affinity of calcium cation toward citrate anion was also reported in 2008.

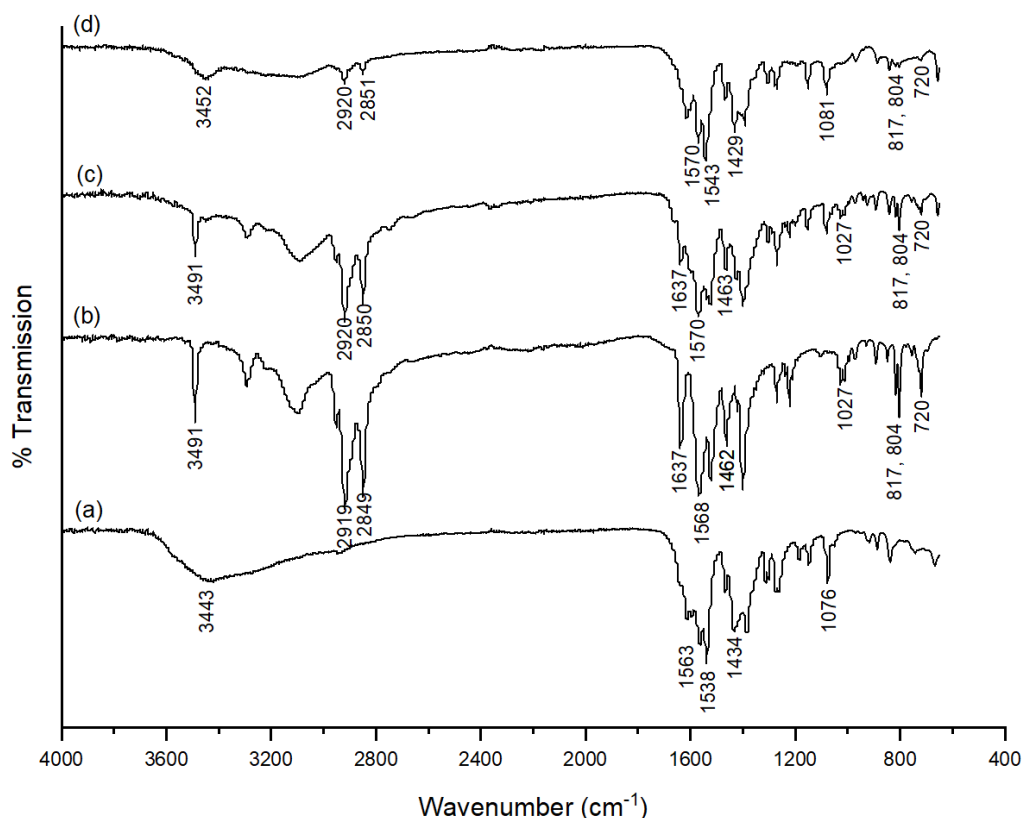


Figure 22. FTIR spectrums of (a) calcium citrate nanoparticles, (b) **2a**, (c) reaction using sodium citrate, and (d) reaction using citric acid with NaOH

From this study, it was found that when sodium citrate was used as the citrate source, the pH of solution required to favour calcium phosphate over calcium citrate formation was only at pH 4.9-6.3.⁹⁹ It could be surmised that the solution mixture of **2a** and sodium citrate was too basic to form the desired calcium citrate-triazine precipitate. Furthermore, sodium citrate has been reported to assist in the dissolution of calcium hydrocarboxylates, such as calcium L-lactate and calcium citrate.¹⁰¹ This finding could support such unsuccessful calcium citrate formation because in the current method, sodium citrate was present in greater amount such that the remaining unreacted sodium citrate could possibly dissolve the already formed calcium citrate precipitate.

Alternatively, calcium citrate could be prepared by using citric acid as the source of citrate ion *via* the acid-base reaction of citric acid and calcium hydroxide or reacting citric acid with calcium carbonate.¹⁰² Citrate anion could be generated from citric acid with

NaOH because citric acid has three pKa values of 2.9, 4.3 and 5.6.^{60, 103} We decided to generate the citrate anion in situ by mixing citric acid with NaOH at the ratio of 1:2 resulting a mixture with pH 6.0 which the citrate anion existed predominantly in the divalent ions form.⁶⁰ Unlike the product from using sodium citrate, citric acid with NaOH resulted in CaCit-triazine precipitate. The FTIR spectrum of product obtained exhibited characteristic peaks of both calcium citrate (3452, 1543, 1429 and 1081 cm^{-1}) and **2a** (2920, 2851, 1570, 817, 804 and 720 cm^{-1}) as shown in Figure 22D. Despite, the ability to prepare 1,3,5-triazine incorporated calcium citrate particles, the morphology and size of the obtained particles were outside of what we expected (Figure 23B). The reaction time could have impacts on the morphology and size of particles as reported by lafisco et al.¹⁰⁴ As the current reaction condition used 16 hours to prepare samples, small aliquots were sampled at different time interval between one to 24 hours in order to study the effect of time.

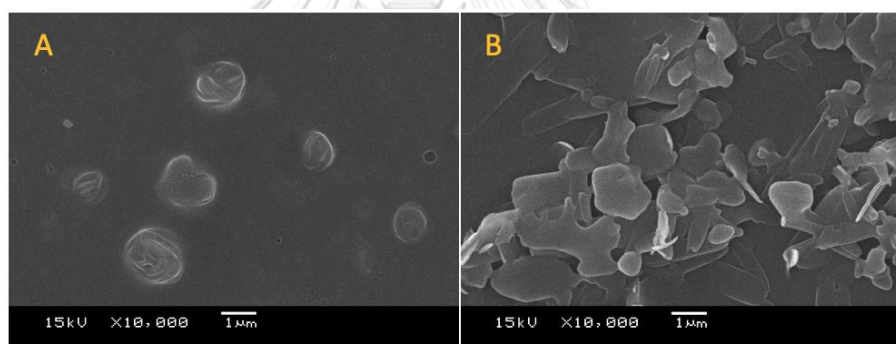


Figure 23. SEM images at x10,000 magnification of product obtained with (A) sodium citrate and (B) citric acid with NaOH

SEM images in Figure 24 demonstrates the morphology and size of particles obtained at different reaction times. It was apparent that longer reaction time resulted in larger particles with aggregation that eventually led to the formation of a large sheet-like morphology. The changes of particles size with respect to time is commonly observed for calcium carbonate and hydroxyapatite particles.^{80, 104, 105} Regardless, nanoparticles were unexpectedly observed at the second (Figure 24ii) and the eighth hour (Figure 24v). In our research groups, we have observed a time-dependent nanoparticle formation of bare CaCit NPs. Calcium citrate was observed as large particles in the initial stage, but the

particles then became smaller eventually forming nanoparticles after some time; then once again grow large into microparticles. A similar behaviour of particle growth was observed for citrate-functionalised nano-apatite which the length decreased by nearly half in the first hour and grew back to its original length after 96 hours, however, this behaviour for drug incorporated calcium citrate particles has not been reported.¹⁰⁶ Even though the nanoparticles formation was possible as observed by the CaCit NPs experiment, the double nanoparticles formation for the CaCit-2a NPs was a very surprising result. The complication on the double nanoparticle formation could occur by having the formation of calcium citrate and the absorption of 2a happening simultaneously. It was suspected that that nanoparticles obtained after 2 hours was the kinetic product that undergo phase

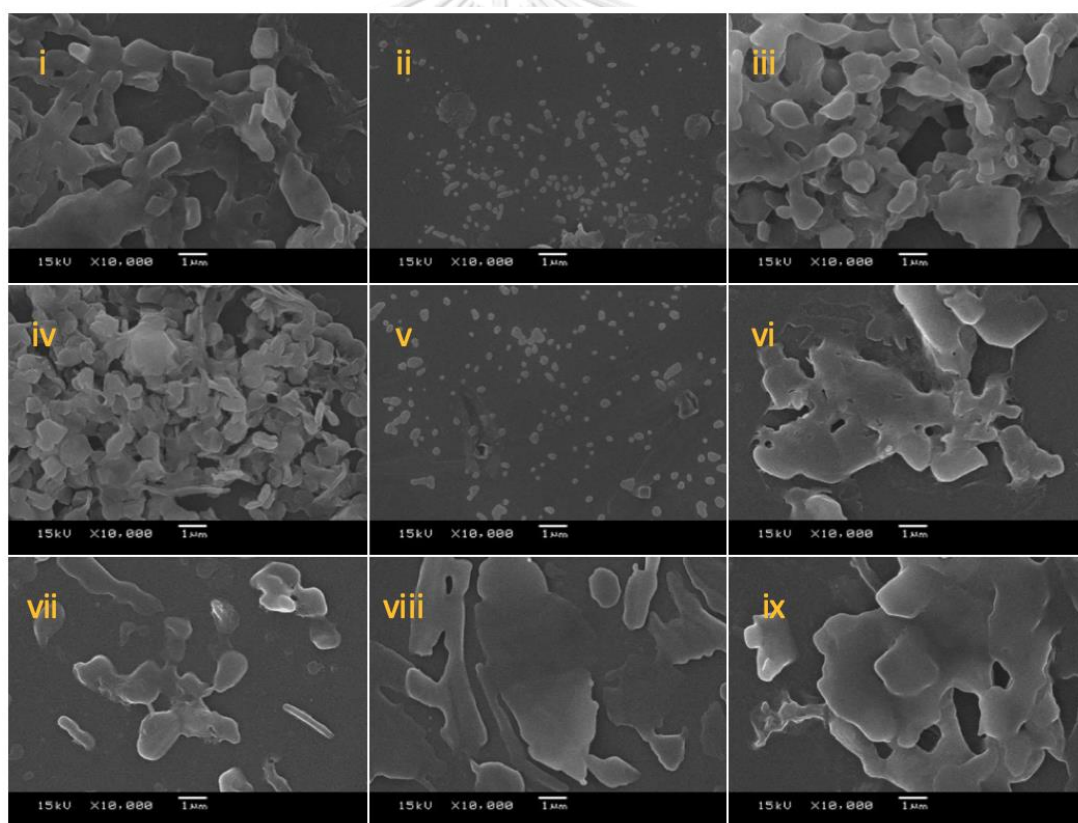


Figure 24. SEM images of Condition C at various synthesis time between 1-24 hours at 10,000x magnification; i (1 hr), ii (2 hrs), iii (4 hrs), iv (6 hrs), v (8 hrs), vi (12 hrs), vii (16 hrs), viii (20 hrs) and ix (24 hrs)

change and reassembled into a more thermodynamically favourable nanoparticles at 8 hours. Substances could undergo changes with respect to time, such as the change of amorphous calcium carbonate into the more stable vaterite then calcite.⁸⁰ Furthermore, the occurrence of nanoparticles at two different time could additionally be due to the EtOH used in the binary solvent system.¹⁰⁷ Ethanol was found to be able to stabilise vaterite phase of calcium carbonate preventing its rapid transformation to calcite.¹⁰⁷ Thus, the nanoparticles formed at two hours did not undergo rapid transformation and its state was maintained allowing the nanoparticles to be observed by SEM.

2.2. Preparation of CaCit-triazine NPs using the optimised method

The optimised method established in the previous section include using EtOH-DI water binary solvent system, citric acid with NaOH as the source of citrate, and reaction time of 8 hours. The method was repeated to verify the feasibility of reaction at the reaction times of 2 (Condition A), 5 (Condition B) and 8 hours (Condition C). White powder products were obtained from all three conditions, so they were characterised by SEM, DLS, IR, EA, and TGA. The size and zeta potential of the products measured by SEM and DLS are tabulated in Table 7. The morphology and size of the particles obtained from all three conditions were consistent with the morphology and size produced from the reaction time optimisation experiment (**Figure 25**). Nanoparticles of condition A was smaller than condition C at around 130 nm and 150 nm, respectively. In contrast, aggregated and plate-like particles with size over 1000 nm was observed for condition B. Particle size was also measured with the dynamic light scattering technique to support the SEM data. Hydrodynamic size of the condition A was found to be slightly higher than condition C at 370 and 300 nm, respectively. The difference between the size determined by SEM and DLS was due to how the size of the nanoparticles was measured in aqueous solvent hence the tendency of nanoparticles to agglomerate in aqueous solvent.¹⁰⁸ The agglomeration could be due to the low negative zeta potentials of the particles. The zeta potentials of the nanoparticles were around -10 mV meaning that the particles might have lower kinetic stability thus not having the ability to repel each other well enough.¹⁰⁹ The effect from the zeta potential could also be reflected in PDI values and the shape of the size distribution

graphs (Figure 26). Despite observing monodispersed systems for both condition A and C, their PDI values were greater than 0.3 thus having potential effects on the use of the nanoparticles *via* intravenous delivery. However, this problem could be overcome by modifying the surface of the nanoparticles with polymer or ligands hence preventing agglomeration by repulsive forces.¹¹⁰ Overall, the size of nanoparticles of both condition A and C satisfied the size requirement for the EPR effect.

Table 7. Characterisation of CaCit-2a NPs by SEM and DLS

Condition	Reaction time (h)	Particle Size by SEM (nm)	Particle size by DLS (nm) [PDI]	Zeta potential (mV)
A	2	134±18.87	369.30±13.44 [0.464]	-8.36
B	5	>1000	n.d. ^a	n.d. ^a
C	8	148±23.69	300.30±12.42 [0.322]	-7.71

^a not determined



Figure 25. SEM of CaCit-triazine at 2, 5 and 8 hours (Condition A-C)

The FTIR spectra of condition A-C confirmed the success of drug incorporation in calcium citrate because both peaks of calcium citrate and **2a** were presented (Figure B-4, Appendix). The extent of drug incorporation was determined by elemental analysis and thermogravimetric analysis. First, the elemental analysis data shown in Table 8 indicated that condition B had the highest %drug loading of 17.8%, followed by condition C (16.3%) and condition A (9.6%). It is noteworthy that despite the similarity of particle size for condition A and C, longer reaction time resulted in a higher %drug loading. Thermogravimetric analysis additionally validated the success of drug incorporation. The TGA curves of calcium citrate nanoparticles, **2a** and particles obtained from condition

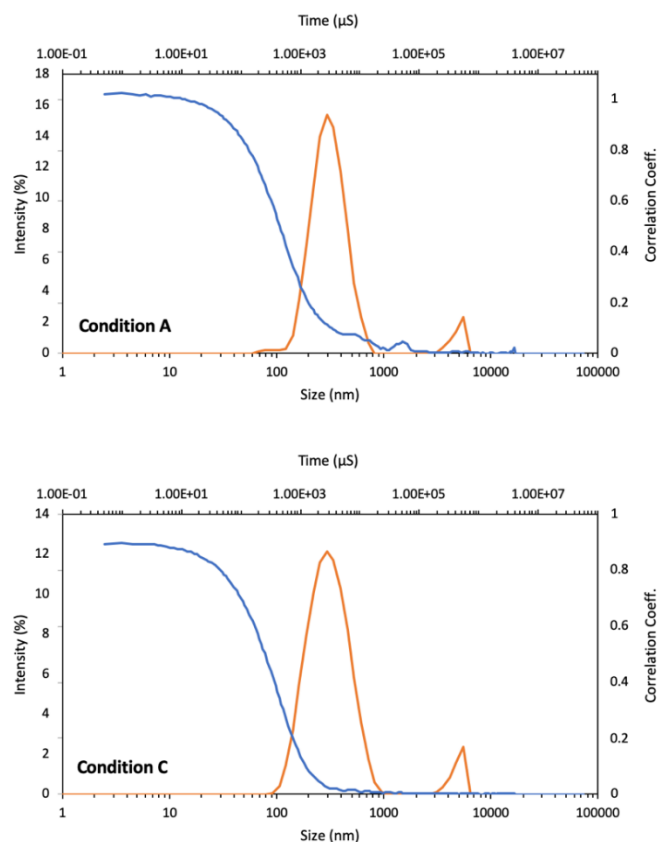


Figure 26. DLS correlograms and size distribution graphs of Condition A and C

A-C are illustrated in Figure 27. The TGA curve of calcium citrate typically has three stages including the loss of water molecules, the decomposition of calcium citrate, and the decomposition of calcium carbonate (Ca_2CO_3).^{63, 66, 111, 112} The first region at around 50-170°C was the loss of surface-adsorbed and water molecules inside the crystal structure of calcium citrate. The second weight loss at temperature between 420-600°C was the decomposition of calcium citrate to Ca_2CO_3 ; and beyond 700°C was the decomposition of Ca_2CO_3 to calcium oxide (CaO). In contrast to calcium citrate, **2a** decomposition was almost a one-step weight loss. The major weight loss started at 200°C and decreased by 84%. Despite the difference in morphologies of the obtained particles, all three TGA curves exhibited a combination of weight loss behaviours of both calcium citrate and **2a**. The first weight loss between 50-150°C indicates the release of water molecules. The second decrease of weight after 200°C was the decomposition of **2a**. The weight loss in this region was used to calculate the %drug loading in the nanoparticles (condition A and

C) which the values agreed with the %drug loading calculated by CHNS analysis method at 13.5% and 15.6%, respectively. The rest of the graph were the same as observed in calcium citrate.

Table 8. Characterisation of CaCit-2a NPs by EA and TGA

Condition	Elemental Analysis			Drug Loading (%)	
	% C	% H	% N	EA	TGA
2a	68.86	11.23	19.59	-	-
A	29.23	3.31	1.88	9.6	13.5
B	33.38	4.13	3.49	17.8	n.d. ^a
C	32.84	3.91	3.19	16.3	15.6

^a not determined

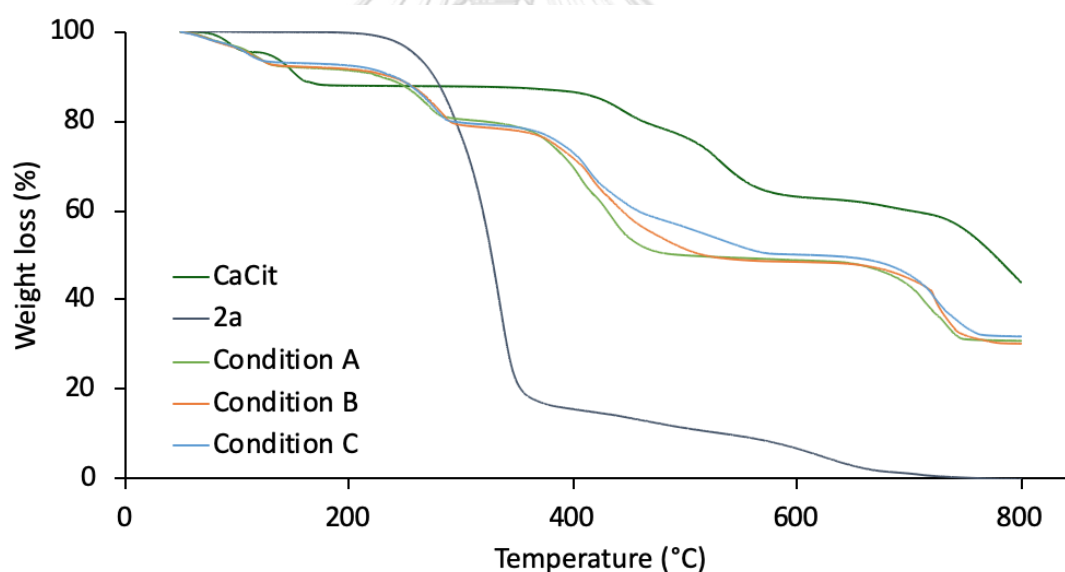


Figure 27. TGA curves of Condition A-C

In sum, the optimised method to prepare CaCit-triazine NPs was identified and the reproducibility of the reaction was verified by repeating condition C. As characterised by FTIR and SEM, the obtained nanoparticles had FTIR similar to condition C and size in the nanometric scale (Figure 28 and Figure B-5 in Appendix).

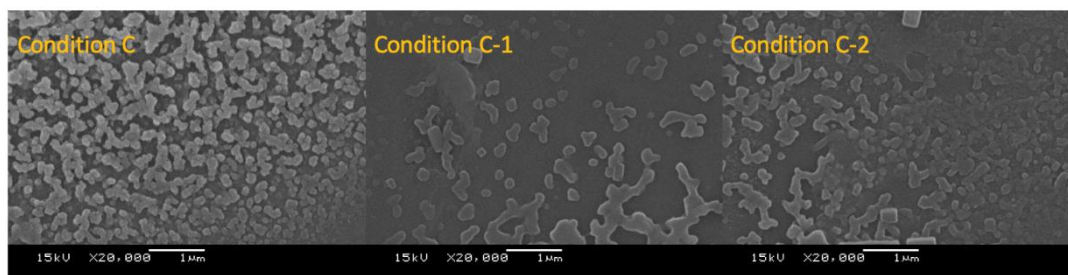


Figure 28. SEM of Repeat A & Repeat B of Condition C

2.3. Calcium citrate nanoparticles (CaCit NPs)

The synthesis of calcium citrate was also carried out in this work. Four conditions were conducted as listed in Table 9. The first condition (condition 9-1) followed the protocol reported by Rimsueb et al.³⁶ The second and third condition used the modified ratio of 1:1.3 $\text{Ca}^{2+}:\text{Cit}^{3-}$, but prepared at different reaction times. The last condition (condition 9-4) used the optimised method without **2a**. Calcium citrate nanoparticles were obtained from three conditions, condition 9-1, 9-3 and 9-4. Overall, the size range of nanoparticles was similar to each other, between 200-300 nm (Figure 29) and their spectra matched the reference calcium citrate produced in bulk in the lab (Figure B-6, Appendix). These results confirm that 8 hours was a suitable time for nanoparticles formation for the 1:1.3 $\text{Ca}^{2+}:\text{Cit}^{3-}$ ratio used in this work.

Table 9. Conditions for the preparation of calcium citrate

Condition	$\text{Ca}^{2+}:\text{Cit}^{3-}$ ratio	Citrate ion source	Solvents	Reaction time (hours)
9-1	1.3:1 [0.13:0.1 M]	sodium citrate	Water 10 mL	16-18
9-2	1:1.3 [0.15:0.195 M]	Sodium citrate	Water 10 mL	16-18
9-3	1:1.3 [0.15:0.195 M]	Sodium citrate	Water 10 mL	8
9-4	1:1.3 [0.15:0.195 M]	Citric acid with NaOH	EtOH/Water	8

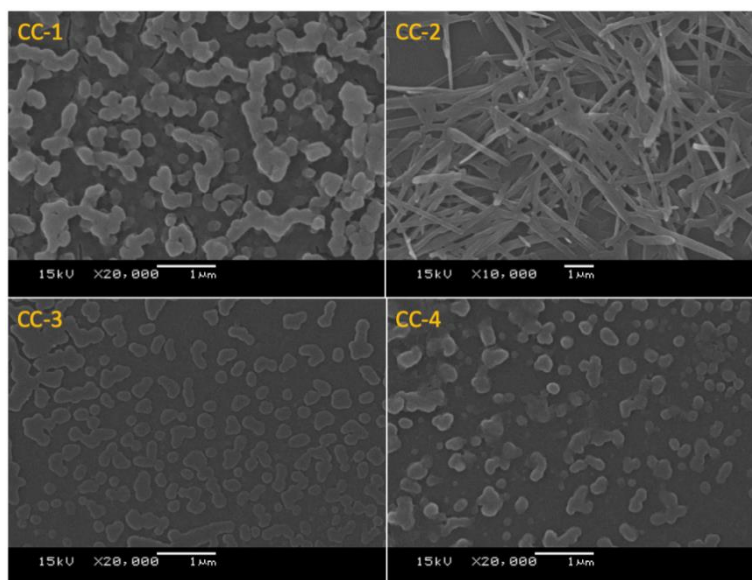


Figure 29. SEM of calcium citrate particles from Condition 9-1 to 9-4

2.4. *In vitro* drug release study

CaCit-triazine NPs produced from the most optimised condition was to be evaluated for anticancer activity, but the observed results were unanticipated. The observed low cytotoxicity of CaCit-2a NPs compared to bare 2a was surmised to be due to two possibilities (data not shown). First, CaCit NPs is expected to be taken into cells by endocytosis and under the acidic condition of lysosome (pH around 4), calcium citrate should dissociate and release the loaded content.¹¹³ However, the zeta potentials of the nanoparticles was found to be close to zero hence the CaCit-2a NPs could have sediment instead of remaining in a suspension state and so the nanoparticles was not taken into cells. In another case, 2a could have not been released from the CaCit-2a NPs. The former possibility was not investigated because cellular uptake has to be observed by a microscope which requires the compound of interest to be fluorescent. Therefore, the release of 2a from CaCit-2a NPs was investigated.

The *in vitro* drug release was performed on the CaCit-2a NPs synthesised from the most optimised condition, condition C. The common method to conduct drug release study especially for water-soluble drug is to use PBS as the release medium.¹¹⁴⁻¹¹⁶ However, this was not applicable for CaCit-2a NPs due to the hydrophobic nature of 2a.

Despite using Tween-80 as the surfactant to help dissolve **2a** in PBS,^{81, 82, 117} it was not dissolvable in PBS. The use of EtOH with PBS has been reported to increase the solubility of compounds, for example, 0.5% Tween-80 and 20% EtOH in PBS as the release medium for curcumin;¹¹⁸ PBS with 10% EtOH for all-trans-retinoic acid and paclitaxel in albumin-bound nanoparticles;¹¹⁹ and PBS:EtOH at 2:1 ratio for the hydrophobic drug C6 in multilayer thin films.¹²⁰ In order to confirm that **2a** is dissolvable in EtOH/PBS, various percentages of EtOH in PBS were experimented. 60% EtOH in PBS could dissolve **2a** completely resulting in a clear colourless solution. For other EtOH contents, there were either not enough EtOH to dissolve **2a** or too much EtOH that dissolved **2a** but not miscible with PBS. In spite of the 60% EtOH in PBS being the suitable release medium, reported literature values for percentage of EtOH in PBS has not exceed 30% hence only 30% EtOH in PBS was used as the release medium. Since the weight of nanoparticles used in this experiment is equivalent to 1 mg of **2a**, 30% EtOH was enough to dissolve **2a**.

Three pH conditions were chosen to compare the drug release performance under different environments. pH 7.4 and 5.0 represent the physiological pH of blood and inside normal tissues and the pH of the tumour environment, respectively.³⁰ Moreover, as the lysosome of cancer cells has pH around 4.5 and calcium citrate was able to dissolve fully under 30%EtOH-PBS solution at pH 3.0, the drug release measurement was extended into pH 3.0.¹²¹ From the cumulative drug release graph, the release of **2a** from CaCit-**2a** NPs was pH-dependent and controlled release behaviour was observed over the 48 hours (Figure 30). In general, higher drug release was observed as the pH of the release medium decreased. This difference in the rate of drug release could be explained by the higher decomposition of calcium citrate carrier under acidic condition. This result was consistent with other drug-loaded calcium carbonate.^{114, 116, 122} After 24 hours, 48.8% and 30.0% of **2a** was released for pH 5.0 and pH 7.4, respectively. A two-fold higher drug release was observed for pH 3.0 at 81.6%. The release of **2a** was sustained for 48 hours with the release of over half of the nanoparticles' loaded content at 63.9% for pH 5.0 and to a lesser extent of 41.9% for pH 7.4. From the graph, we predicted that it would be probable for more **2a** to be release from CaCit-**2a** NPs.

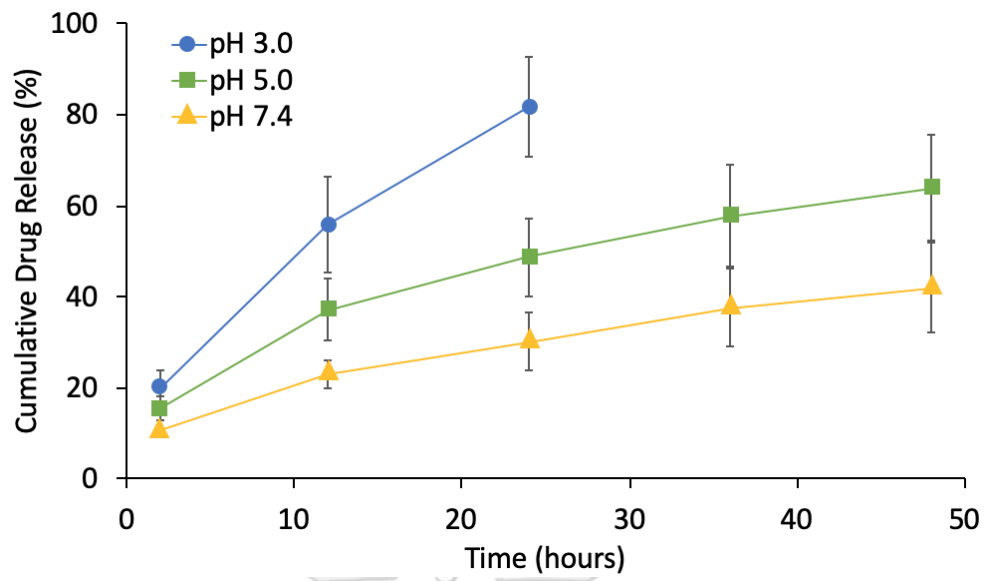


Figure 30. Cumulative drug release (%) graph



CHAPTER IV

CONCLUSION

In conclusion, metformin derived (**2a-2f**) and phenylbiguanide derived (**3a-3f**) 1,3,5-triazine derivatives were synthesised with either synthesis pathway I or II. Preliminary %cytotoxicity screening of the 12 1,3,5-triazine derivatives showed that compound **2a** and **3d** bearing hydrophobic substituents were the two most cytotoxic compounds with comparable activity to cisplatin at %cytotoxicity as high as $96.02 \pm 0.06\%$. However, **2b**, **2e/3e** and **2f/3f** exhibited low %cytotoxicity at around 5-20%. Subsequently, the six selected derivatives – **2a**, **2c** and **3a-3d** – were evaluated for IC_{50} values and the results were in contrast to the %cytotoxicity results. **2c** and **3c** exhibited the lowest IC_{50} values of $25.25 \pm 1.12 \mu\text{M}$ and $22.80 \pm 1.06 \mu\text{M}$ for SW620 cell line, and of $26.29 \pm 1.07 \mu\text{M}$ and $20.79 \pm 1.07 \mu\text{M}$ for HCT116 cell line, respectively. Moreover, the incorporation of **2a** in CaCit NPs was successful by using the optimised preparation method. Under the EtOH-DI water binary solvent system, the use of 1:2 citric acid/NaOH as the citrate source with a reaction time of 8 hours provided the best CaCit-**2a** NPs. The obtained nanoparticles was monodispersed with particle size of around 150 nm and %drug loading up to 16.3%. Furthermore, the *in vitro* drug release study showed that the release of **2a** from CaCit-**2a** NPs was pH-dependent and controlled for 48 hours. From this research, the influence of substituents on the anticancer activity of 1,3,5-triazine derivatives was demonstrated in which this information could assist in the future development of novel anticancer agent containing the 1,3,5-triazine scaffold. In addition, the possibility of using CaCit NPs was verified in which the formulated preparation method could be applicable for other anticancer drugs in the future.

REFERENCES

1. Cancer, I. A. o. R. o. Estimated number of deaths from 2020 to 2040, Both sexes, age [0-85+].
https://gco.iarc.fr/tomorrow/en/dataviz/bars?types=1&single_unit=500000&mode=population (accessed 22 February 2021).
2. Cancer, I. A. o. R. o. All cancers fact sheet.
<https://gco.iarc.fr/today/data/factsheets/cancers/39-All-cancers-fact-sheet.pdf> (accessed 22 February 2021).
3. Das, M.; Mohanty, C.; Sahoo, S. K., Ligand-based targeted therapy for cancer tissue. *Expert Opinion on Drug Delivery* **2009**, *6* (3), 285-304.
4. Banerjee, A.; Pathak, S.; Subramaniam, V. D.; G, D.; Murugesan, R.; Verma, R. S., Strategies for targeted drug delivery in treatment of colon cancer: current trends and future perspectives. *Drug Discovery Today* **2017**, *22* (8), 1224-1232.
5. Marín-Ocampo, L.; Veloza, L. A.; Abonia, R.; Sepúlveda-Arias, J. C., Anti-inflammatory activity of triazine derivatives: A systematic review. *European Journal of Medicinal Chemistry* **2019**, *162*, 435-447.
6. Zhou, C.; Min, J.; Liu, Z.; Young, A.; Deshazer, H.; Gao, T.; Chang, Y.-T.; Kallenbach, N. R., Synthesis and biological evaluation of novel 1,3,5-triazine derivatives as antimicrobial agents. *Bioorganic & Medicinal Chemistry Letters* **2008**, *18* (4), 1308-1311.
7. Melato, S.; Prospero, D.; Coghi, P.; Basilico, N.; Monti, D., A Combinatorial Approach to 2,4,6-Trisubstituted Triazines with Potent Antimalarial Activity: Combining Conventional Synthesis and Microwave-Assistance. *ChemMedChem* **2008**, *3* (6), 873-876.
8. Singla, P.; Luxami, V.; Paul, K., Synthesis and in vitro evaluation of novel triazine analogues as anticancer agents and their interaction studies with bovine serum albumin. *European Journal of Medicinal Chemistry* **2016**, *117*, 59-69.

9. Koh, M.; Lee, J.-C.; Min, C.; Moon, A., A novel metformin derivative, HL010183, inhibits proliferation and invasion of triple-negative breast cancer cells. *Bioorganic & Medicinal Chemistry* **2013**, *21* (8), 2305-2313.
10. Lee, C. R.; Faulds, D., Altretamine. *Drugs* **1995**, *49* (6), 932-953.
11. Mallon, R.; Feldberg, L. R.; Lucas, J.; Chaudhary, I.; Dehnhardt, C.; Santos, E. D.; Chen, Z.; dos Santos, O.; Ayral-Kaloustian, S.; Venkatesan, A.; Hollander, I., Antitumor Efficacy of PKI-587, a Highly Potent Dual PI3K/mTOR Kinase Inhibitor. *Clinical Cancer Research* **2011**, *17* (10), 3193.
12. Junaid, A.; Lim, F. P. L.; Tiekink, E. R. T.; Dolzhenko, A. V., Design, synthesis, and biological evaluation of new 6,N2-diaryl-1,3,5-triazine-2,4-diamines as anticancer agents selectively targeting triple negative breast cancer cells. *RSC Advances* **2020**, *10* (43), 25517-25528.
13. Junaid, A.; Lim, F. P. L.; Tiekink, E. R. T.; Dolzhenko, A. V., New One-Pot Synthesis of 1,3,5-Triazines: Three-Component Condensation, Dimroth Rearrangement, and Dehydrogenative Aromatization. *ACS Combinatorial Science* **2019**, *21* (7), 548-555.
14. Zeng, M.; Wang, T.; Cui, D.-M.; Zhang, C., Ruthenium-catalyzed synthesis of tri-substituted 1,3,5-triazines from alcohols and biguanides. *New Journal of Chemistry* **2016**, *40* (10), 8225-8228.
15. Zeng, M.; Xie, Z. P.; Cui, D.-M.; Zhang, C., Ruthenium-catalyzed synthesis of arylethyl 1,3,5-triazines from arylallyl alcohols and biguanides. *Organic & Biomolecular Chemistry* **2018**, *16* (33), 6140-6145.
16. Xu, Y.; Shen, B.; Liu, L.; Qiao, C., Metal free [4+1] and [5+1] annulation reactions to prepare heterocycles using DMF and its derivatives as one-carbon source. *Tetrahedron Letters* **2020**, *61* (19), 151844.
17. Cao, H.; Liao, S.; Zhong, W.; Xiao, X.; Zhu, J.; Li, W.; Wu, X.; Feng, Y., Synthesis, Characterization, and Biological Evaluations of 1,3,5-Triazine Derivatives of Metformin Cyclization with Berberine and Magnolol in the Presence of Sodium Methylate. *Molecules (Basel, Switzerland)* **2017**, *22* (10), 1752.

18. Makowska, A.; Sączewski, F.; Bednarski, P. J.; Sączewski, J.; Balewski, Ł., Hybrid Molecules Composed of 2,4-Diamino-1,3,5-triazines and 2-Imino-Coumarins and Coumarins. Synthesis and Cytotoxic Properties. *Molecules (Basel, Switzerland)* **2018**, *23* (7), 1616.
19. Pryor, R.; Cabreiro, F., Repurposing metformin: an old drug with new tricks in its binding pockets. *Biochemical Journal* **2015**, *471* (3), 307.
20. DeCensi, A.; Puntoni, M.; Goodwin, P.; Cazzaniga, M.; Gennari, A.; Bonanni, B.; Gandini, S., Metformin and Cancer Risk in Diabetic Patients: A Systematic Review and Meta-analysis. *Cancer Prevention Research* **2010**, *3* (11), 1451.
21. Franciosi, M.; Lucisano, G.; Lapice, E.; Strippoli, G. F. M.; Pellegrini, F.; Nicolucci, A., Metformin therapy and risk of cancer in patients with type 2 diabetes: systematic review. *PloS one* **2013**, *8* (8), e71583-e71583.
22. Chaurasia, S. R.; Dange, R.; Bhanage, B. M., Graphene oxide as a carbo-catalyst for the synthesis of tri-substituted 1,3,5-triazines using biguanides and alcohols. *Catalysis Communications* **2020**, *137*, 105933.
23. Yao, W.; Duan, Z.-C.; Zhang, Y.; Sang, X.; Xia, X.-F.; Wang, D., Iridium Supported on Phosphorus-Doped Porous Organic Polymers: Active and Recyclable Catalyst for Acceptorless Dehydrogenation and Borrowing Hydrogen Reaction. *Advanced Synthesis & Catalysis* **2019**, *361* (24), 5695-5703.
24. Lam, T. G.; Jeong, Y. S.; Kim, S.-A.; Ahn, S.-G., New metformin derivative HL156A prevents oral cancer progression by inhibiting the insulin-like growth factor/AKT/mammalian target of rapamycin pathways. *Cancer science* **2018**, *109* (3), 699-709.
25. Kothayer, H.; Spencer, S. M.; Tripathi, K.; Westwell, A. D.; Palle, K., Synthesis and in vitro anticancer evaluation of some 4,6-diamino-1,3,5-triazine-2-carbohydrazides as Rad6 ubiquitin conjugating enzyme inhibitors. *Bioorganic & Medicinal Chemistry Letters* **2016**, *26* (8), 2030-2034.

26. Sączewski, F.; Bułakowska, A.; Bednarski, P.; Grunert, R., Synthesis, structure and anticancer activity of novel 2,4-diamino-1,3,5-triazine derivatives. *European Journal of Medicinal Chemistry* **2006**, *41* (2), 219-225.
27. McDonald, D. M.; Baluk, P., Significance of Blood Vessel Leakiness in Cancer. *Cancer Research* **2002**, *62* (18), 5381.
28. Hickey, J. W.; Santos, J. L.; Williford, J.-M.; Mao, H.-Q., Control of polymeric nanoparticle size to improve therapeutic delivery. *Journal of Controlled Release* **2015**, *219*, 536-547.
29. Bae, Y. H.; Park, K., Targeted drug delivery to tumors: Myths, reality and possibility. *Journal of Controlled Release* **2011**, *153* (3), 198-205.
30. Estrella, V.; Chen, T.; Lloyd, M.; Wojtkowiak, J.; Cornell, H. H.; Ibrahim-Hashim, A.; Bailey, K.; Balagurunathan, Y.; Rothberg, J. M.; Sloane, B. F.; Johnson, J.; Gatenby, R. A.; Gillies, R. J., Acidity Generated by the Tumor Microenvironment Drives Local Invasion. *Cancer Research* **2013**, *73* (5), 1524.
31. Vito, I.; Vittoria, I., Citrate – new functions for an old metabolite. *Biological Chemistry* **2014**, *395* (4), 387-399.
32. Rodríguez-Ruiz, I.; Delgado-López, J. M.; Durán-Olivencia, M. A.; Iafisco, M.; Tampieri, A.; Colangelo, D.; Prat, M.; Gómez-Morales, J., pH-Responsive Delivery of Doxorubicin from Citrate–Apatite Nanocrystals with Tailored Carbonate Content. *Langmuir* **2013**, *29* (26), 8213-8221.
33. Mehbuba Hossain, S.; Chowdhury, E. H., Citrate- and Succinate-Modified Carbonate Apatite Nanoparticles with Loaded Doxorubicin Exhibit Potent Anticancer Activity against Breast Cancer Cells. *Pharmaceutics* **2018**, *10* (1), 32.
34. Di Mauro, V.; Iafisco, M.; Salvarani, N.; Vacchiano, M.; Carullo, P.; Ramírez-Rodríguez, G. B.; Patricio, T.; Tampieri, A.; Miragoli, M.; Catalucci, D., Bioinspired negatively charged calcium phosphate nanocarriers for cardiac delivery of MicroRNAs. *Nanomedicine* **2016**, *11* (8), 891-906.

35. Oungeun, P.; Rojanathanes, R.; Pinsornsak, P.; Wanichwecharungruang, S., Sustaining Antibiotic Release from a Poly(methyl methacrylate) Bone-Spacer. *ACS Omega* **2019**, *4* (12), 14860-14867.
36. Rimsueb, N.; Cherdchom, S.; Aksornkitti, V.; Khotavivattana, T.; Sereemasapun, A.; Rojanathanes, R., Feeding Cells with a Novel "Trojan" Carrier: Citrate Nanoparticles. *ACS Omega* **2020**, *5* (13), 7418-7423.
37. Bailey, C.; Day, C., Metformin: its botanical background. **2004**, *21* (3), 115-117.
38. Sośnicki, S.; Kapral, M.; Węglarz, L., Molecular targets of metformin antitumor action. *Pharmacological Reports* **2016**, *68* (5), 918-925.
39. Del Barco, S.; Vazquez-Martin, A.; Cufi, S.; Oliveras-Ferraros, C.; Bosch-Barrera, J.; Joven, J.; Martin-Castillo, B.; Menendez, J. A., Metformin: multi-faceted protection against cancer. *Oncotarget* **2011**, *2* (12), 896-917.
40. Graham, G. G.; Punt, J.; Arora, M.; Day, R. O.; Doogue, M. P.; Duong, J.; Furlong, T. J.; Greenfield, J. R.; Greenup, L. C.; Kirkpatrick, C. M.; Ray, J. E.; Timmins, P.; Williams, K. M., Clinical Pharmacokinetics of Metformin. *Clinical Pharmacokinetics* **2011**, *50* (2), 81-98.
41. Ju, K. D.; Kim, H. J.; Tsogbadrakh, B.; Lee, J.; Ryu, H.; Cho, E. J.; Hwang, Y.-H.; Kim, K.; Yang, J.; Ahn, C.; Oh, K.-H., HL156A, a novel AMP-activated protein kinase activator, is protective against peritoneal fibrosis in an in vivo and in vitro model of peritoneal fibrosis. *American Journal of Physiology-Renal Physiology* **2016**, *310* (5), F342-F350.
42. Markowicz-Piasecka, M.; Huttunen, J.; Sikora, J.; Huttunen, K. M., Sulfenamide derivatives can improve transporter-mediated cellular uptake of metformin and induce cytotoxicity in human breast adenocarcinoma cell lines. *Bioorganic Chemistry* **2019**, *87*, 321-334.
43. Łażewska, D.; Więcek, M.; Ner, J.; Kamińska, K.; Kottke, T.; Schwed, J. S.; Zygmunt, M.; Karcz, T.; Olejarz, A.; Kuder, K.; Latacz, G.; Grosicki, M.; Sapa, J.; Karolak-Wojciechowska, J.; Stark, H.; Kieć-Kononowicz, K., Aryl-1,3,5-triazine

- derivatives as histamine H4 receptor ligands. *European Journal of Medicinal Chemistry* **2014**, *83*, 534-546.
44. Sanders, M. A.; Brahehi, G.; Nangia-Makker, P.; Balan, V.; Morelli, M.; Kothayer, H.; Westwell, A. D.; Shekhar, M. P. V., Novel Inhibitors of Rad6 Ubiquitin Conjugating Enzyme: Design, Synthesis, Identification, and Functional Characterization. *Molecular Cancer Therapeutics* **2013**, *12* (4), 373.
45. Kothayer, H.; Elshanawani, A. A.; Abu Kull, M. E.; El-Sabbagh, O. I.; Shekhar, M. P. V.; Brancale, A.; Jones, A. T.; Westwell, A. D., Design, synthesis and in vitro anticancer evaluation of 4,6-diamino-1,3,5-triazine-2-carbohydrazides and -carboxamides. *Bioorganic & Medicinal Chemistry Letters* **2013**, *23* (24), 6886-6889.
46. Sączewski, F.; Bułakowska, A., Synthesis, structure and anticancer activity of novel alkenyl-1,3,5-triazine derivatives. *European Journal of Medicinal Chemistry* **2006**, *41* (5), 611-615.
47. Wang, X.; Yi, Y.; Lv, Q.; Zhang, J.; Wu, K.; Wu, W.; Zhang, W., Novel 1,3,5-triazine derivatives exert potent anti-cervical cancer effects by modulating Bax, Bcl2 and Caspases expression. *Chemical Biology & Drug Design* **2018**, *91* (3), 728-734.
48. Jain, R. K.; Stylianopoulos, T., Delivering nanomedicine to solid tumors. *Nature Reviews Clinical Oncology* **2010**, *7* (11), 653-664.
49. Maleki Dizaj, S.; Barzegar-Jalali, M.; Zarrintan, M. H.; Adibkia, K.; Lotfipour, F., Calcium carbonate nanoparticles as cancer drug delivery system. *Expert Opinion on Drug Delivery* **2015**, *12* (10), 1649-1660.
50. Matsumura, Y.; Maeda, H., A New Concept for Macromolecular Therapeutics in Cancer Chemotherapy: Mechanism of Tumor-tropic Accumulation of Proteins and the Antitumor Agent Smancs. *Cancer Research* **1986**, *46* (12 Part 1), 6387-6392.
51. Tee, J. K.; Yip, L. X.; Tan, E. S.; Santitewagun, S.; Prasath, A.; Ke, P. C.; Ho, H. K.; Leong, D. T., Nanoparticles' interactions with vasculature in diseases. *Chemical Society Reviews* **2019**, *48* (21), 5381-5407.
52. Azzi, S.; Hebda, J.; GAVARD, J., Vascular Permeability and Drug Delivery in Cancers. *Frontiers in Oncology* **2013**, *3* (211).

53. Yuan, F.; Dellian, M.; Fukumura, D.; Leunig, M.; Berk, D. A.; Torchilin, V. P.; Jain, R. K., Vascular Permeability in a Human Tumor Xenograft: Molecular Size Dependence and Cutoff Size. *Cancer Research* **1995**, *55* (17), 3752-3756.
54. Barbé, C.; Bartlett, J.; Kong, L.; Finnie, K.; Lin, H. Q.; Larkin, M.; Calleja, S.; Bush, A.; Calleja, G., Silica Particles: A Novel Drug-Delivery System. *Advanced Materials* **2004**, *16* (21), 1959-1966.
55. Soo Choi, H.; Liu, W.; Misra, P.; Tanaka, E.; Zimmer, J. P.; Itty Ipe, B.; Bawendi, M. G.; Frangioni, J. V., Renal clearance of quantum dots. *Nature Biotechnology* **2007**, *25* (10), 1165-1170.
56. Moghimi, S. M.; Hunter, A. C.; Murray, J. C., Long-circulating and target-specific nanoparticles: theory to practice. *Pharmacol Rev* **2001**, *53* (2), 283-318.
57. Rippe, B.; Rosengren, B. I.; Carlsson, O.; Venturoli, D., Transendothelial Transport: The Vesicle Controversy. *Journal of Vascular Research* **2002**, *39* (5), 375-390.
58. Abedini, F.; Ebrahimi, M.; Roozbehani, A. H.; Domb, A. J.; Hosseinkhani, H., Overview on natural hydrophilic polysaccharide polymers in drug delivery. *Polymers for Advanced Technologies* **2018**, *29* (10), 2564-2573.
59. Alaqad, K.; A Saleh, T., *Gold and Silver Nanoparticles: Synthesis Methods, Characterization Routes and Applications towards Drugs*. 2016; Vol. 6.
60. Ma, C.; Gerhard, E.; Lu, D.; Yang, J., Citrate chemistry and biology for biomaterials design. *Biomaterials* **2018**, *178*, 383-400.
61. Mycielska, M. E.; Patel, A.; Rizaner, N.; Mazurek, M. P.; Keun, H.; Patel, A.; Ganapathy, V.; Djamgoz, M. B. A., Citrate transport and metabolism in mammalian cells. *BioEssays* **2009**, *31* (1), 10-20.
62. Huang, L.; Wang, C.; Xu, H.; Peng, G., Targeting citrate as a novel therapeutic strategy in cancer treatment. *Biochimica et Biophysica Acta (BBA) - Reviews on Cancer* **2020**, *1873* (1), 188332.
63. Li, J.; Liu, Y.; Gao, Y.; Zhong, L.; Zou, Q.; Lai, X., Preparation and properties of calcium citrate nanosheets for bone graft substitute. *Bioengineered* **2016**, *7* (5), 376-381.

64. Huang, S.; Chen, J. C.; Hsu, C. W.; Chang, W. H., Effects of nano calcium carbonate and nano calcium citrate on toxicity in ICR mice and on bone mineral density in an ovariectomized mice model. *Nanotechnology* **2009**, *20* (37), 375102.
65. Herdtweck, E.; Kornprobst, T.; Sieber, R.; Straver, L.; Plank, J., Crystal Structure, Synthesis, and Properties of tri-Calcium di-Citrate tetra-Hydrate $[Ca_3(C_6H_5O_7)_2(H_2O)_2] \cdot 2H_2O$. *Zeitschrift für anorganische und allgemeine Chemie* **2011**, *637* (6), 655-659.
66. Li, J. F.; Gao, Y.; Zhong, L. Z.; Liu, Y. Q.; Liu, H. Q.; Zou, Q.; Lai, X. F., Facile Self-Assembly Synthesis of Hierarchical 3D Flowerlike Calcium Citrate Microspheres. *Journal of Nano Research* **2017**, *45*, 185-192.
67. Erfanian, A.; Mirhosseini, H.; Rasti, B.; Hair-Bejo, M.; Mustafa, S. B.; Manap, M. Y. A., Absorption and Bioavailability of Nano-Size Reduced Calcium Citrate Fortified Milk Powder in Ovariectomized and Ovariectomized-Osteoporosis Rats. *Journal of Agricultural and Food Chemistry* **2015**, *63* (24), 5795-5804.
68. Hanzlik, R. P.; Fowler, S. C.; Fisher, D. H., Relative Bioavailability of Calcium from Calcium Formate, Calcium Citrate, and Calcium Carbonate. *Journal of Pharmacology and Experimental Therapeutics* **2005**, *313* (3), 1217.
69. Tondapu, P.; Provost, D.; Adams-Huet, B.; Sims, T.; Chang, C.; Sakhaee, K., Comparison of the Absorption of Calcium Carbonate and Calcium Citrate after Roux-en-Y Gastric Bypass. *Obesity Surgery* **2009**, *19* (9), 1256-1261.
70. Zhang, W.; Wang, W.; Chen, Q.-Y.; Lin, Z.-Q.; Cheng, S.-W.; Kou, D.-Q.; Ying, X.-Z.; Shen, Y.; Cheng, X.-J.; Nie, P.-F.; Li, X.-C.; Rompis, F. A.; Huang, H.; Zhang, H.; Mu, Z.-L.; Peng, L., Effect of calcium citrate on bone integration in a rabbit femur defect model. *Asian Pacific Journal of Tropical Medicine* **2012**, *5* (4), 310-314.
71. Kothayer, H.; Morelli, M.; Braheimi, G.; Elshanawani, A. A.; Abu Kull, M. E.; El-Sabbagh, O. I.; Shekhar, M. P. V.; Westwell, A. D., Optimised synthesis of diamino-triazinylmethyl benzoates as inhibitors of Rad6B ubiquitin conjugating enzyme. *Tetrahedron Letters* **2014**, *55* (51), 7015-7018.

72. Mayer, S.; Daigle, D. M.; Brown, E. D.; Khatri, J.; Organ, M. G., An Expedient and Facile One-Step Synthesis of a Biguanide Library by Microwave Irradiation Coupled with Simple Product Filtration. Inhibitors of Dihydrofolate Reductase. *Journal of Combinatorial Chemistry* **2004**, *6* (5), 776-782.
73. LeBel, O.; Maris, T.; Duval, H.; Wuest, J. D., A practical guide to arylbiguanides — Synthesis and structural characterization. *Canadian Journal of Chemistry* **2005**, *83* (6-7), 615-625.
74. Liu, C., Synthesis of the derivatives of 2-Amino-4-dimethylamino-1,3,5-triazine. *Journal of Guangdong College of Pharmacy* **2005**, Vol. 21 No. 2.
75. Shapiro, S. L.; Parrino, V. A.; Freedman, L., Guanamines. VIII. 6-(Substituted Phenyl)guanamines. *The Journal of Organic Chemistry* **1961**, *26* (9), 3331-3334.
76. Liu, C.; Lin, J.; Leftheris, K., A novel one-pot synthesis of N,6-disubstituted 1,3,5-triazine-4,6-diamines from isothiocyanates and amidines. *Tetrahedron Letters* **2007**, *48* (3), 435-437.
77. Lebel, O.; Perron, M.-È.; Maris, T.; Zalzal, S. F.; Nanci, A.; Wuest, J. D., A New Class of Selective Low-Molecular-Weight Gelators Based on Salts of Diaminotriazinecarboxylic Acids. *Chemistry of Materials* **2006**, *18* (16), 3616-3626.
78. Xu, M.; McCanna, D. J.; Sivak, J. G., Use of the viability reagent PrestoBlue in comparison with alamarBlue and MTT to assess the viability of human corneal epithelial cells. *Journal of Pharmacological and Toxicological Methods* **2015**, *71*, 1-7.
79. Peng, H.; Li, K.; Wang, T.; Wang, J.; Wang, J.; Zhu, R.; Sun, D.; Wang, S., Preparation of hierarchical mesoporous CaCO₃ by a facile binary solvent approach as anticancer drug carrier for etoposide. *Nanoscale Research Letters* **2013**, *8* (1), 321.
80. Xiao, H.; Hu, C.; Chen, C.; Tao, C.; Wu, Y.; Jiang, J., The advantage of alcohol–calcium method on the formation and the stability of vaterite against ethanol–water binary solvent method. *Journal of Materials Research* **2020**, *35* (3), 289-298.

81. Hardiansyah, A.; Yang, M.-C.; Liu, T.-Y.; Kuo, C.-Y.; Huang, L.-Y.; Chan, T.-Y., Hydrophobic Drug-Loaded PEGylated Magnetic Liposomes for Drug-Controlled Release. *Nanoscale Research Letters* **2017**, *12* (1), 355.
82. Wu, J.-L.; Wang, C.-Q.; Zhuo, R.-X.; Cheng, S.-X., Multi-drug delivery system based on alginate/calcium carbonate hybrid nanoparticles for combination chemotherapy. *Colloids and Surfaces B: Biointerfaces* **2014**, *123*, 498-505.
83. Chhikara, B. S.; St. Jean, N.; Mandal, D.; Kumar, A.; Parang, K., Fatty acyl amide derivatives of doxorubicin: Synthesis and in vitro anticancer activities. *European Journal of Medicinal Chemistry* **2011**, *46* (6), 2037-2042.
84. Pathi, S.; Jutooru, I.; Chadalapaka, G.; Nair, V.; Lee, S.-O.; Safe, S., Aspirin Inhibits Colon Cancer Cell and Tumor Growth and Downregulates Specificity Protein (Sp) Transcription Factors. *PLOS ONE* **2012**, *7* (10), e48208.
85. Xu, Q.-B.; Chen, X.-F.; Feng, J.; Miao, J.-F.; Liu, J.; Liu, F.-T.; Niu, B.-X.; Cai, J.-Y.; Huang, C.; Zhang, Y.; Ling, Y., Design, synthesis and biological evaluation of hybrids of β -carboline and salicylic acid as potential anticancer and apoptosis inducing agents. *Scientific Reports* **2016**, *6* (1), 36238.
86. Natella, F.; Nardini, M.; Di Felice, M.; Scaccini, C., Benzoic and Cinnamic Acid Derivatives as Antioxidants: Structure–Activity Relation. *Journal of Agricultural and Food Chemistry* **1999**, *47* (4), 1453-1459.
87. Chavarria, D.; Silva, T.; Martins, D.; Bravo, J.; Summavielle, T.; Garrido, J.; Borges, F., Exploring cinnamic acid scaffold: development of promising neuroprotective lipophilic antioxidants. *MedChemComm* **2015**, *6* (6), 1043-1053.
88. Silva, R. H. N.; Andrade, A. C. M.; Nóbrega, D. F.; Castro, R. D. d.; Pessôa, H. L. F.; Rani, N.; de Sousa, D. P., Antimicrobial Activity of 4-Chlorocinnamic Acid Derivatives. *BioMed Research International* **2019**, *2019*, 3941242.
89. Narasimhan, B.; Belsare, D.; Pharande, D.; Mourya, V.; Dhake, A., Esters, amides and substituted derivatives of cinnamic acid: synthesis, antimicrobial activity and QSAR investigations. *European Journal of Medicinal Chemistry* **2004**, *39* (10), 827-834.

90. Ismail, I. A.; Kang, H. S.; Lee, H. J.; Kwon, B. M.; Hong, S. H., 2'-Benzoyloxycinnamaldehyde-mediated DJ-1 upregulation protects MCF-7 cells from mitochondrial damage. *Biol Pharm Bull* **2012**, *35* (6), 895-902.
91. Menezes, J. C. J. M. D. S.; Edraki, N.; Kamat, S. P.; Khoshneviszadeh, M.; Kayani, Z.; Mirzaei, H. H.; Miri, R.; Erfani, N.; Nejati, M.; Cavaleiro, J. A. S.; Silva, T.; Saso, L.; Borges, F.; Firuzi, O., Long Chain Alkyl Esters of Hydroxycinnamic Acids as Promising Anticancer Agents: Selective Induction of Apoptosis in Cancer Cells. *Journal of Agricultural and Food Chemistry* **2017**, *65* (33), 7228-7239.
92. Baj-Krzyworzeka, M.; Mytar, B.; Szatanek, R.; Surmiak, M.; Węglarczyk, K.; Baran, J.; Siedlar, M., Colorectal cancer-derived microvesicles modulate differentiation of human monocytes to macrophages. *Journal of Translational Medicine* **2016**, *14* (1), 36.
93. Zhou, J.; Li, P.; Xue, X.; He, S.; Kuang, Y.; Zhao, H.; Chen, S.; Zhi, Q.; Guo, X., Salinomycin induces apoptosis in cisplatin-resistant colorectal cancer cells by accumulation of reactive oxygen species. *Toxicology Letters* **2013**, *222* (2), 139-145.
94. Moreno, L. M.; Quiroga, J.; Abonia, R.; Ramírez-Prada, J.; Insuasty, B., Synthesis of New 1,3,5-Triazine-Based 2-Pyrazolines as Potential Anticancer Agents. *Molecules (Basel, Switzerland)* **2018**, *23* (8), 1956.
95. Srivastava, J. K.; Pillai, G. G.; Bhat, H. R.; Verma, A.; Singh, U. P., Design and discovery of novel monastrol-1,3,5-triazines as potent anti-breast cancer agent via attenuating Epidermal Growth Factor Receptor tyrosine kinase. *Scientific Reports* **2017**, *7* (1), 5851.
96. Ng, H.-L.; Ma, X.; Chew, E.-H.; Chui, W.-K., Design, Synthesis, and Biological Evaluation of Coupled Bioactive Scaffolds as Potential Anticancer Agents for Dual Targeting of Dihydrofolate Reductase and Thioredoxin Reductase. *Journal of Medicinal Chemistry* **2017**, *60* (5), 1734-1745.

97. Junaid, A.; Lim, F. P. L.; Chuah, L. H.; Dolzhenko, A. V., 6,N2-Diaryl-1,3,5-triazine-2,4-diamines: synthesis, antiproliferative activity and 3D-QSAR modeling. *RSC Advances* **2020**, *10* (21), 12135-12144.
98. Santos, C.; Almeida, M. M.; Costa, M. E., Morphological Evolution of Hydroxyapatite Particles in the Presence of Different Citrate:Calcium Ratios. *Crystal Growth & Design* **2015**, *15* (9), 4417-4426.
99. Garcia, A. C.; Vavrusova, M.; Skibsted, L. H., Supersaturation of calcium citrate as a mechanism behind enhanced availability of calcium phosphates by presence of citrate. *Food Research International* **2018**, *107*, 195-205.
100. Um, N.; Hirato, T., Precipitation behavior of $\text{Ca}(\text{OH})_2$, $\text{Mg}(\text{OH})_2$, and $\text{Mn}(\text{OH})_2$ from CaCl_2 , MgCl_2 , and MnCl_2 in $\text{NaOH-H}_2\text{O}$ solutions and study of lithium recovery from seawater via two-stage precipitation process. *Hydrometallurgy* **2014**, *146*, 142-148.
101. Vavrusova, M.; Garcia, A. C.; Danielsen, B. P.; Skibsted, L. H., Spontaneous supersaturation of calcium citrate from simultaneous isothermal dissolution of sodium citrate and sparingly soluble calcium hydroxycarboxylates in water. *RSC Advances* **2017**, *7* (6), 3078-3088.
102. Al-Khaldi, M. H.; Nasr-El-Din, H. A.; Mehta, S.; Al-Aamri, A. D., Reaction of citric acid with calcite. *Chemical Engineering Science* **2007**, *62* (21), 5880-5896.
103. Krukowski, S.; Karasiewicz, M.; Kolodziejcki, W., Convenient UV-spectrophotometric determination of citrates in aqueous solutions with applications in the pharmaceutical analysis of oral electrolyte formulations. *Journal of Food and Drug Analysis* **2017**, *25* (3), 717-722.
104. Iafisco, M.; Ramírez-Rodríguez, G. B.; Sakhno, Y.; Tampieri, A.; Martra, G.; Gómez-Morales, J.; Delgado-López, J. M., The growth mechanism of apatite nanocrystals assisted by citrate: relevance to bone biomineralization. *CrystEngComm* **2015**, *17* (3), 507-511.
105. YAO, C.; XIE, A.; SHEN, Y.; ZHU, J.; LI, T., Green synthesis of calcium carbonate with unusual morphologies in the presence of fruit extracts. *Journal of the Chilean Chemical Society* **2013**, *58*, 2235-2238.

106. Delgado-López, J. M.; Lafisco, M.; Rodríguez, I.; Tampieri, A.; Prat, M.; Gómez-Morales, J., Crystallization of bioinspired citrate-functionalized nanoapatite with tailored carbonate content. *Acta Biomaterialia* **2012**, *8* (9), 3491-3499.
107. Sand, K. K.; Rodríguez-Blanco, J. D.; Makovicky, E.; Benning, L. G.; Stipp, S. L. S., Crystallization of CaCO₃ in Water-Alcohol Mixtures: Spherulitic Growth, Polymorph Stabilization, and Morphology Change. *Crystal Growth & Design* **2012**, *12* (2), 842-853.
108. Hebeish, A.; El-Rafie, M. H.; El-Sheikh, M. A.; El-Naggar, M. E., Ultra-Fine Characteristics of Starch Nanoparticles Prepared Using Native Starch With and Without Surfactant. *Journal of Inorganic and Organometallic Polymers and Materials* **2014**, *24* (3), 515-524.
109. Shao, X.-R.; Wei, X.-Q.; Song, X.; Hao, L.-Y.; Cai, X.-X.; Zhang, Z.-R.; Peng, Q.; Lin, Y.-F., Independent effect of polymeric nanoparticle zeta potential/surface charge, on their cytotoxicity and affinity to cells. *Cell Proliferation* **2015**, *48* (4), 465-474.
110. Sperling, R. A.; Parak, W. J., Surface modification, functionalization and bioconjugation of colloidal inorganic nanoparticles. *Philosophical Transactions of the Royal Society A: Mathematical, Physical and Engineering Sciences* **2010**, *368* (1915), 1333-1383.
111. Zhang, H.; Zeng, X.; Gao, Y.; Shi, F.; Zhang, P.; Chen, J.-F., A Facile Method To Prepare Superhydrophobic Coatings by Calcium Carbonate. *Industrial & Engineering Chemistry Research* **2011**, *50* (6), 3089-3094.
112. Mansour, S. A. A., Thermal decomposition of calcium citrate tetrahydrate. *Thermochimica Acta* **1994**, *233* (2), 243-256.
113. Casey, J. R.; Grinstein, S.; Orlowski, J., Sensors and regulators of intracellular pH. *Nature Reviews Molecular Cell Biology* **2010**, *11* (1), 50-61.
114. Yang, T.; Wan, Z.; Liu, Z.; Li, H.; Wang, H.; Lu, N.; Chen, Z.; Mei, X.; Ren, X., In situ mineralization of anticancer drug into calcium carbonate monodisperse

- nanospheres and their pH-responsive release property. *Materials Science and Engineering: C* **2016**, *63*, 384-392.
115. Vergaro, V.; Papadia, P.; Leporatti, S.; De Pascali, S. A.; Fanizzi, F. P.; Ciccarella, G., Synthesis of biocompatible polymeric nano-capsules based on calcium carbonate: A potential cisplatin delivery system. *Journal of Inorganic Biochemistry* **2015**, *153*, 284-292.
116. Guo, Y.; Li, H.; Shi, W.; Zhang, J.; Feng, J.; Yang, X.; Wang, K.; Zhang, H.; Yang, L., Targeted delivery and pH-responsive release of doxorubicin to cancer cells using calcium carbonate/hyaluronate/glutamate mesoporous hollow spheres. *Journal of Colloid and Interface Science* **2017**, *502*, 59-66.
117. Xie, J.; Wang, C.-H., Self-Assembled Biodegradable Nanoparticles Developed by Direct Dialysis for the Delivery of Paclitaxel. *Pharmaceutical Research* **2005**, *22* (12), 2079-2090.
118. Chen, Y.; Wu, Q.; Zhang, Z.; Yuan, L.; Liu, X.; Zhou, L., Preparation of curcumin-loaded liposomes and evaluation of their skin permeation and pharmacodynamics. *Molecules (Basel, Switzerland)* **2012**, *17* (5), 5972-5987.
119. Huang, H.; Shi, H.; Liu, J.; Min, Y.; Wang, Y.; Wang, A. Z.; Wang, J.; Liu, Y., Co-delivery of all-trans-retinoic acid enhances the anti-metastasis effect of albumin-bound paclitaxel nanoparticles. *Chemical Communications* **2017**, *53* (1), 212-215.
120. Han, U.; Seo, Y.; Hong, J., Effect of pH on the structure and drug release profiles of layer-by-layer assembled films containing polyelectrolyte, micelles, and graphene oxide. *Scientific Reports* **2016**, *6* (1), 24158.
121. Zhou, C.; Chen, T.; Wu, C.; Zhu, G.; Qiu, L.; Cui, C.; Hou, W.; Tan, W., Aptamer CaCO₃ Nanostructures: A Facile, pH-Responsive, Specific Platform for Targeted Anticancer Theranostics. *Chemistry – An Asian Journal* **2015**, *10* (1), 166-171.
122. Wang, C.; Liu, X.; Chen, S.; Hu, F.; Sun, J.; Yuan, H., Facile preparation of phospholipid–amorphous calcium carbonate hybrid nanoparticles: toward controllable burst drug release and enhanced tumor penetration. *Chemical Communications* **2018**, *54* (93), 13080-13083.

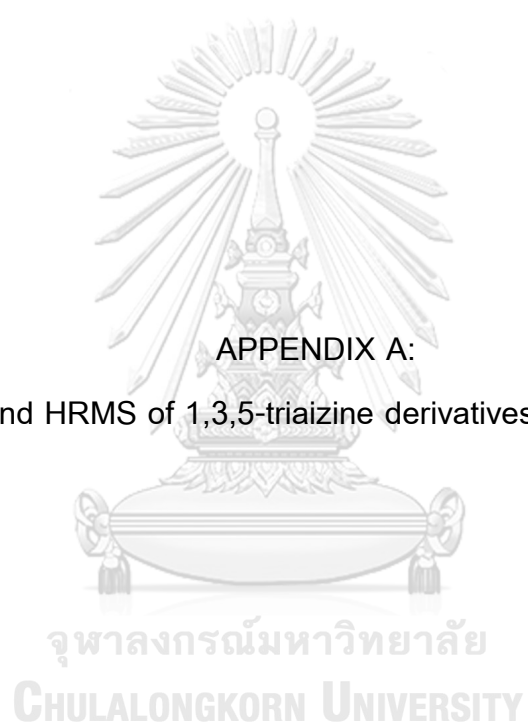


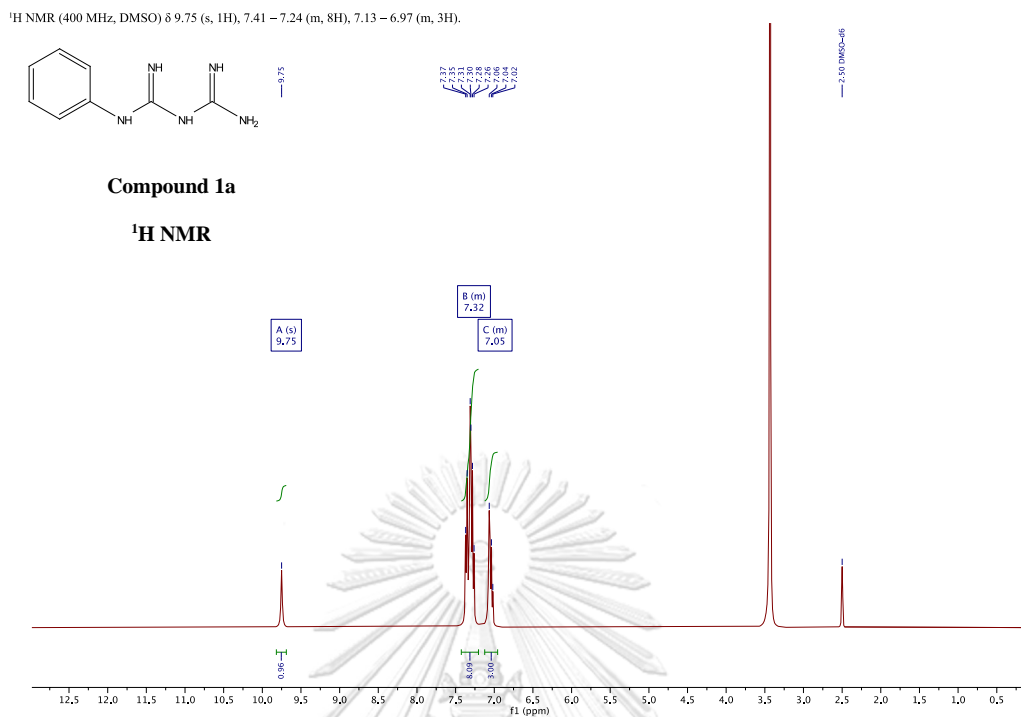
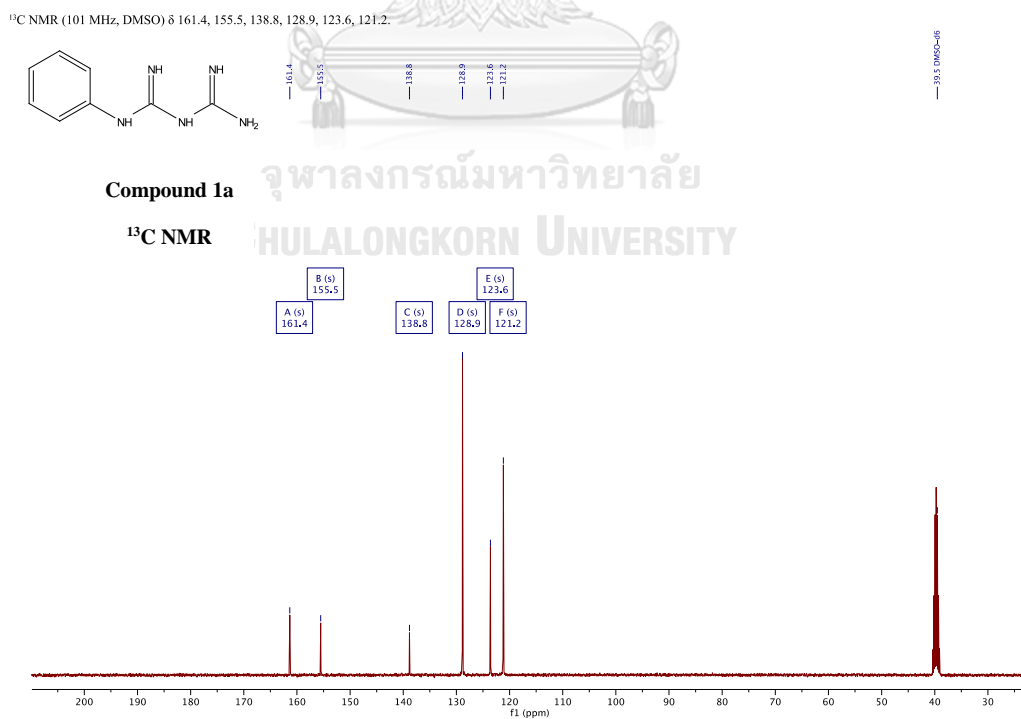
จุฬาลงกรณ์มหาวิทยาลัย
CHULALONGKORN UNIVERSITY

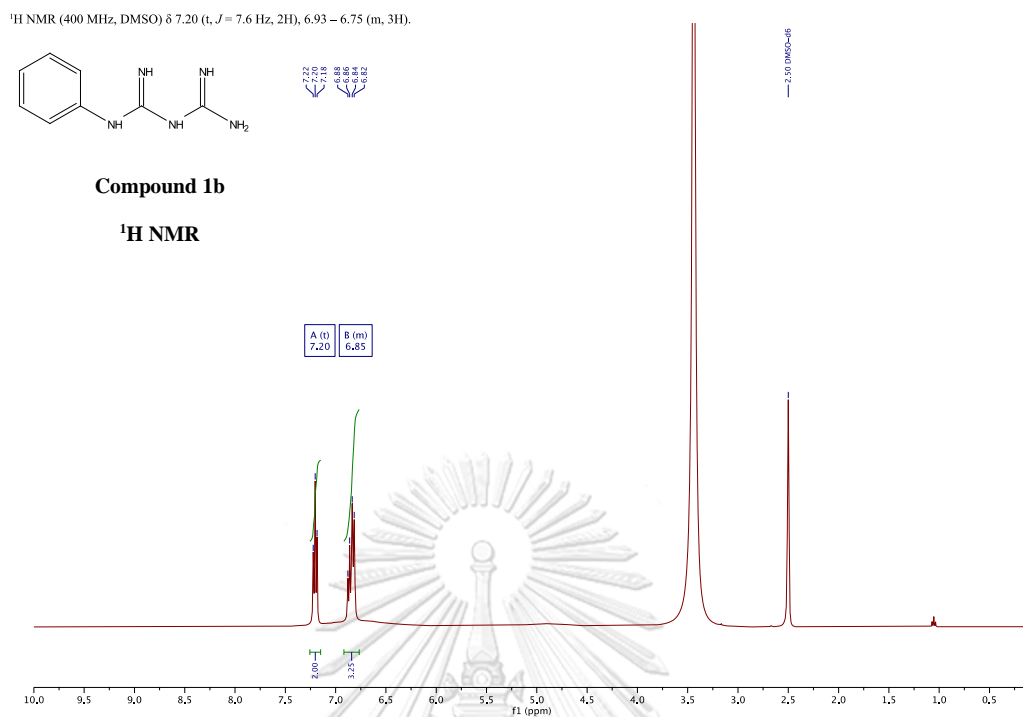
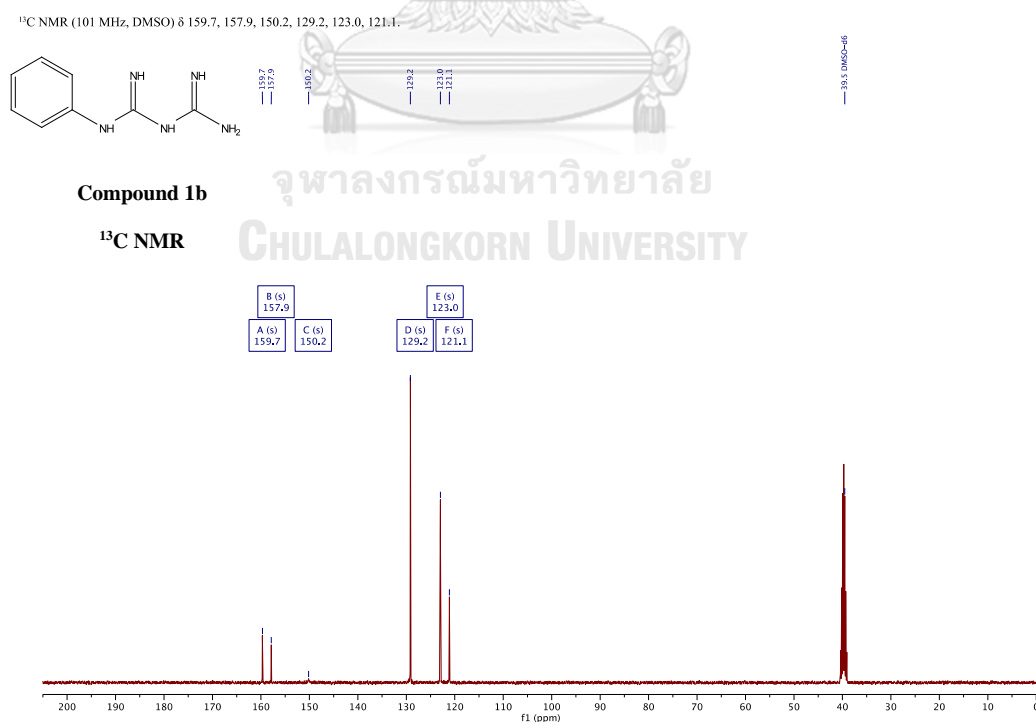


APPENDICES

จุฬาลงกรณ์มหาวิทยาลัย
CHULALONGKORN UNIVERSITY



Figure A-1. ¹H-NMR of Phenylbiguanide hydrochloride (1a)Figure A-2. ¹³C-NMR of Phenylbiguanide hydrochloride (1a)

Figure A-3. ¹H-NMR of Phenylbiguanide (1b)Figure A-4. ¹³C-NMR of Phenylbiguanide (1b)

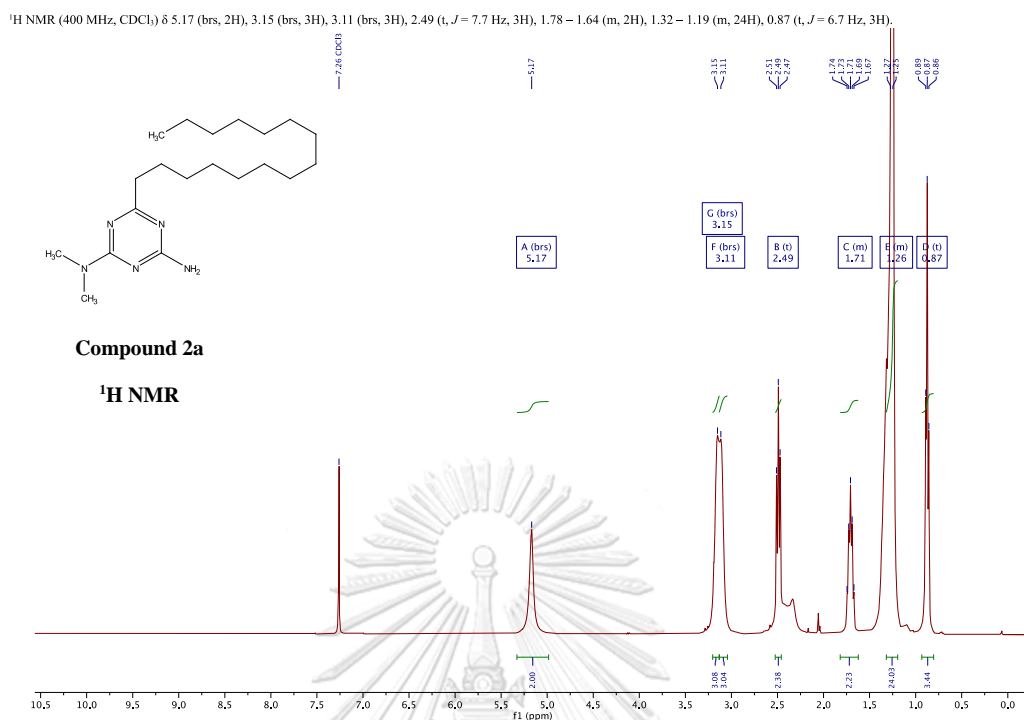


Figure A-5. ¹H-NMR of *N,N*-dimethyl-6-pentadecyl-1,3,5-triazine-2,4-diamine (**2a**)

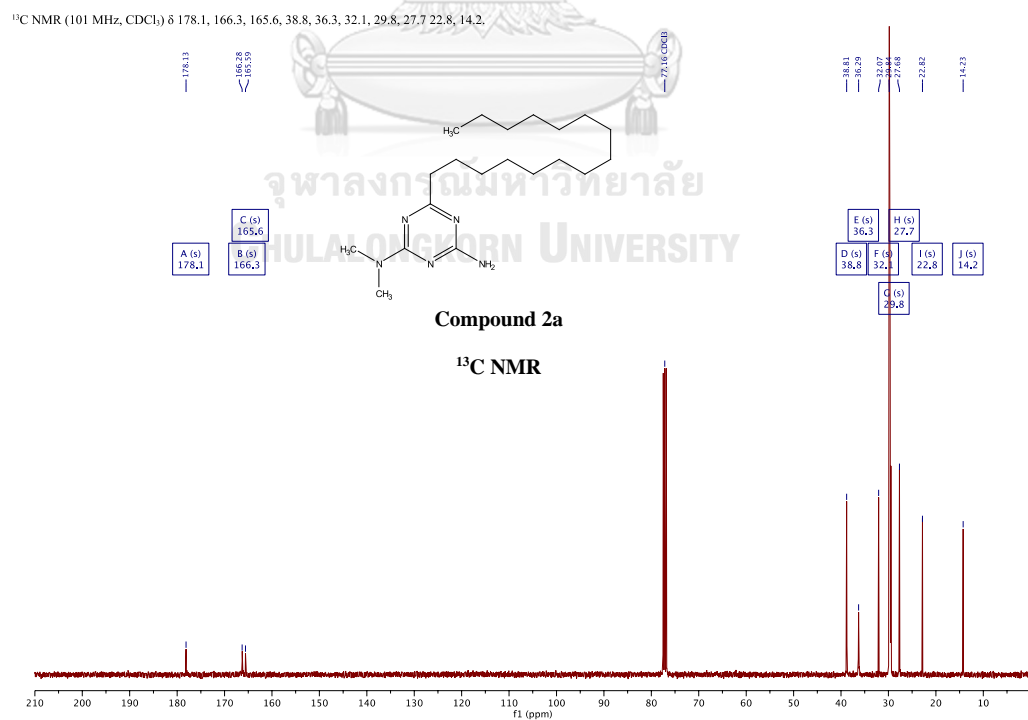


Figure A-6. ¹³C-NMR of *N,N*-dimethyl-6-pentadecyl-1,3,5-triazine-2,4-diamine (**2a**)

$^1\text{H NMR}$ (400 MHz, CDCl_3) δ 8.37 (d, $J = 7.5$ Hz, 2H), 7.53 – 7.38 (m, 3H), 5.26 (brs, 2H), 3.30 (brs, 3H), 3.17 (brs, 3H).

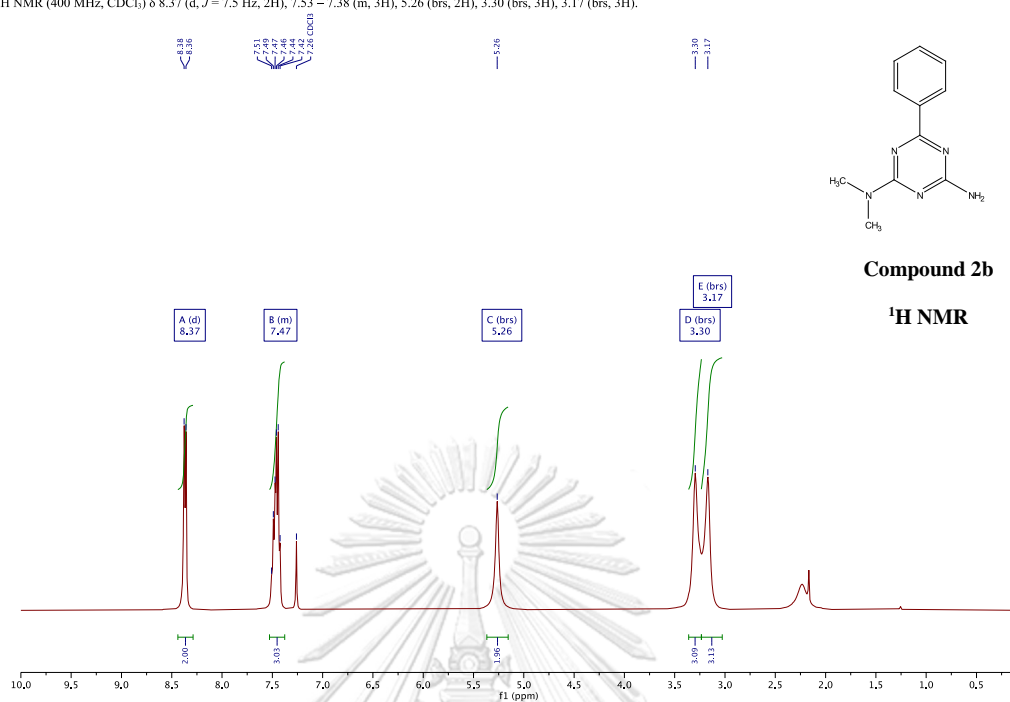


Figure A-7. $^1\text{H-NMR}$ of N,N -dimethyl-6-phenyl-1,3,5-triazine-2,4-diamine (2b)

$^{13}\text{C NMR}$ (101 MHz, CDCl_3) δ 171.0, 167.4, 166.0, 131.4, 130.1, 128.5, 128.3, 36.4.

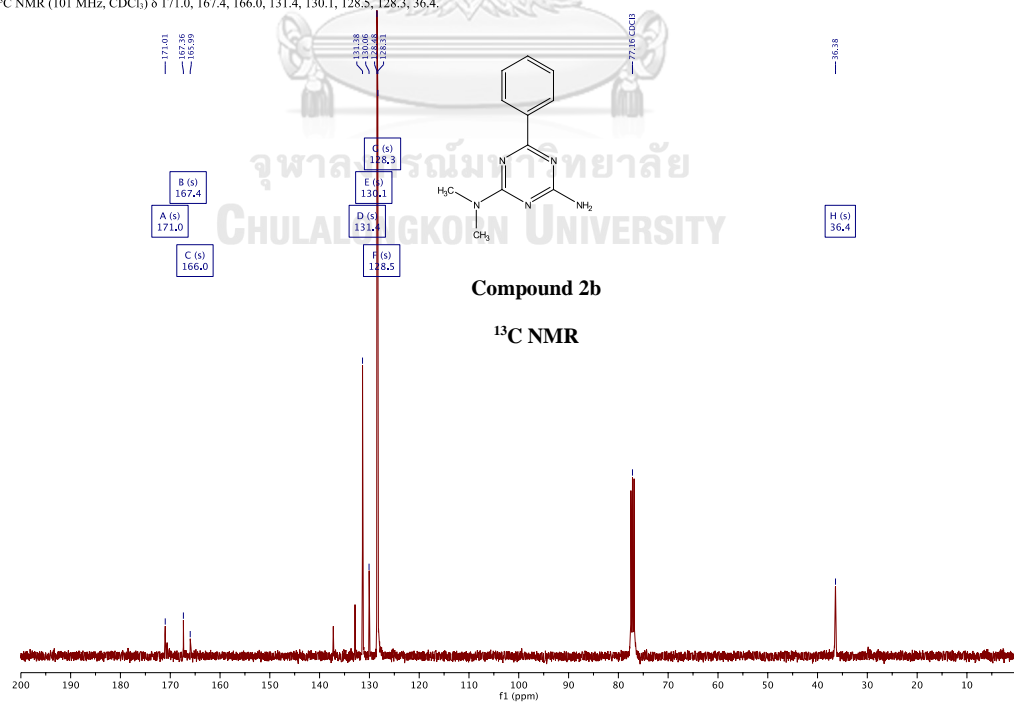
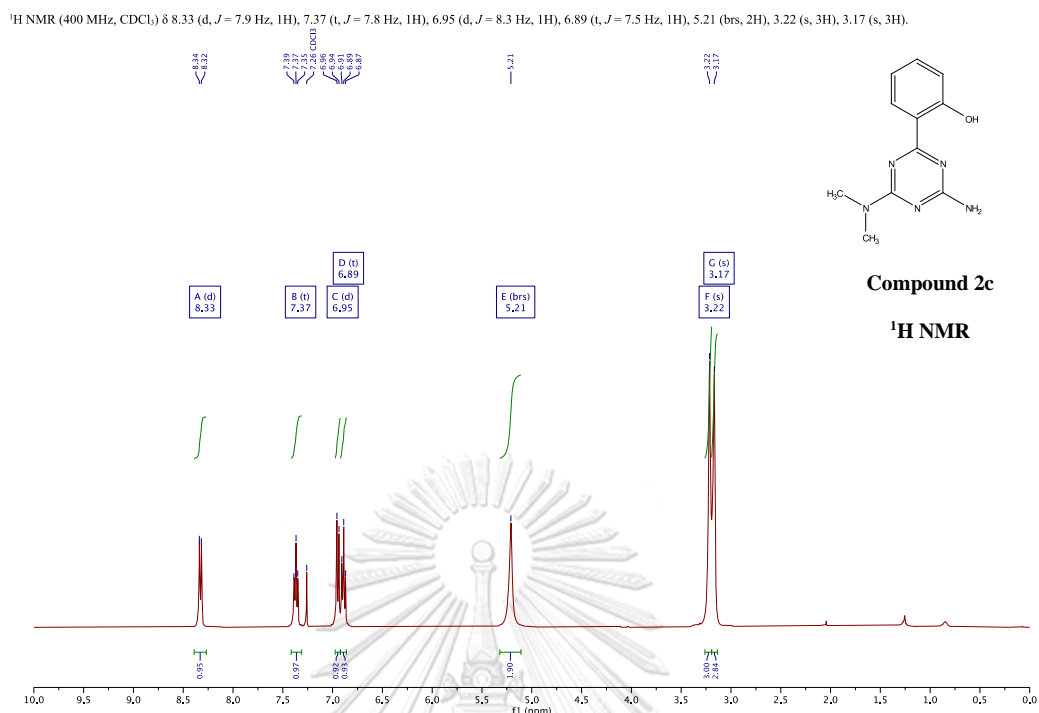
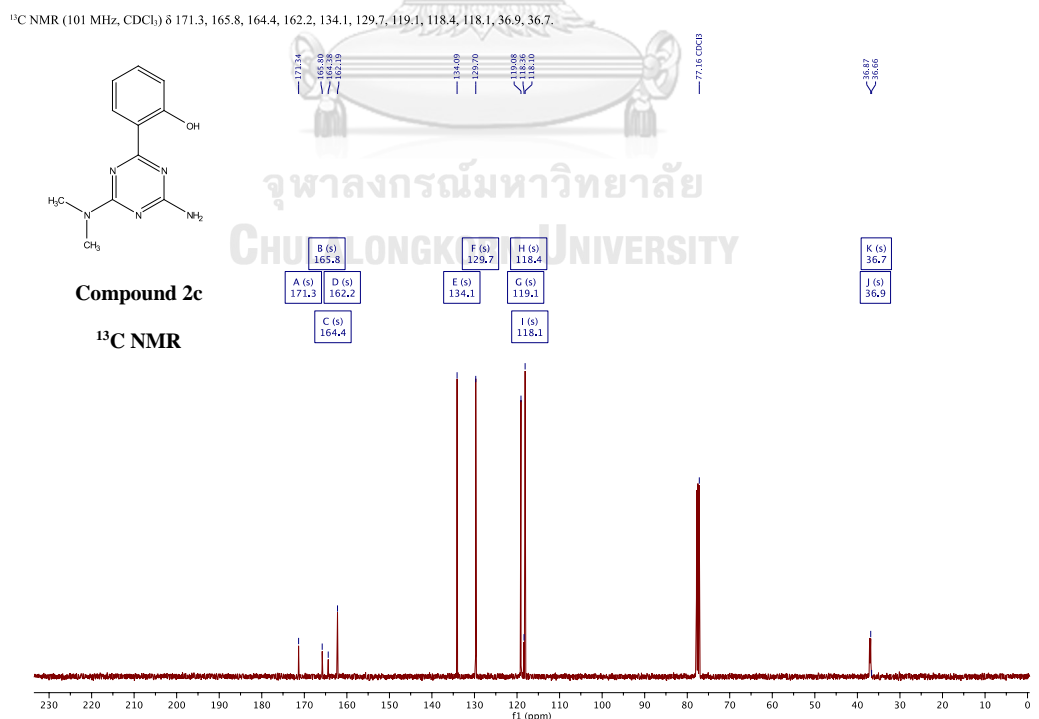


Figure A-8. $^{13}\text{C-NMR}$ of N,N -dimethyl-6-phenyl-1,3,5-triazine-2,4-diamine (2b)

Figure A-9. ¹H-NMR of 2-(4-amino-6-(dimethylamino)-1,3,5-triazin-2-yl)phenol (2c)Figure A-10. ¹³C-NMR of 2-(4-amino-6-(dimethylamino)-1,3,5-triazin-2-yl)phenol (2c)

Mass Spectrum List Report

Analysis Info

Analysis Name D:\Data\Data Service\190819\A46_RC6_01_2982.d
Method nv_pos_6min_profile_wguardcol_190624.m
Sample Name A46
Comment

Acquisition Date 8/19/2019 10:23:02 PM

Operator CU.
Instrument / Ser# micrOTOF-Q II 10335

Acquisition Parameter

Source Type	ESI	Ion Polarity	Positive	Set Nebulizer	3.0 Bar
Focus	Not active	Set Capillary	4000 V	Set Dry Heater	200 °C
Scan Begin	100 m/z	Set End Plate Offset	-500 V	Set Dry Gas	8.0 l/min
Scan End	1500 m/z	Set Collision Cell RF	250.0 Vpp	Set Divert Valve	Waste

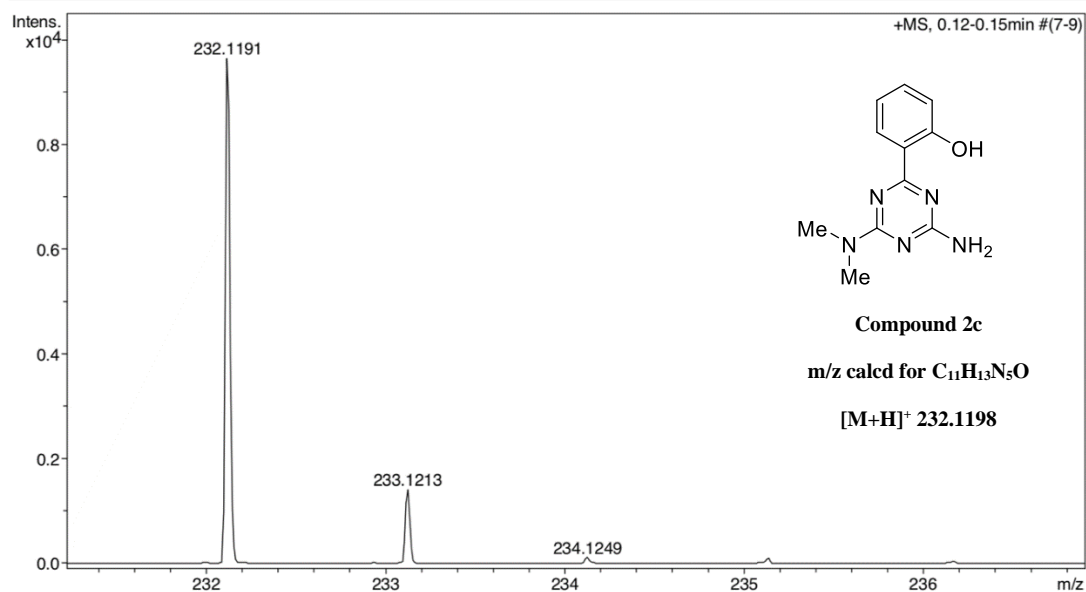


Figure A-11. HRMS spectrum of 2-(4-amino-6-(dimethylamino)-1,3,5-triazin-2-yl)phenol (2c)

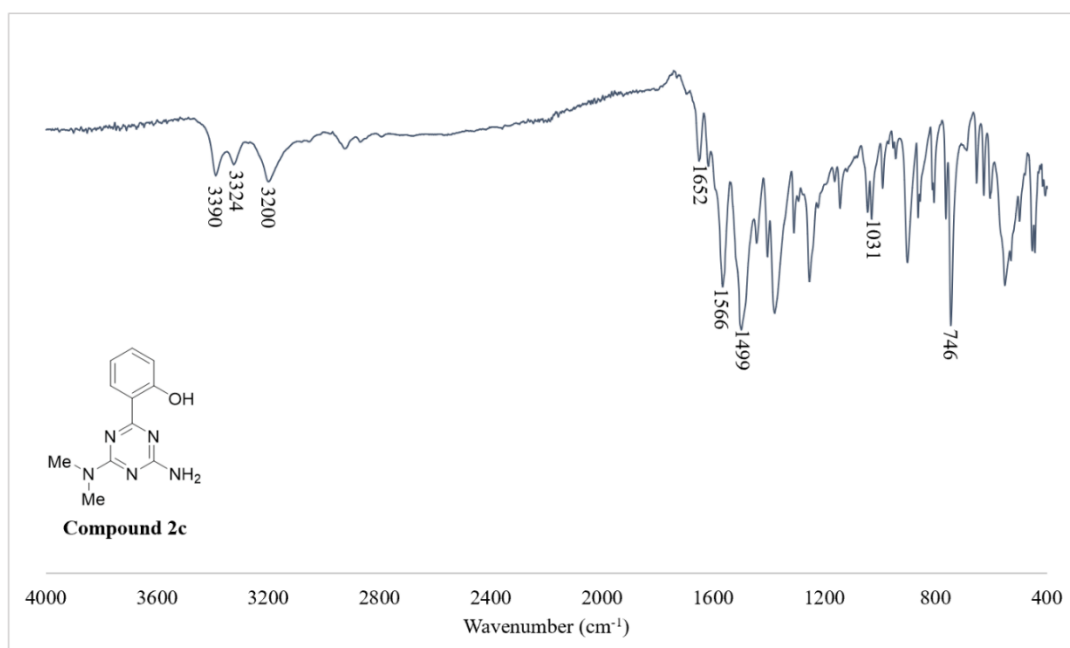


Figure A-12. IR spectrum of 2-(4-amino-6-(dimethylamino)-1,3,5-triazin-2-yl)phenol (2c)

$^1\text{H NMR}$ (400 MHz, CDCl_3) δ 7.95 (d, $J = 15.9$ Hz, 1H), 7.58 (d, $J = 7.0$ Hz, 2H), 7.43 – 7.30 (m, 3H), 6.83 (d, $J = 15.9$ Hz, 1H), 5.28 (brs, 2H), 3.22 (brs, 3H), 3.15 (brs, 3H).

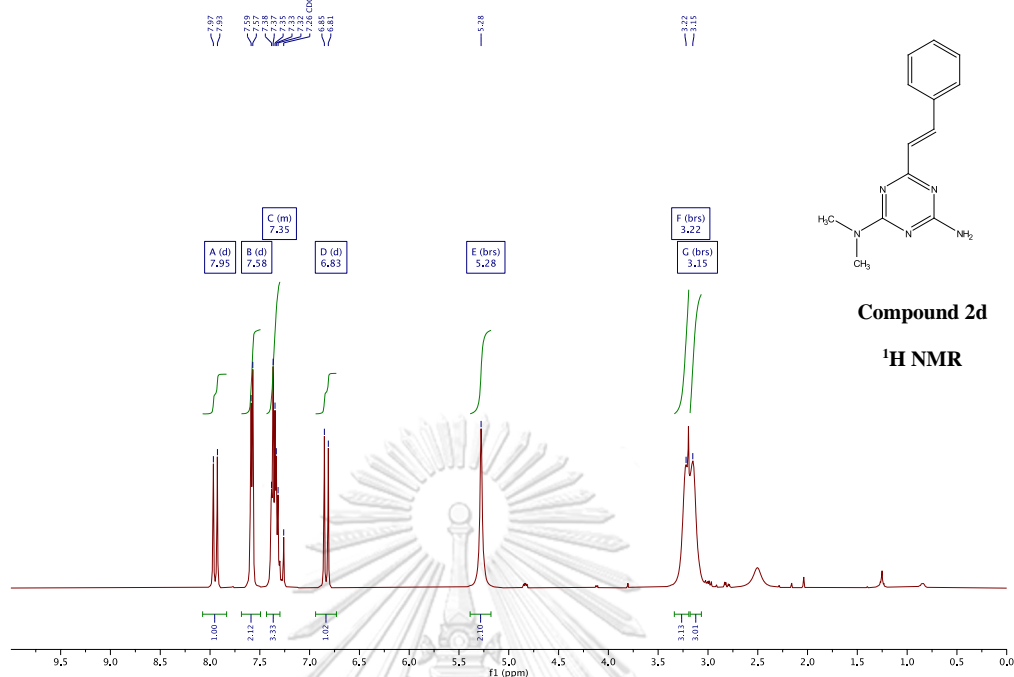


Figure A-13. $^1\text{H-NMR}$ of (*E*)- N^2,N^2 -dimethyl-6-styryl-1,3,5-triazine-2,4-diamine (2d)

$^{13}\text{C NMR}$ (101 MHz, CDCl_3) δ 171.0, 167.2, 166.1, 139.7, 136.3, 129.6, 129.2, 128.3, 127.5, 36.7.

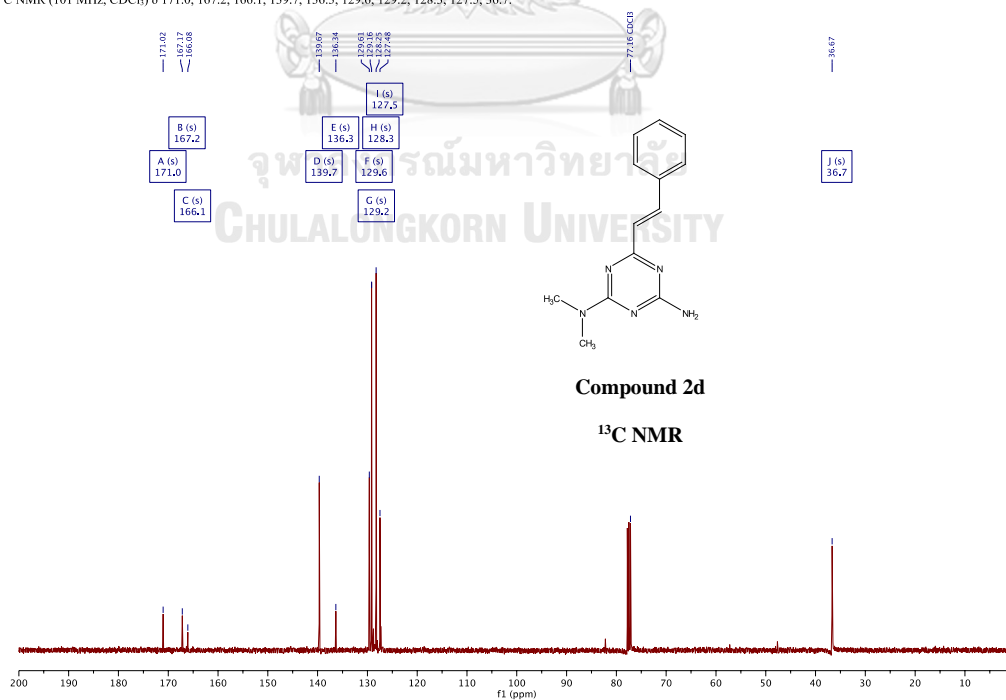
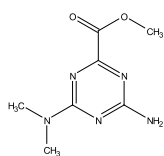


Figure A-14. $^{13}\text{C-NMR}$ of (*E*)- N^2,N^2 -dimethyl-6-styryl-1,3,5-triazine-2,4-diamine (2d)

^1H NMR (400 MHz, CDCl_3) δ 5.68 (brs, 2H), 3.95 (s, 3H), 3.23 (s, 3H), 3.13 (s, 3H).



Compound 2e

^1H NMR

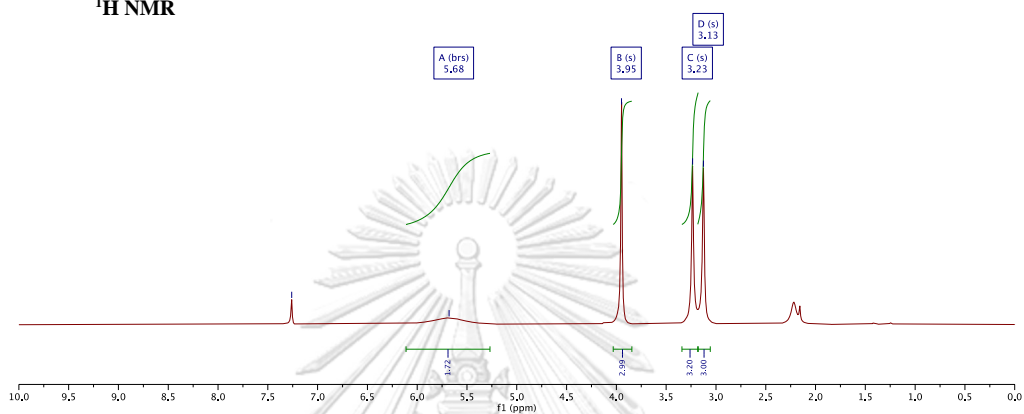


Figure A-15. ^1H -NMR of Methyl 4-amino-6-(dimethylamino)-1,3,5-triazine-2-carboxylate (2e)

^{13}C NMR (101 MHz, CDCl_3) δ 166.5, 165.4, 164.0, 163.1, 53.1, 36.4, 36.2.

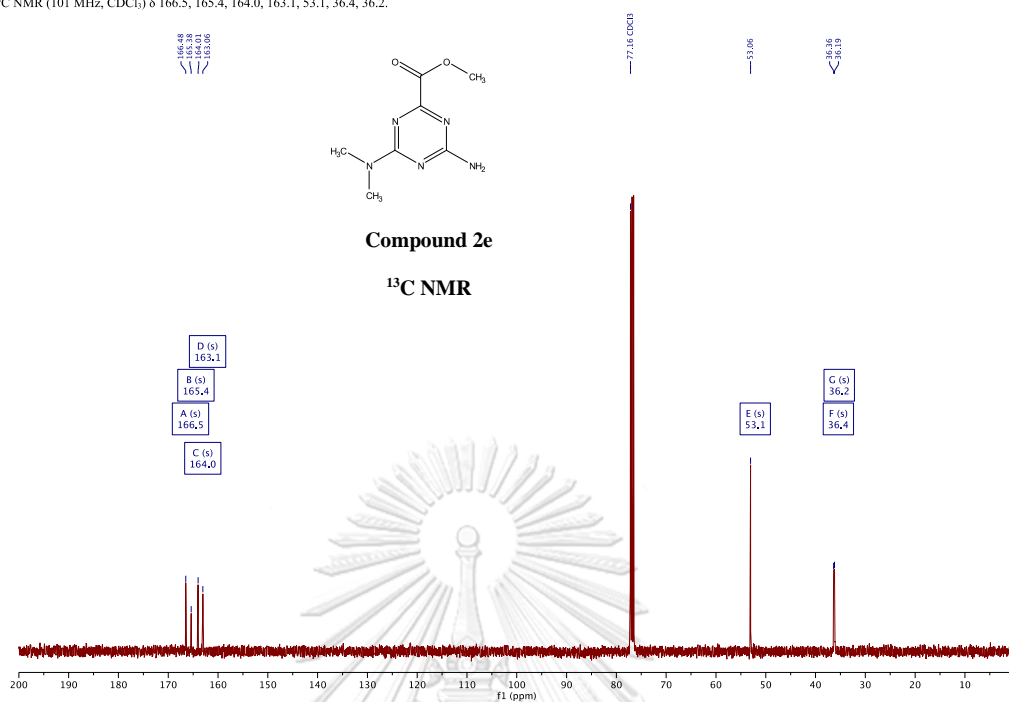


Figure A-16. ^{13}C -NMR of Methyl 4-amino-6-(dimethylamino)-1,3,5-triazine-2-carboxylate (2e)

Mass Spectrum List Report

Analysis Info
Analysis Name D:\Data\Data Service\190819\A52_RC7_01_2983.d
Method nv_pos_6min_profile_wguardcol_190624.m
Sample Name A52
Comment
Acquisition Date 8/19/2019 10:29:30 PM
Operator CU.
Instrument / Ser# micrOTOF-Q II 10335

Acquisition Parameter

Source Type	ESI	Ion Polarity	Positive	Set Nebulizer	3.0 Bar
Focus	Not active	Set Capillary	4000 V	Set Dry Heater	200 °C
Scan Begin	100 m/z	Set End Plate Offset	-500 V	Set Dry Gas	8.0 l/min
Scan End	1500 m/z	Set Collision Cell RF	250.0 Vpp	Set Divert Valve	Waste

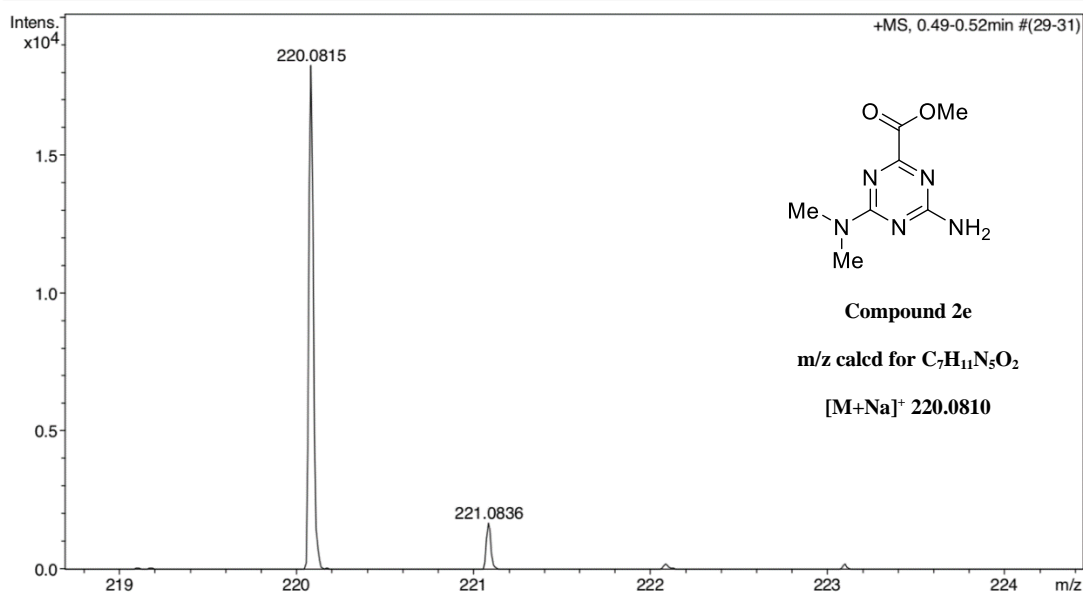


Figure A-17. HRMS spectrum of Methyl 4-amino-6-(dimethylamino)-1,3,5-triazine-2-carboxylate (2e)

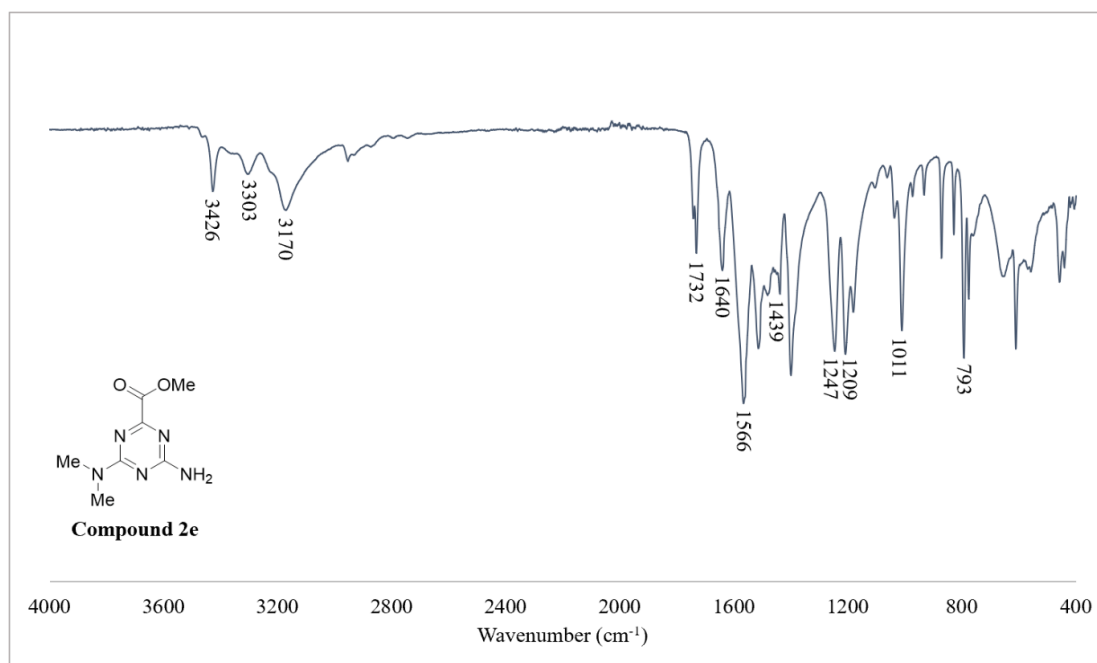


Figure A-18. IR spectrum of Methyl 4-amino-6-(dimethylamino)-1,3,5-triazine-2-carboxylate (**2e**)

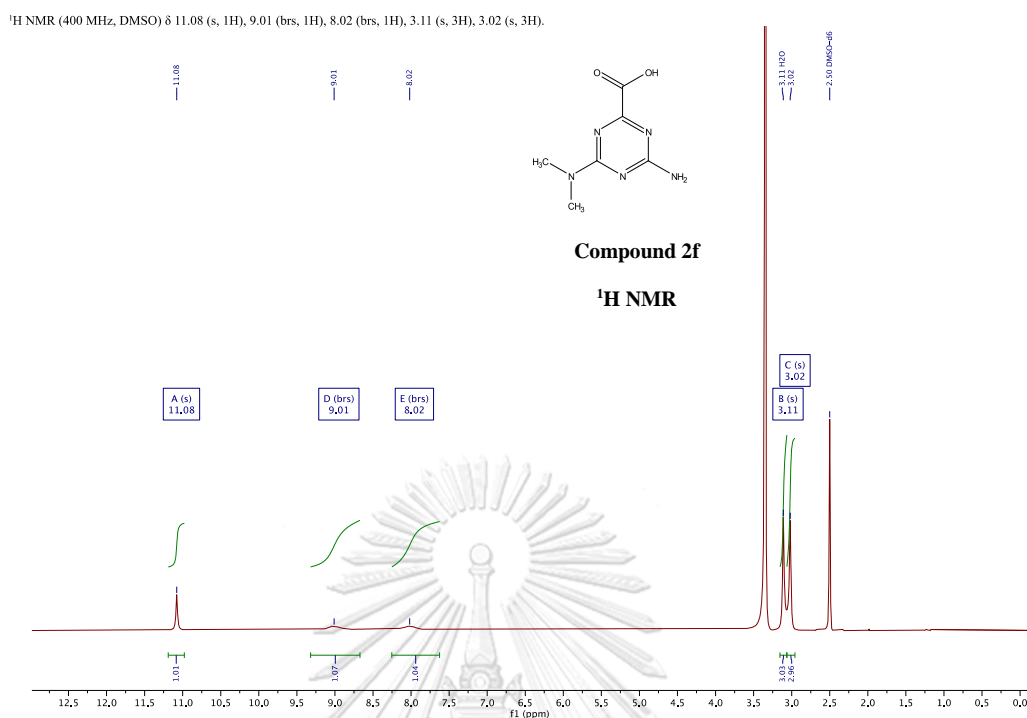


Figure A-19. ¹H-NMR of 4-amino-6-(dimethylamino)-1,3,5-triazine-2-carboxylic acid (2f)

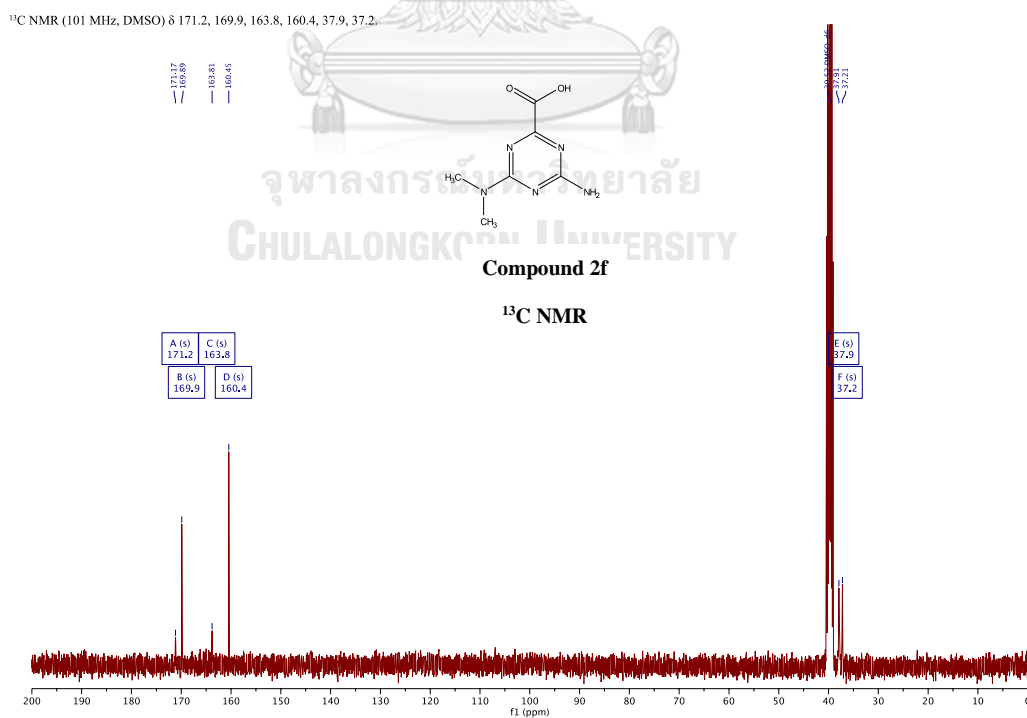


Figure A-20. ¹³C-NMR of 4-amino-6-(dimethylamino)-1,3,5-triazine-2-carboxylic acid (2f)

Mass Spectrum List Report

Analysis Info

Analysis Name D:\Data\Data Service\190819\A30_RA8_01_2948.d
Method nv_pos_6min_profile_wguardcol_190624.m
Sample Name A30
Comment

Acquisition Date 8/19/2019 5:48:44 PM

Operator CU.
Instrument / Ser# micrOTOF-Q II 10335

Acquisition Parameter

Source Type	ESI	Ion Polarity	Positive	Set Nebulizer	3.0 Bar
Focus	Not active	Set Capillary	4000 V	Set Dry Heater	200 °C
Scan Begin	100 m/z	Set End Plate Offset	-500 V	Set Dry Gas	8.0 l/min
Scan End	1500 m/z	Set Collision Cell RF	250.0 Vpp	Set Divert Valve	Waste

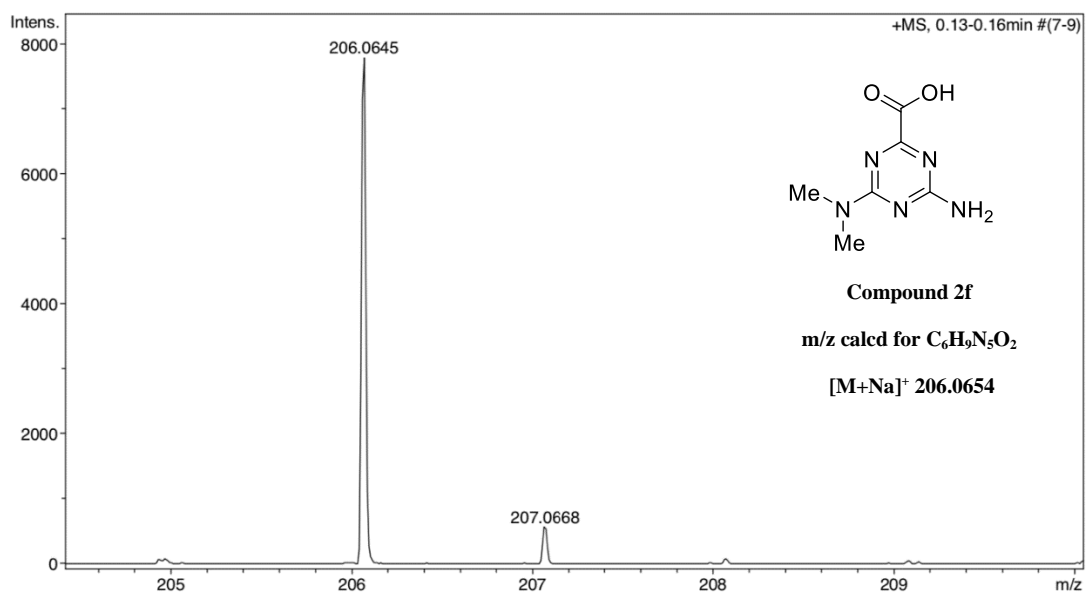


Figure A-21. HRMS spectrum of 4-amino-6-(dimethylamino)-1,3,5-triazine-2-carboxylic acid (2f)

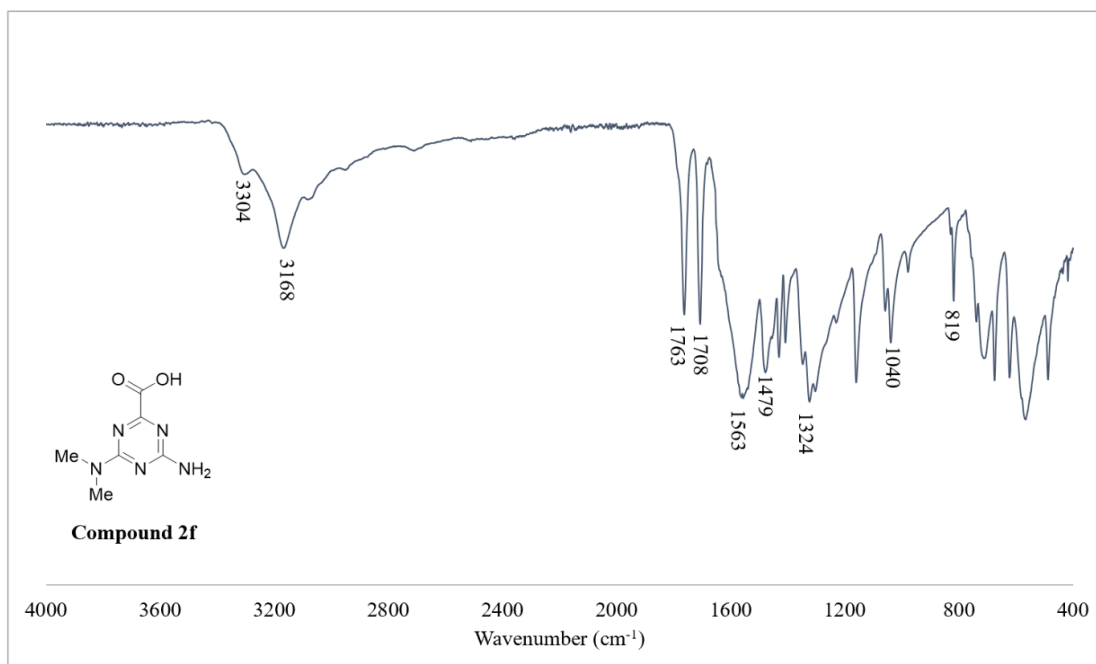


Figure A-22. IR spectrum of 4-amino-6-(dimethylamino)-1,3,5-triazine-2-carboxylic acid (2f)

^1H NMR (400 MHz, DMSO) δ 9.38 (s, 1H), 7.77 (d, $J = 7.9$ Hz, 2H), 7.24 (t, $J = 7.9$ Hz, 2H), 6.94 (t, $J = 7.2$ Hz, 3H), 2.41 (t, $J = 7.6$ Hz, 2H), 1.73 – 1.60 (m, 2H), 1.29 – 1.20 (m, 23H), 0.84 (t, $J = 6.7$ Hz, 3H).

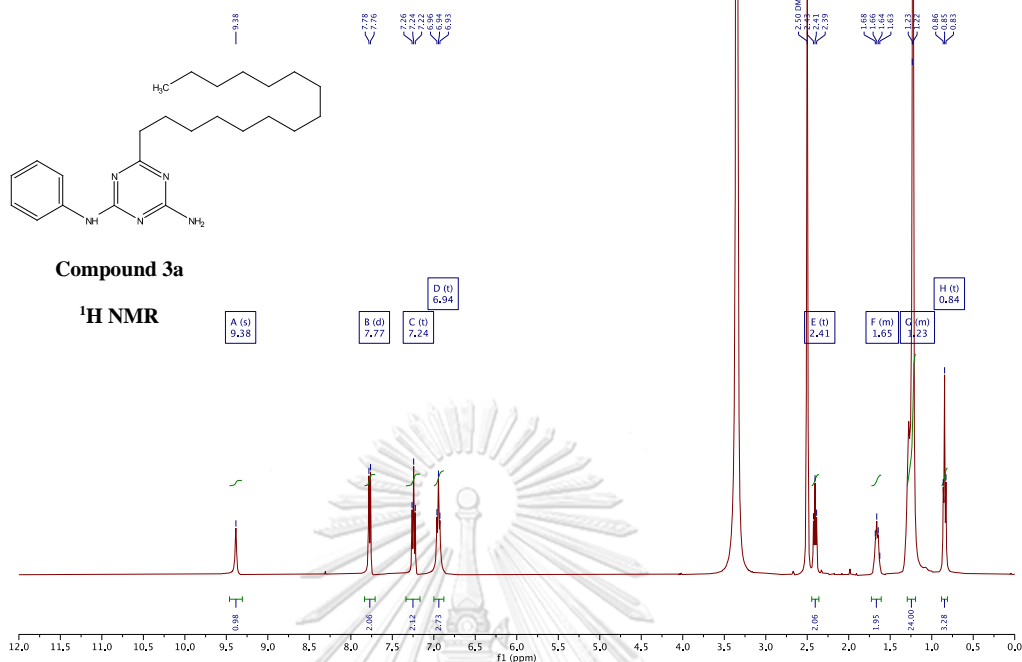


Figure A-23. ^1H -NMR of 6-pentadecyl- N^2 -phenyl-1,3,5-triazine-2,4-diamine (3a)

^{13}C NMR (101 MHz, DMSO) δ 177.8, 166.6, 164.2, 140.0, 128.3, 121.7, 119.7, 37.9, 31.2, 29.0, 26.9, 22.0, 13.9.

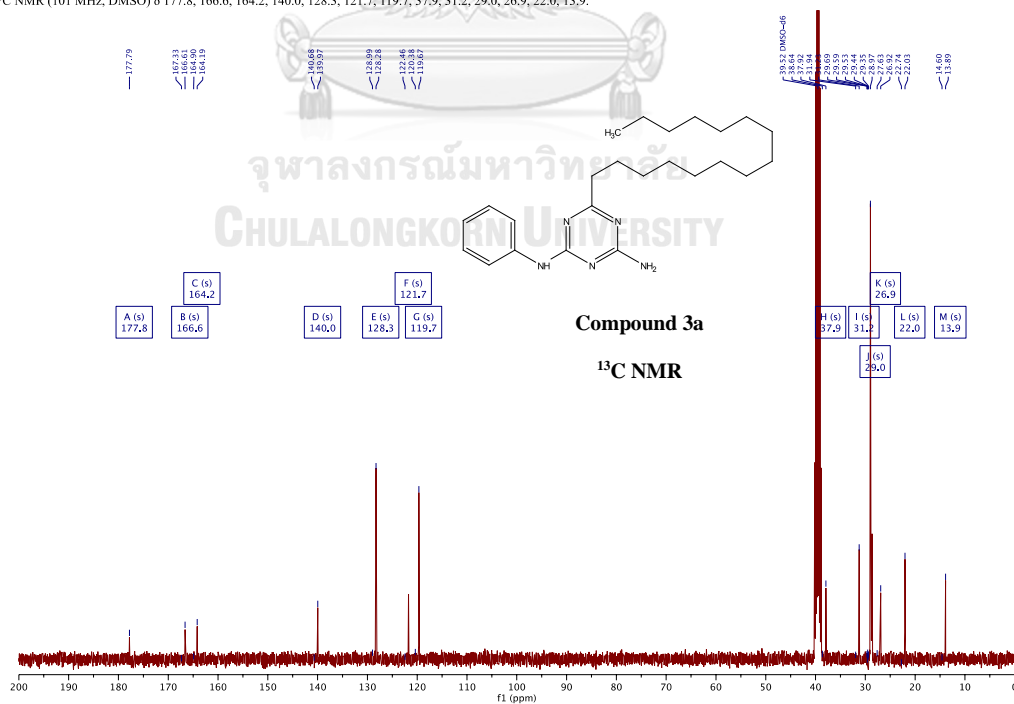


Figure A-24. ^{13}C -NMR of 6-pentadecyl- N^2 -phenyl-1,3,5-triazine-2,4-diamine (3a)

Mass Spectrum List Report

Analysis Info

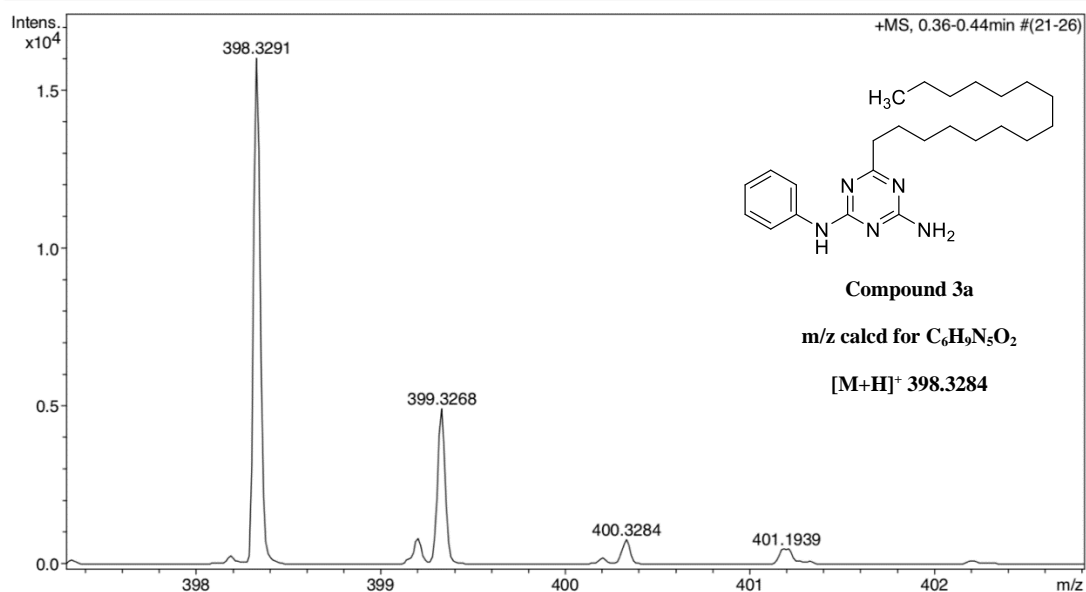
Analysis Name D:\Data\Data Service\190819\A40_RC5_01_2981.d
Method nv_pos_6min_profile_wguardcol_190624.m
Sample Name A40
Comment

Acquisition Date 8/19/2019 10:16:34 PM

Operator CU.
Instrument / Ser# micrOTOF-Q II 10335

Acquisition Parameter

Source Type	ESI	Ion Polarity	Positive	Set Nebulizer	3.0 Bar
Focus	Not active	Set Capillary	4000 V	Set Dry Heater	200 °C
Scan Begin	100 m/z	Set End Plate Offset	-500 V	Set Dry Gas	8.0 l/min
Scan End	1500 m/z	Set Collision Cell RF	250.0 Vpp	Set Divert Valve	Waste

Figure A-25. HRMS spectrum of 6-pentadecyl-*N*²-phenyl-1,3,5-triazine-2,4-diamine (3a)

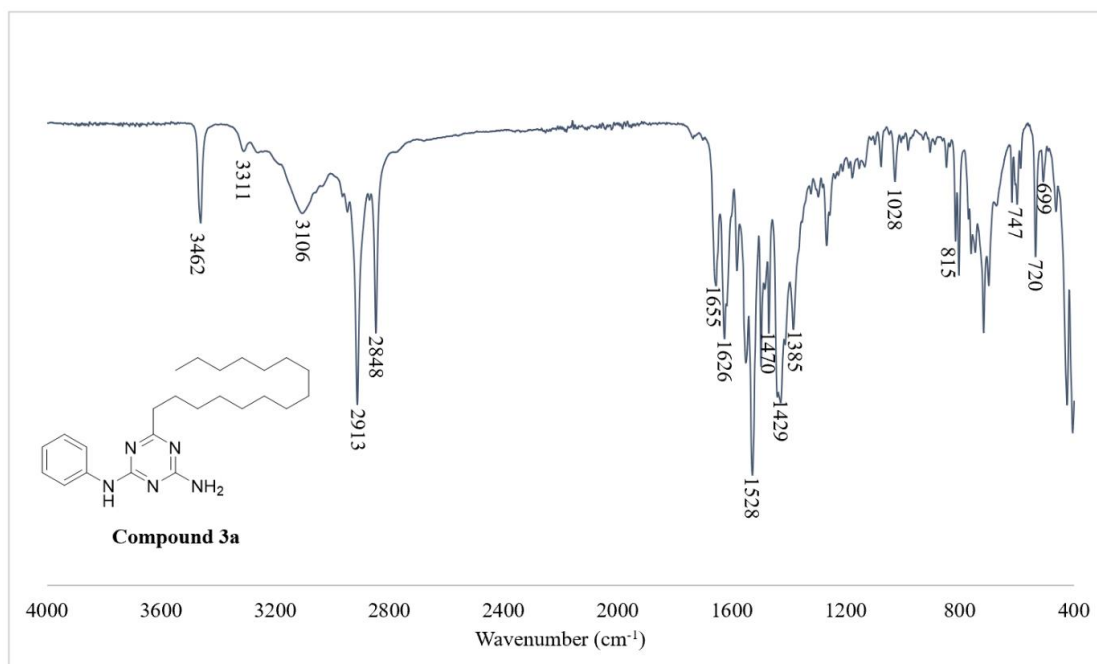
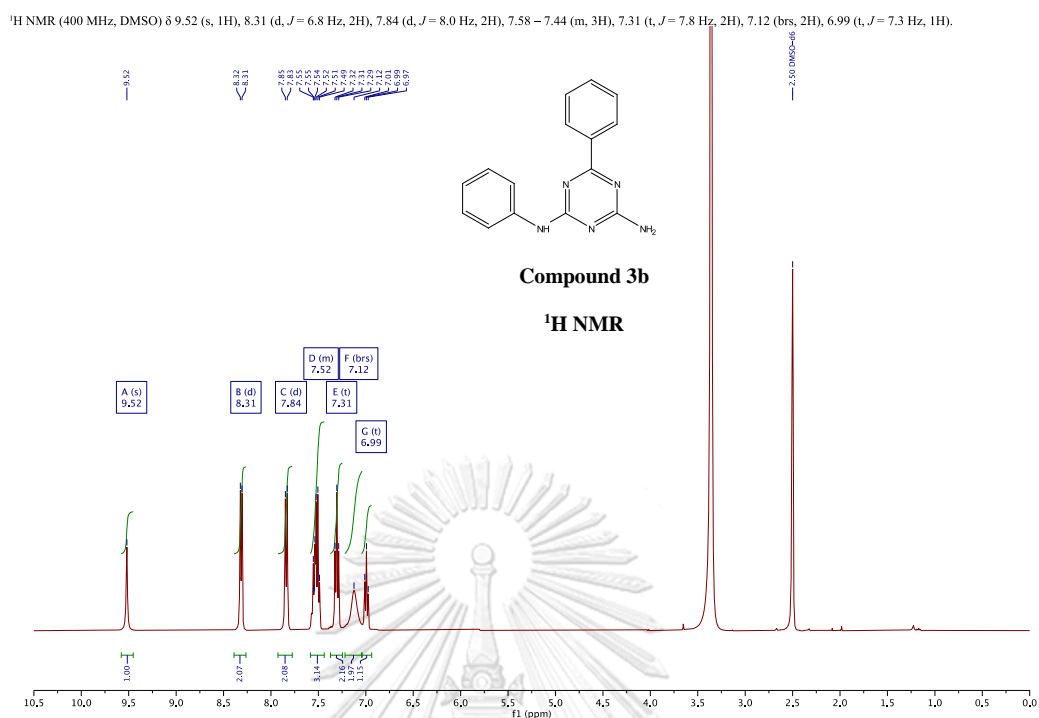
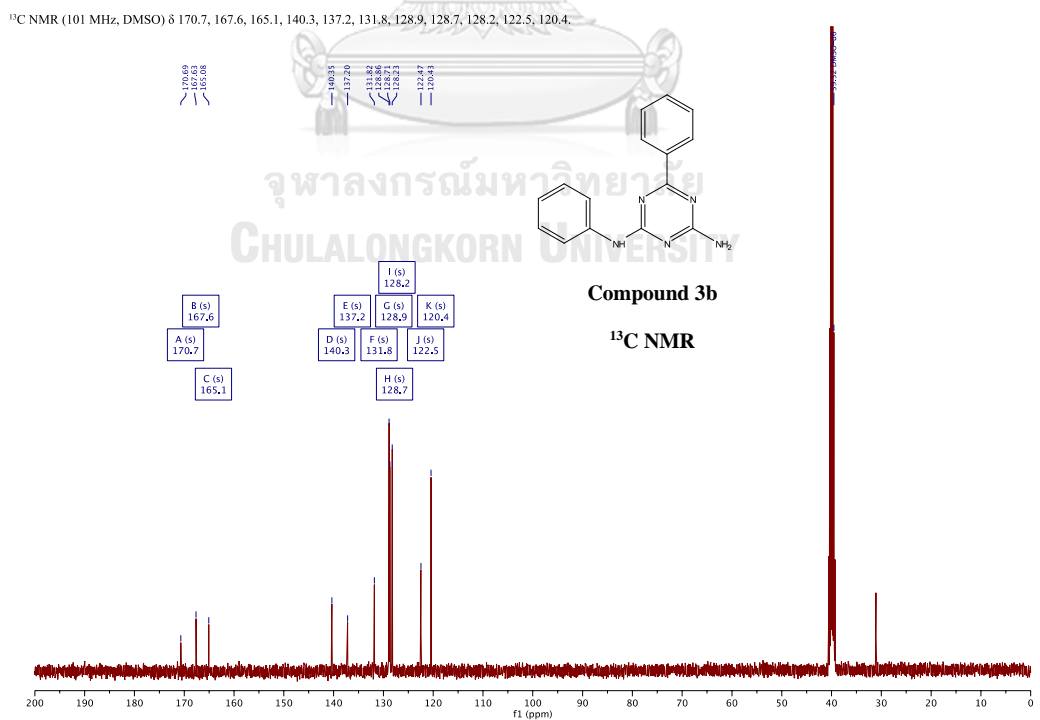


Figure A-26. IR spectrum of 6-pentadecyl-*N*²-phenyl-1,3,5-triazine-2,4-diamine (3a)

Figure A-27. $^1\text{H-NMR}$ of $N^2,6$ -diphenyl-1,3,5-triazine-2,4-diamine (3b)Figure A-28. $^{13}\text{C-NMR}$ of $N^2,6$ -diphenyl-1,3,5-triazine-2,4-diamine (3b)

$^1\text{H NMR}$ (400 MHz, DMSO) δ 13.49 (s, 1H), 9.77 (brs, 1H), 8.26 (d, $J = 7.3$ Hz, 1H), 7.76 (brs, 2H), 7.55 (brs, 1H), 7.44 – 7.35 (m, 2H), 7.33 (t, $J = 7.2$ Hz, 2H), 7.04 (t, $J = 7.5$ Hz, 1H), 6.90 (t, $J = 8.0$ Hz, 2H).

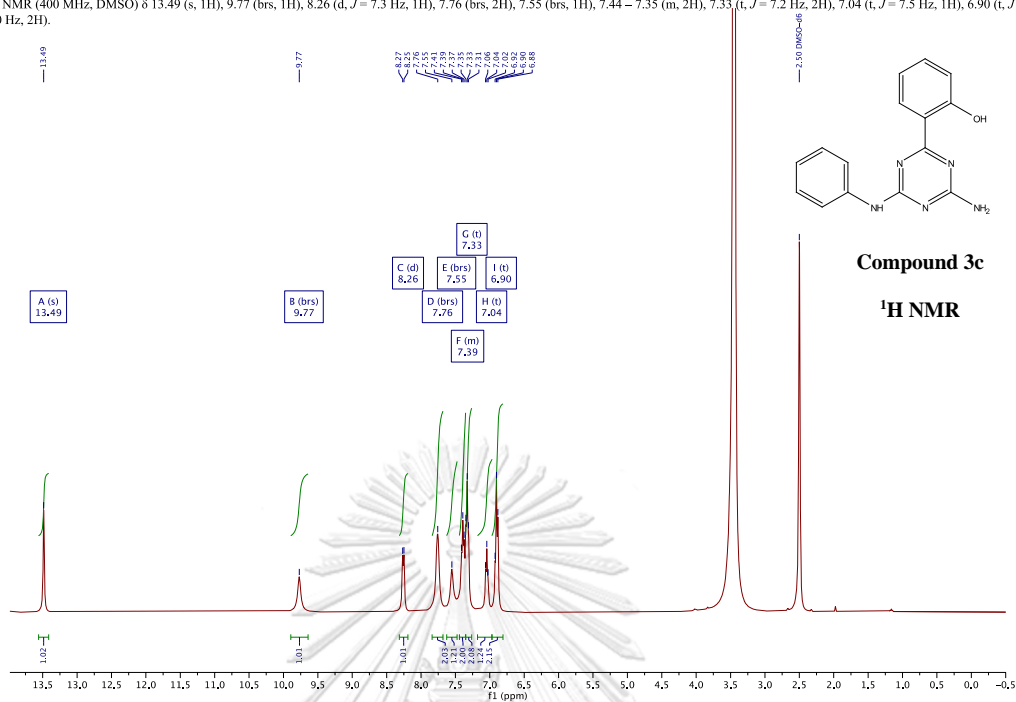


Figure A-29. $^1\text{H-NMR}$ of 2-(4-amino-6-(phenylamino)-1,3,5-triazin-2-yl)phenol (3c)

$^{13}\text{C NMR}$ (101 MHz, DMSO) δ 169.9, 164.7, 160.8, 138.8, 133.2, 128.5, 128.1, 122.3, 120.2, 117.9, 117.2, 117.1.

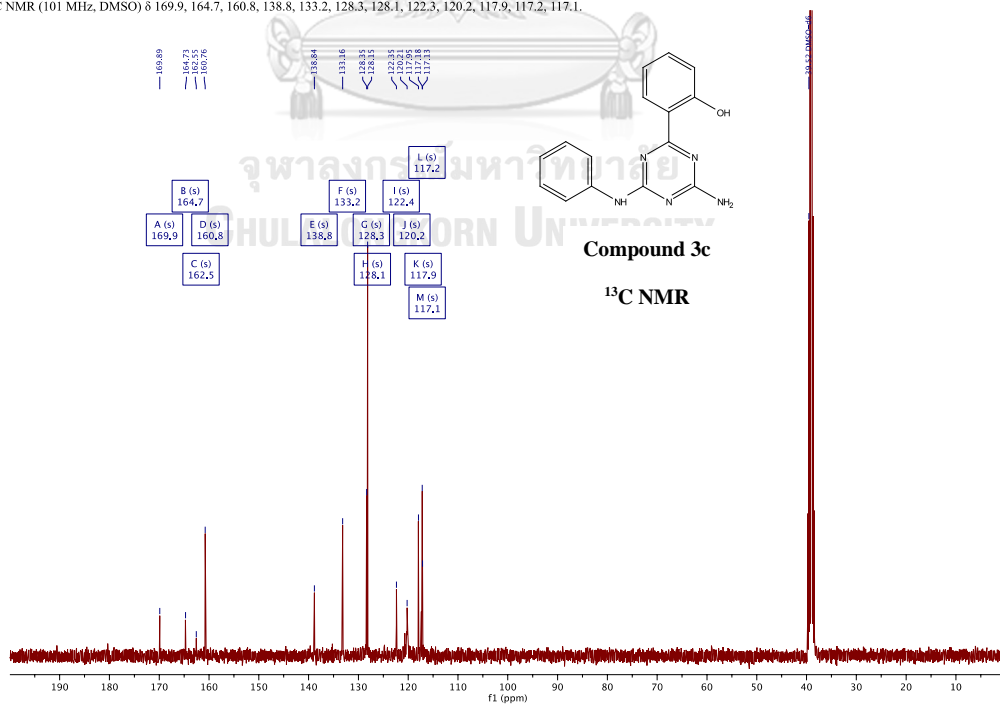


Figure A-30. $^{13}\text{C-NMR}$ of 2-(4-amino-6-(phenylamino)-1,3,5-triazin-2-yl)phenol (3c)

Mass Spectrum List Report

Analysis Info
Analysis Name D:\Data\Data Service\190819\A38_RC4_01_2980.d
Method nv_pos_6min_profile_wguardcol_190624.m
Sample Name A38
Comment
Acquisition Date 8/19/2019 10:10:06 PM
Operator CU.
Instrument / Ser# micrOTOF-Q II 10335

Acquisition Parameter

Source Type	ESI	Ion Polarity	Positive	Set Nebulizer	3.0 Bar
Focus	Not active	Set Capillary	4000 V	Set Dry Heater	200 °C
Scan Begin	100 m/z	Set End Plate Offset	-500 V	Set Dry Gas	8.0 l/min
Scan End	1500 m/z	Set Collision Cell RF	250.0 Vpp	Set Divert Valve	Waste

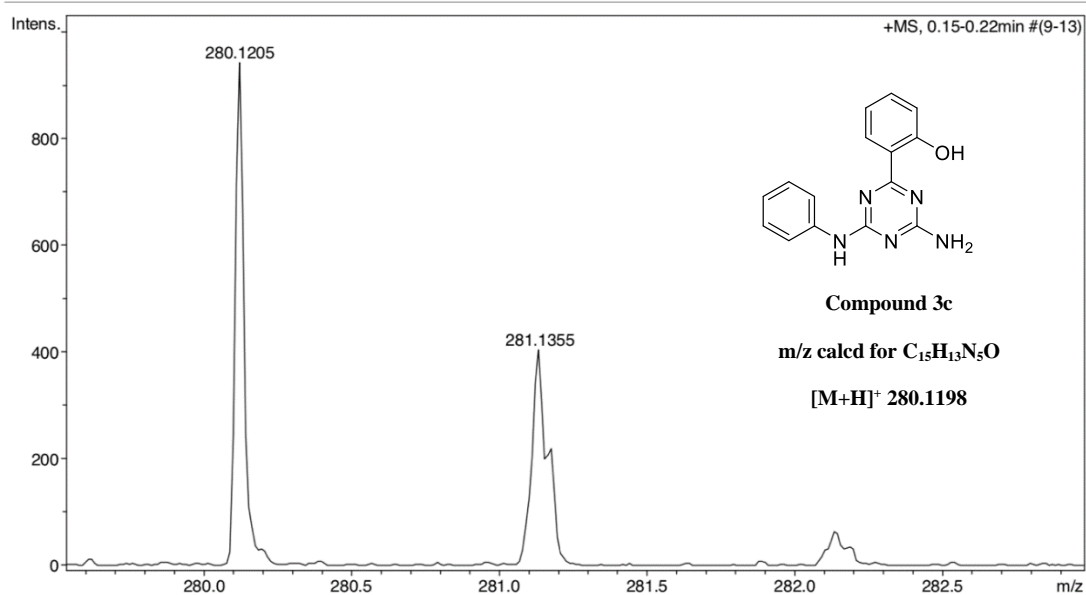


Figure A-31. HRMS spectrum of 2-(4-amino-6-(phenylamino)-1,3,5-triazin-2-yl)phenol (3c)

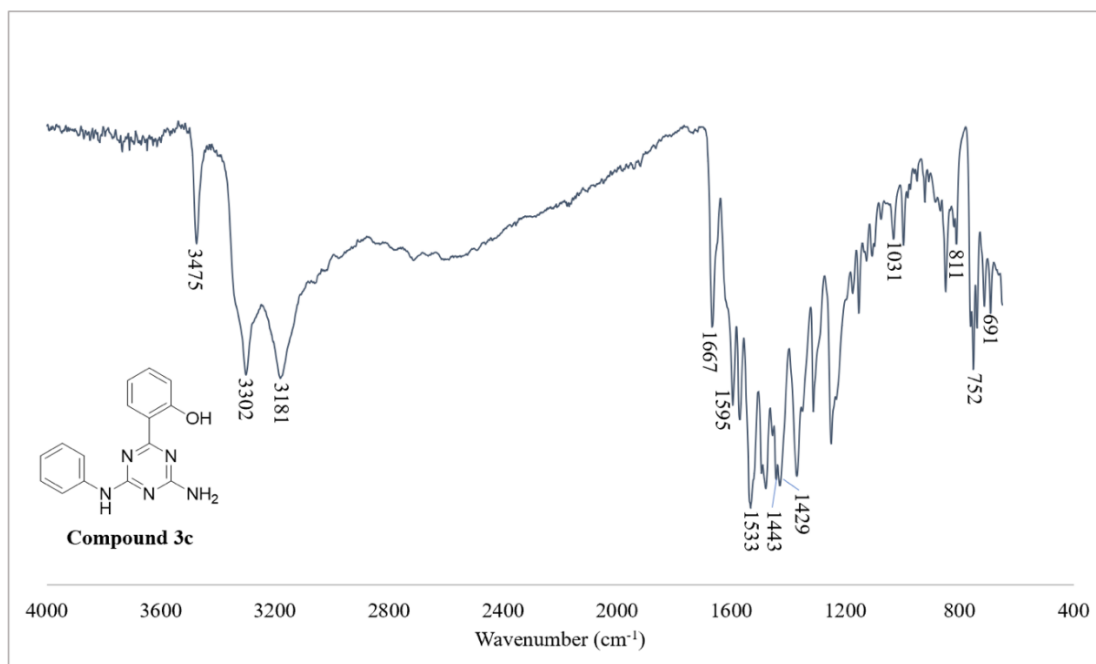


Figure A-32. IR spectrum of 2-(4-amino-6-(phenylamino)-1,3,5-triazin-2-yl)phenol (3c)

$^1\text{H NMR}$ (500 MHz,) δ 9.47 (s, 1H), 7.87 (d, $J = 15.9$ Hz, 1H), 7.81 (dd, $J = 8.7, 1.2$ Hz, 2H), 7.66 (d, $J = 7.5$ Hz, 2H), 7.46–7.36 (m, 3H), 7.28 (t, $J = 7.6$ Hz, 2H), 7.03 (brs, 2H), 6.97 (tt, $J = 7.3, 1.2$ Hz, 1H), 6.82 (d, $J = 16.0$ Hz, 1H).

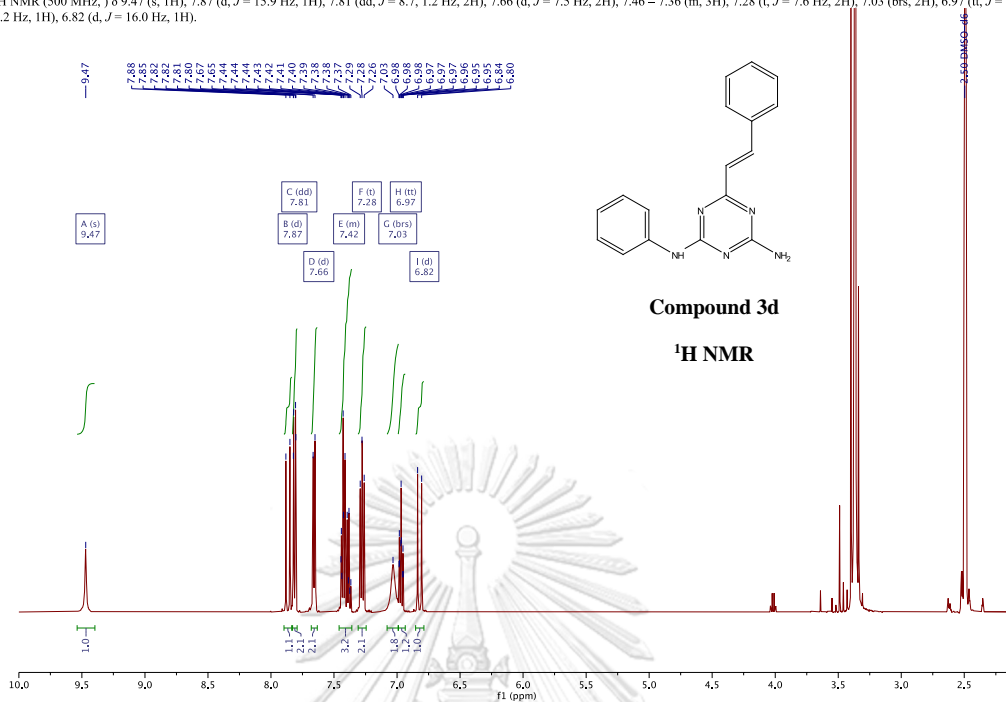


Figure A-33. $^1\text{H-NMR}$ of (*E*)-*N*²-phenyl-6-styryl-1,3,5-triazine-2,4-diamine (3d)

$^{13}\text{C NMR}$ (101 MHz, CDCl_3) δ 171.0, 166.6, 164.3, 141.2, 138.3, 135.5, 129.9, 129.1, 129.0, 128.2, 125.5, 124.0, 121.0.

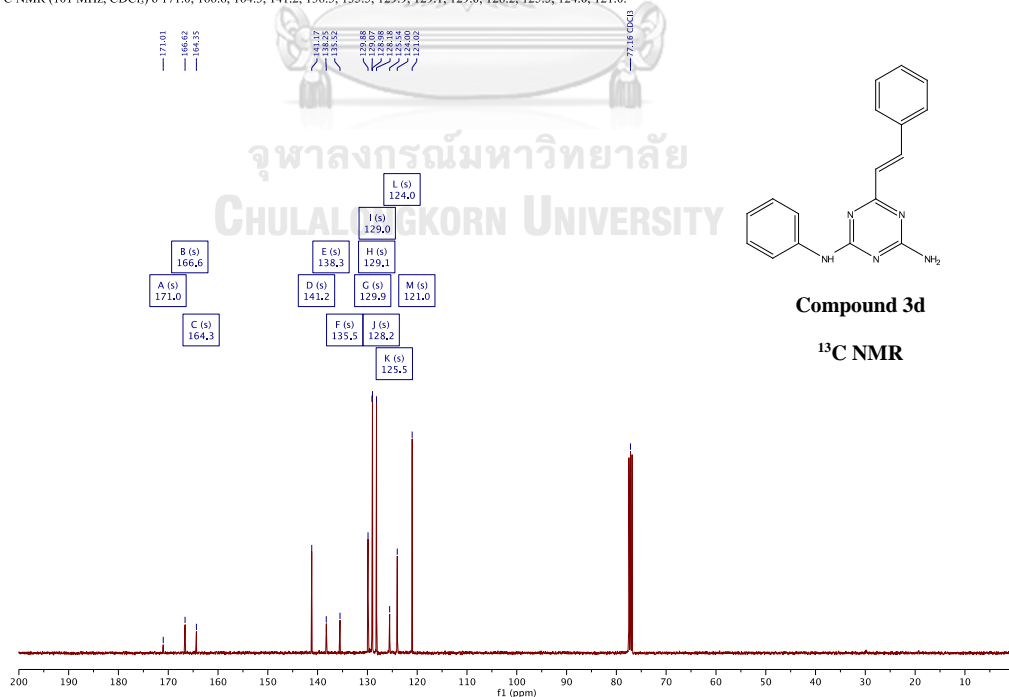
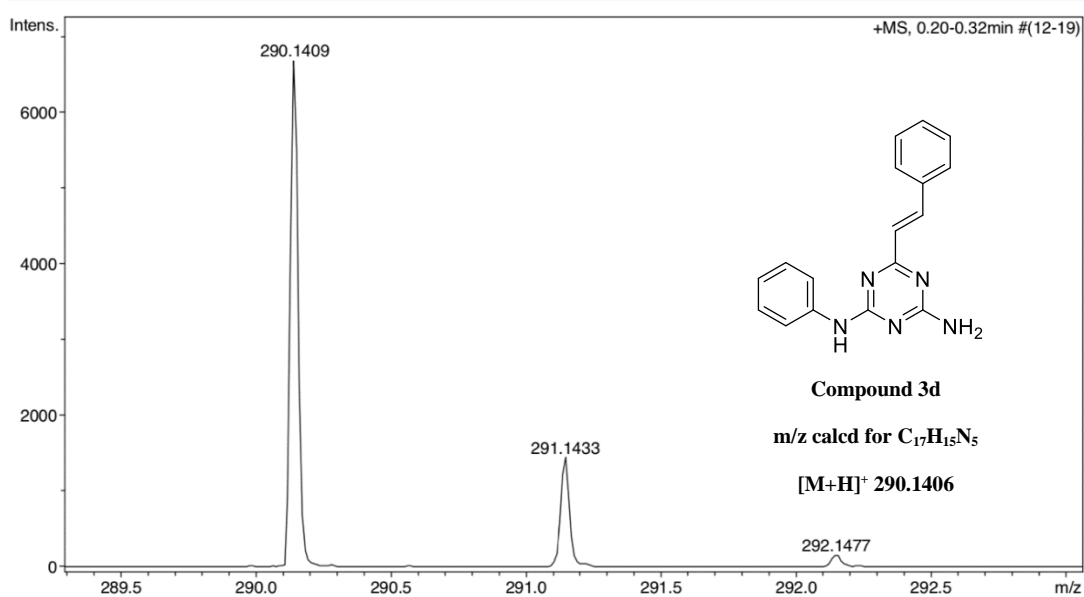


Figure A-34. $^{13}\text{C-NMR}$ of (*E*)-*N*²-phenyl-6-styryl-1,3,5-triazine-2,4-diamine (3d)

Mass Spectrum List Report

Analysis Info		Acquisition Date	8/19/2019 10:03:39 PM
Analysis Name	D:\Data\Data Service\190819VA37_RC3_01_2979.d	Operator	CU.
Method	nv_pos_6min_profile_wguardcol_190624.m	Instrument / Ser#	microTOF-Q II 10335
Sample Name	A37		
Comment			

Acquisition Parameter					
Source Type	ESI	Ion Polarity	Positive	Set Nebulizer	3.0 Bar
Focus	Not active	Set Capillary	4000 V	Set Dry Heater	200 °C
Scan Begin	100 m/z	Set End Plate Offset	-500 V	Set Dry Gas	8.0 l/min
Scan End	1500 m/z	Set Collision Cell RF	250.0 Vpp	Set Divert Valve	Waste

Figure A-35. HRMS spectrum of (*E*)-*N*²-phenyl-6-styryl-1,3,5-triazine-2,4-diamine (3d)

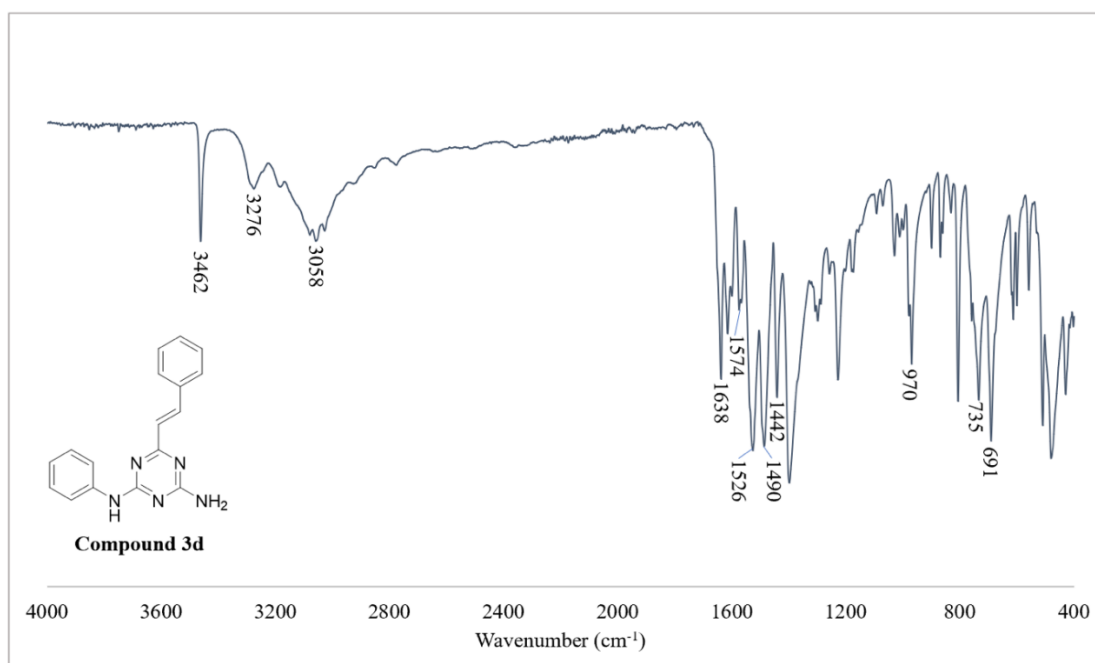


Figure A-36. IR spectrum of (*E*)-*N*²-phenyl-6-styryl-1,3,5-triazine-2,4-diamine (3d)



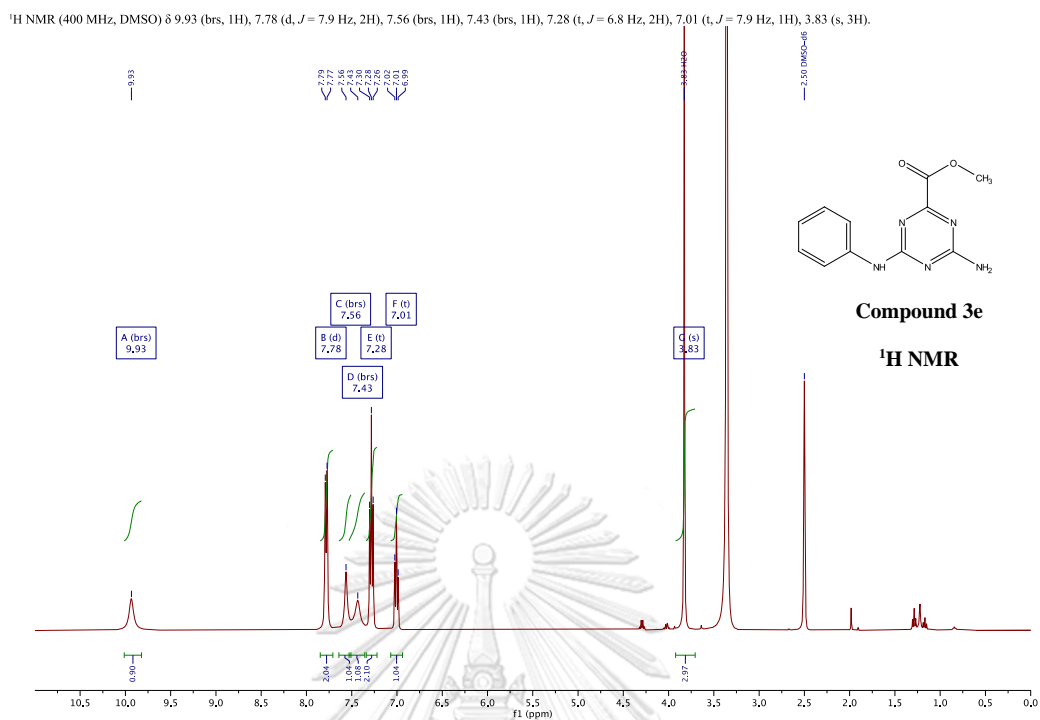


Figure A-37. ¹H-NMR of Methyl 4-amino-6-(phenylamino)-1,3,5-triazine-2-carboxylate (3e)

^{13}C NMR (101 MHz, DMSO) δ 167.3, 164.5, 164.2, 164.1, 139.5, 128.7, 122.7, 120.3, 52.6.

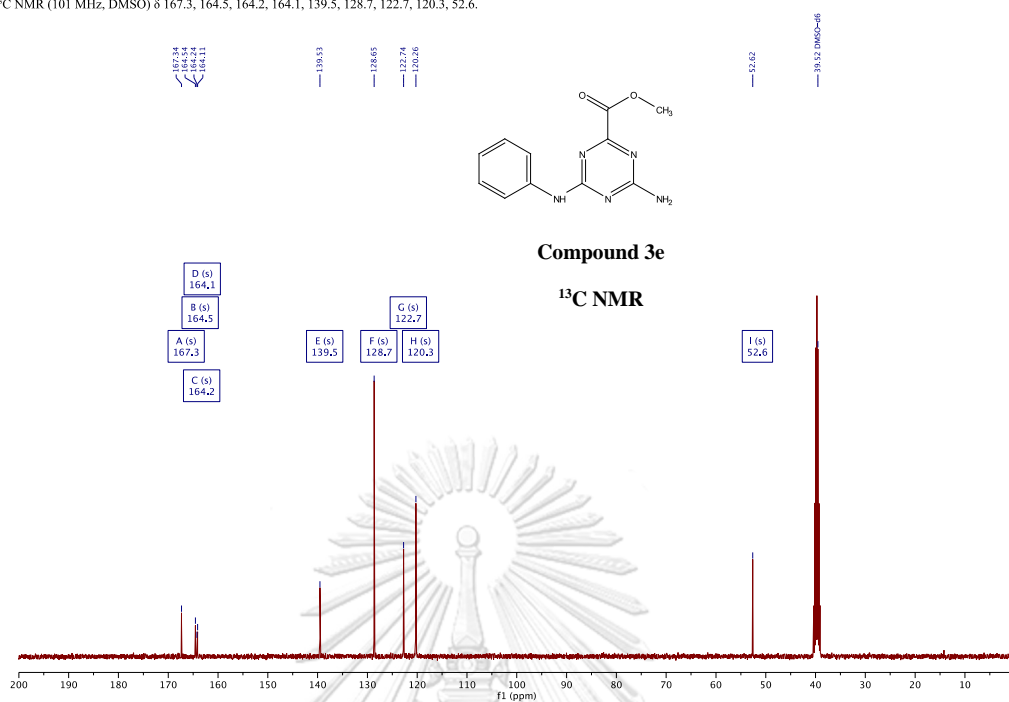


Figure A-38. ^{13}C -NMR of Methyl 4-amino-6-(phenylamino)-1,3,5-triazine-2-carboxylate (3e)

^1H NMR (400 MHz, DMSO) δ 9.89 (brs, 1H), 7.78 (d, $J = 8.1$ Hz, 2H), 7.47 (brs, 2H), 7.28 (t, $J = 7.3$ Hz, 2H), 7.00 (t, $J = 7.5, 6.7$ Hz, 1H).

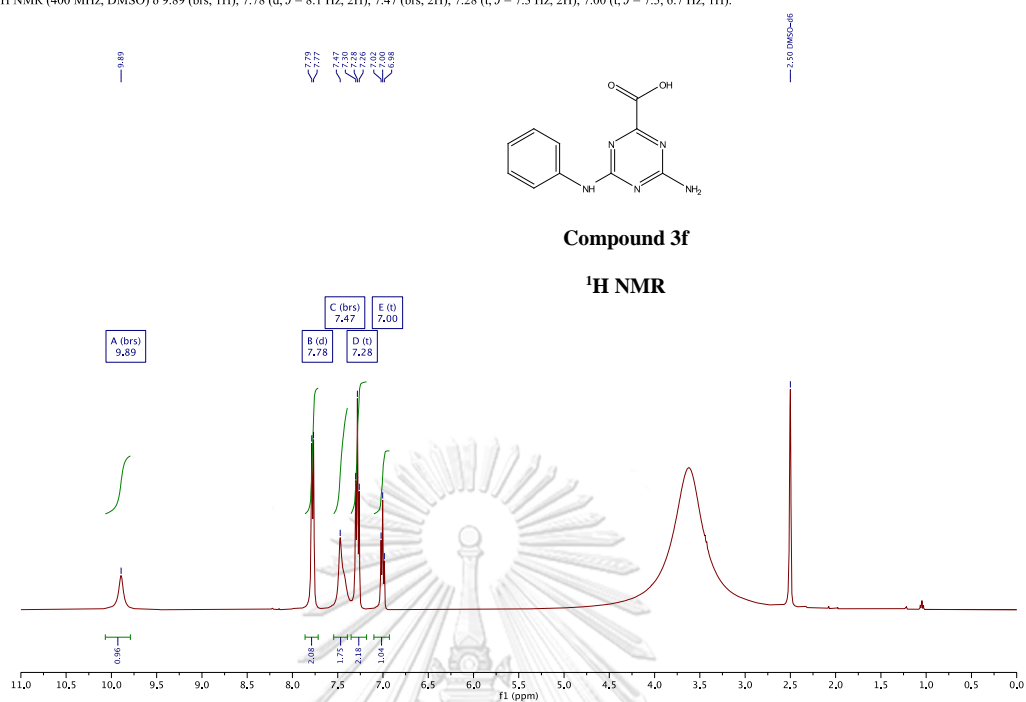


Figure A-39. ^1H -NMR of 4-amino-6-(phenylamino)-1,3,5-triazine-2-carboxylic acid (3f)

^{13}C NMR (101 MHz, DMSO) δ 166.9, 165.4, 165.0, 164.3, 139.4, 128.5, 122.6, 120.2.

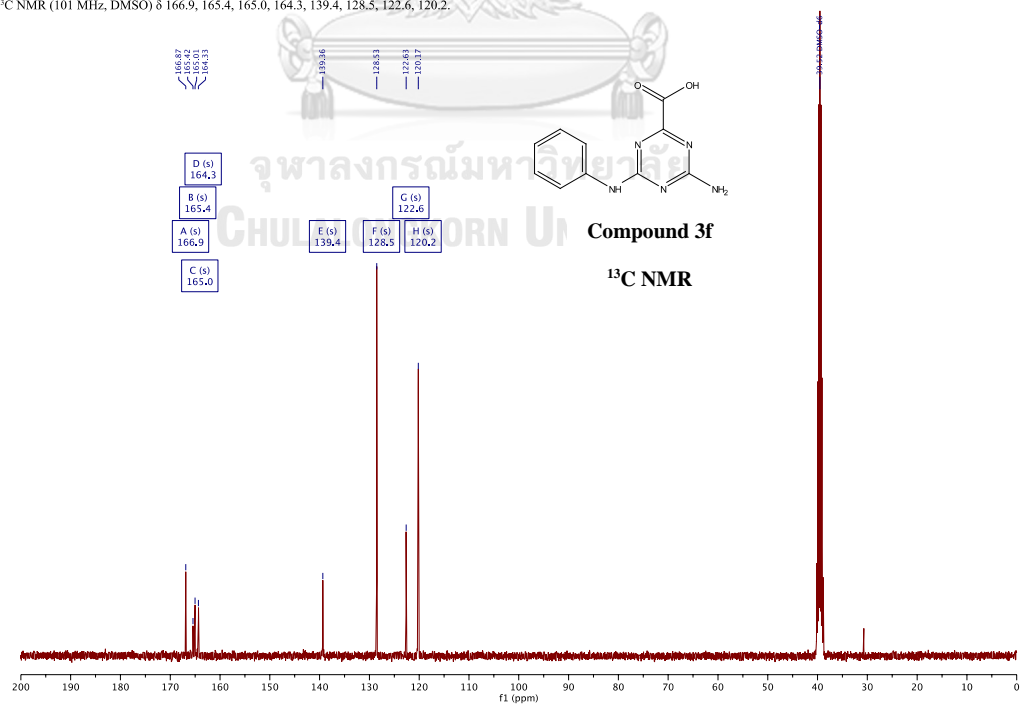


Figure A-40. ^{13}C -NMR of 4-amino-6-(phenylamino)-1,3,5-triazine-2-carboxylic acid (3f)

Mass Spectrum List Report

Analysis Info

Analysis Name D:\Data\Data Service\190827\A53_RB1_01_3017.d
Method nv_pos_6min_profile_wguardcol_190624.m
Sample Name A53
Comment

Acquisition Date 8/27/2019 9:33:05 PM

Operator CU.
Instrument / Ser# micrOTOF-Q II 10335

Acquisition Parameter

Source Type	ESI	Ion Polarity	Positive	Set Nebulizer	3.0 Bar
Focus	Not active	Set Capillary	4000 V	Set Dry Heater	200 °C
Scan Begin	100 m/z	Set End Plate Offset	-500 V	Set Dry Gas	8.0 l/min
Scan End	1500 m/z	Set Collision Cell RF	250.0 Vpp	Set Divert Valve	Waste

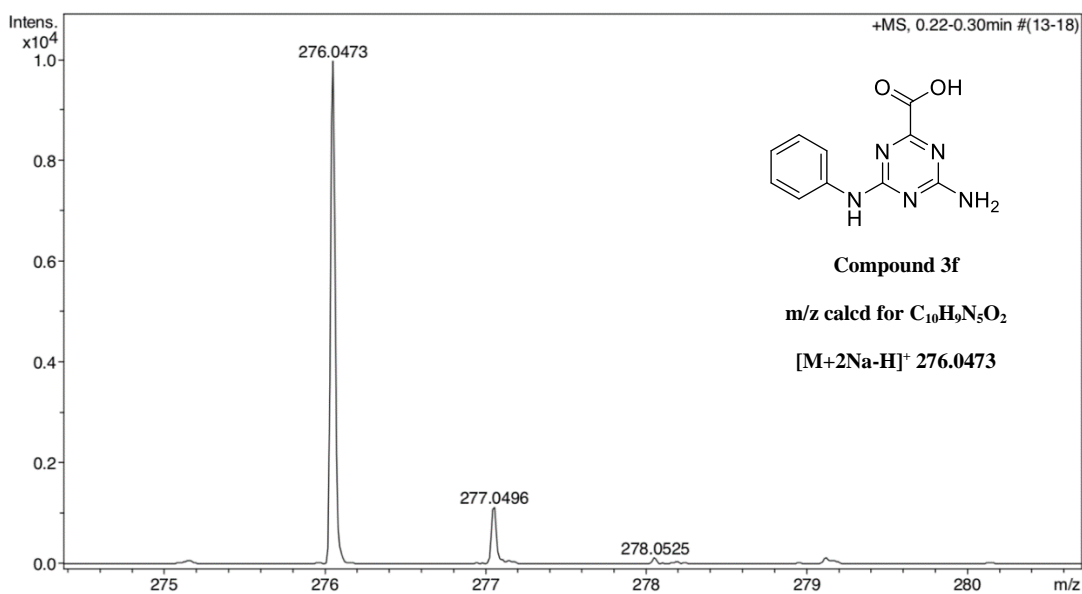


Figure A-41. HRMS spectrum of 4-amino-6-(phenylamino)-1,3,5-triazine-2-carboxylic acid (3f)

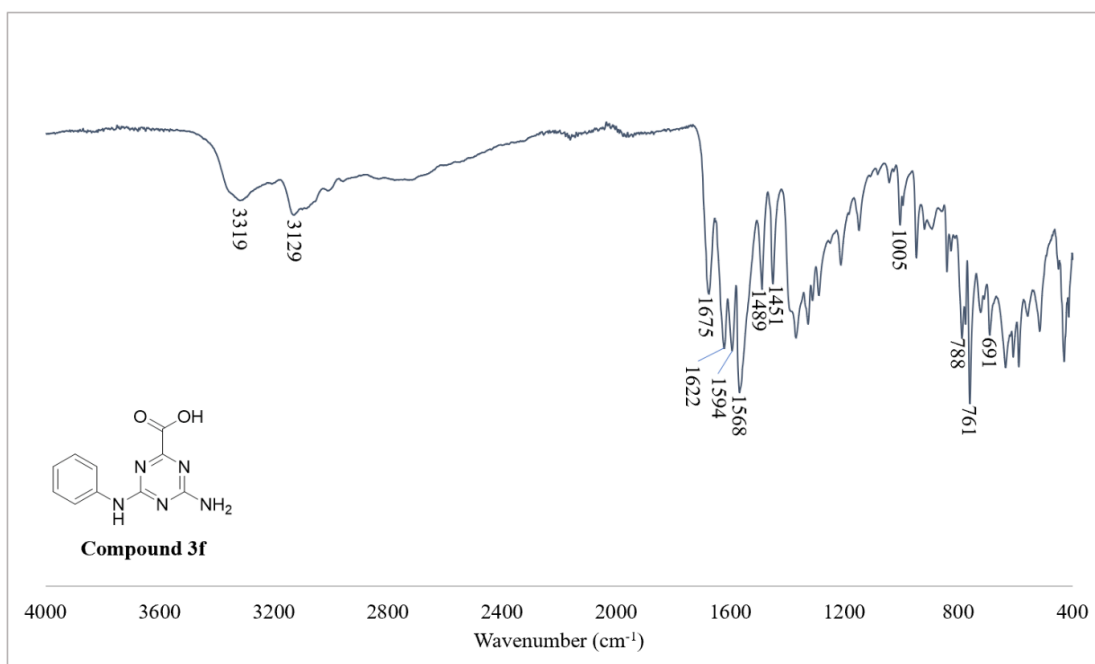
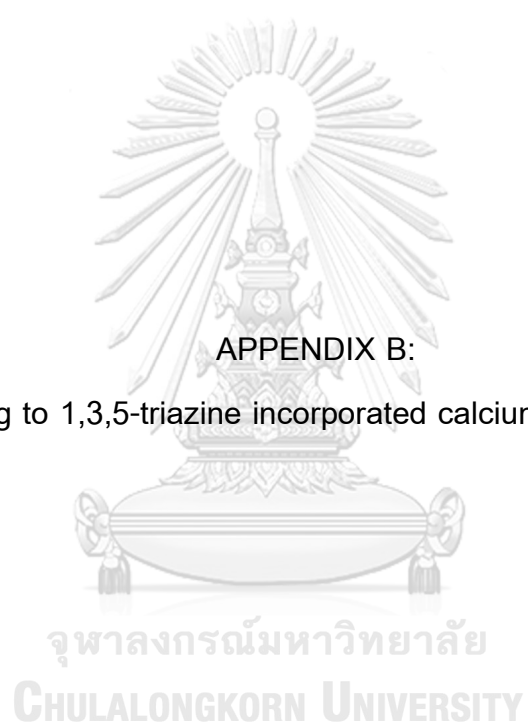


Figure A-42. IR spectrum of 4-amino-6-(phenylamino)-1,3,5-triazine-2-carboxylic acid (3f)



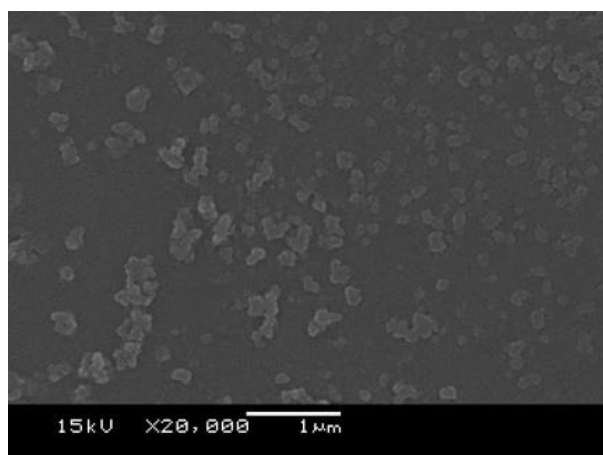


Figure B-1. SEM of the product obtained from condition 6-3, Table 6

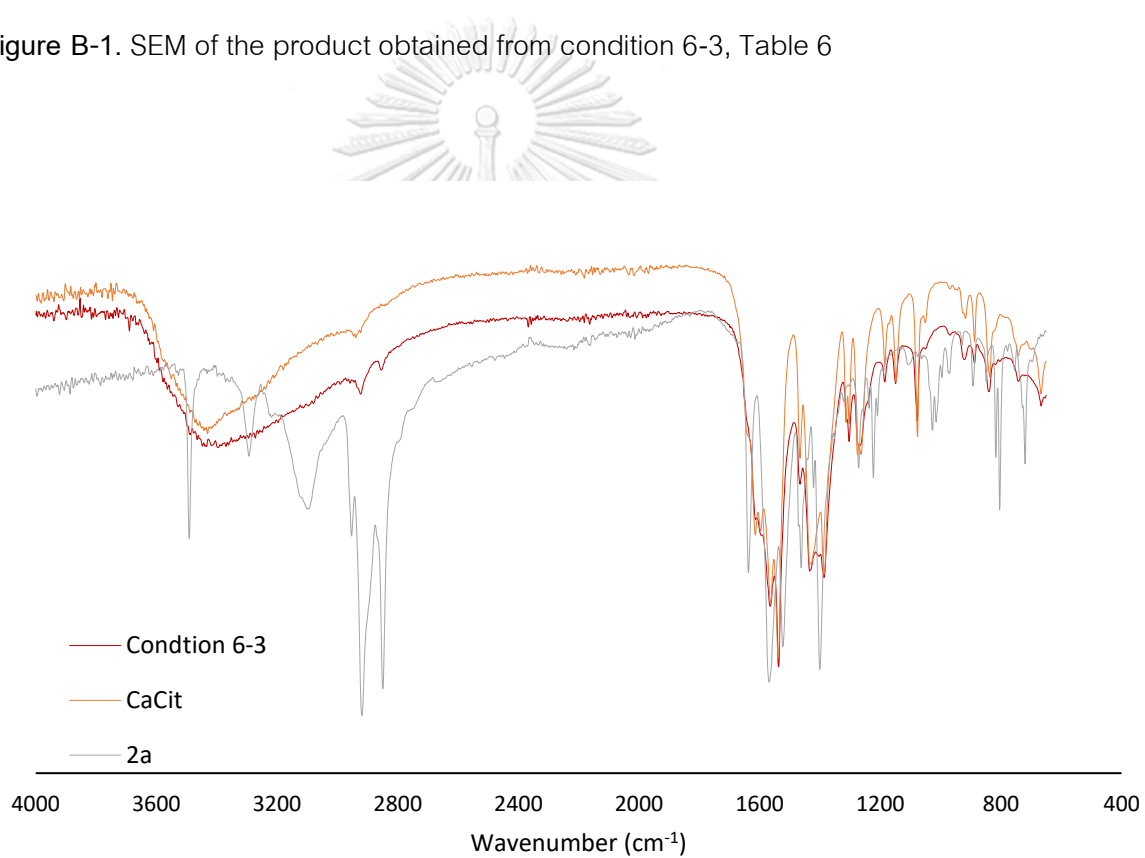


Figure B-2. FTIR spectrum of the product obtained from condition 6-3, Table 6

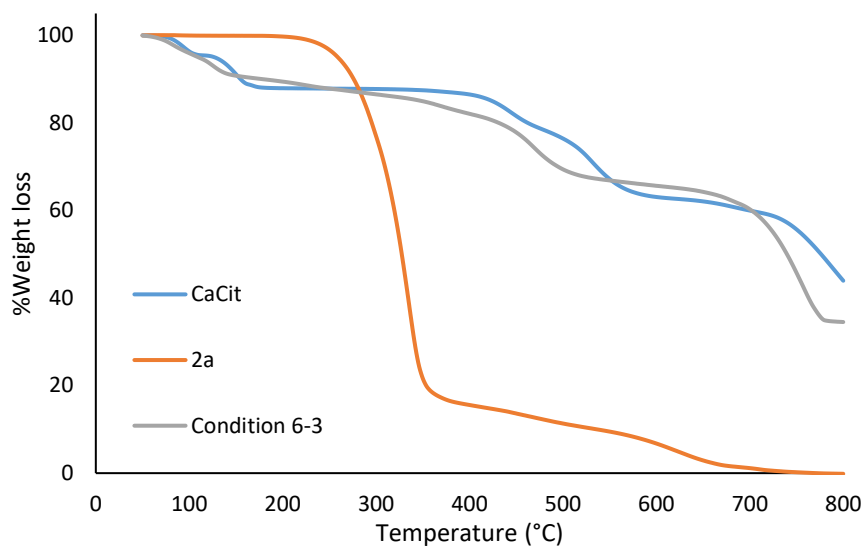


Figure B-3. TGA curves of the product obtained from condition 6-3, Table 6

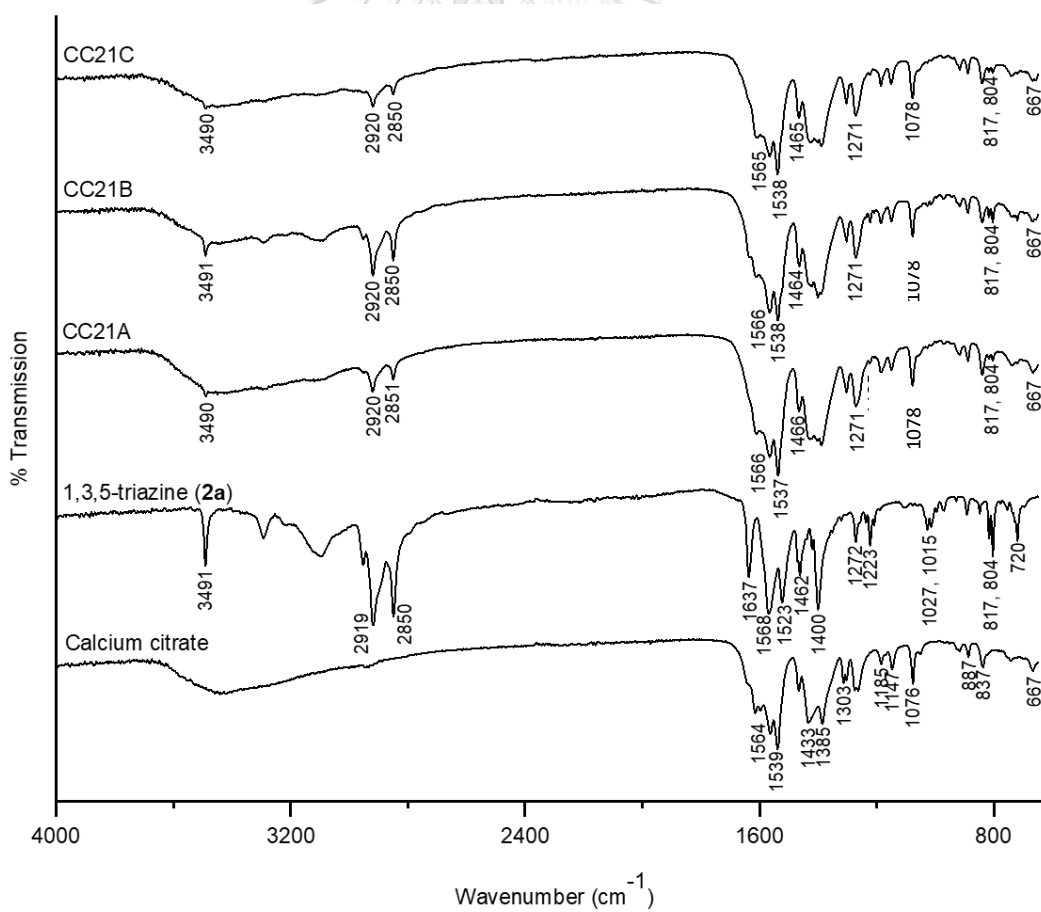


Figure B-4. FTIR spectra of condition A-C

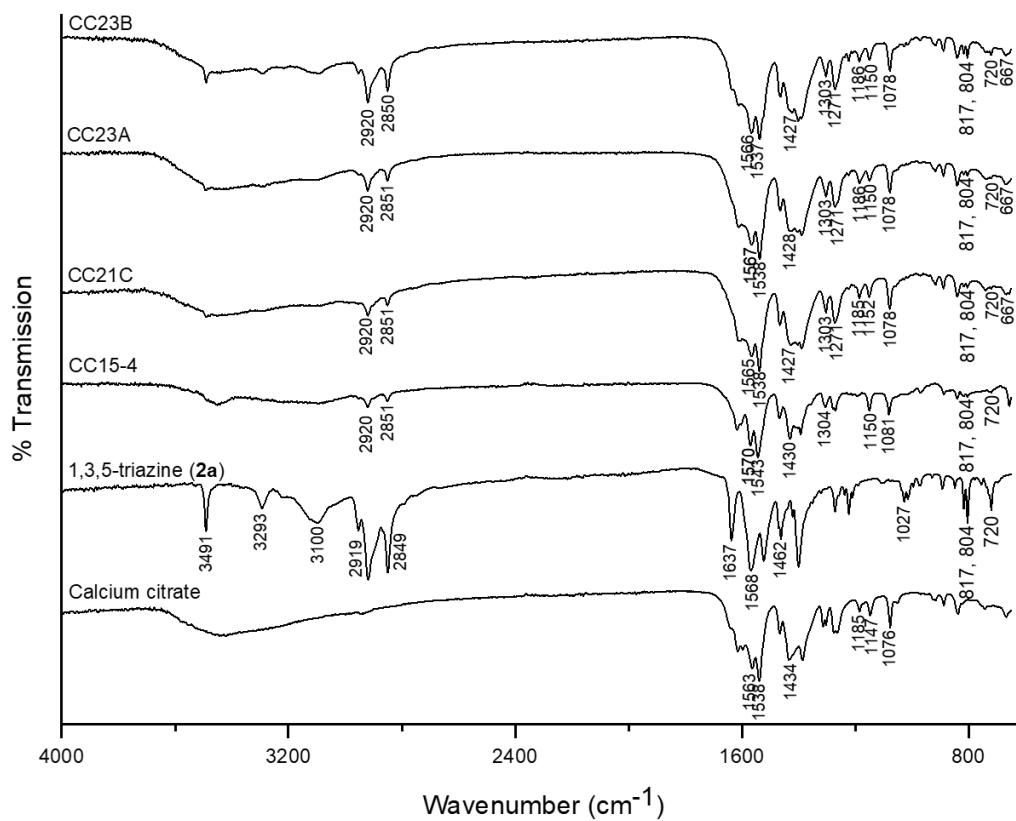


Figure B-5. FTIR spectra of Repeat A and Repeat B of condition C

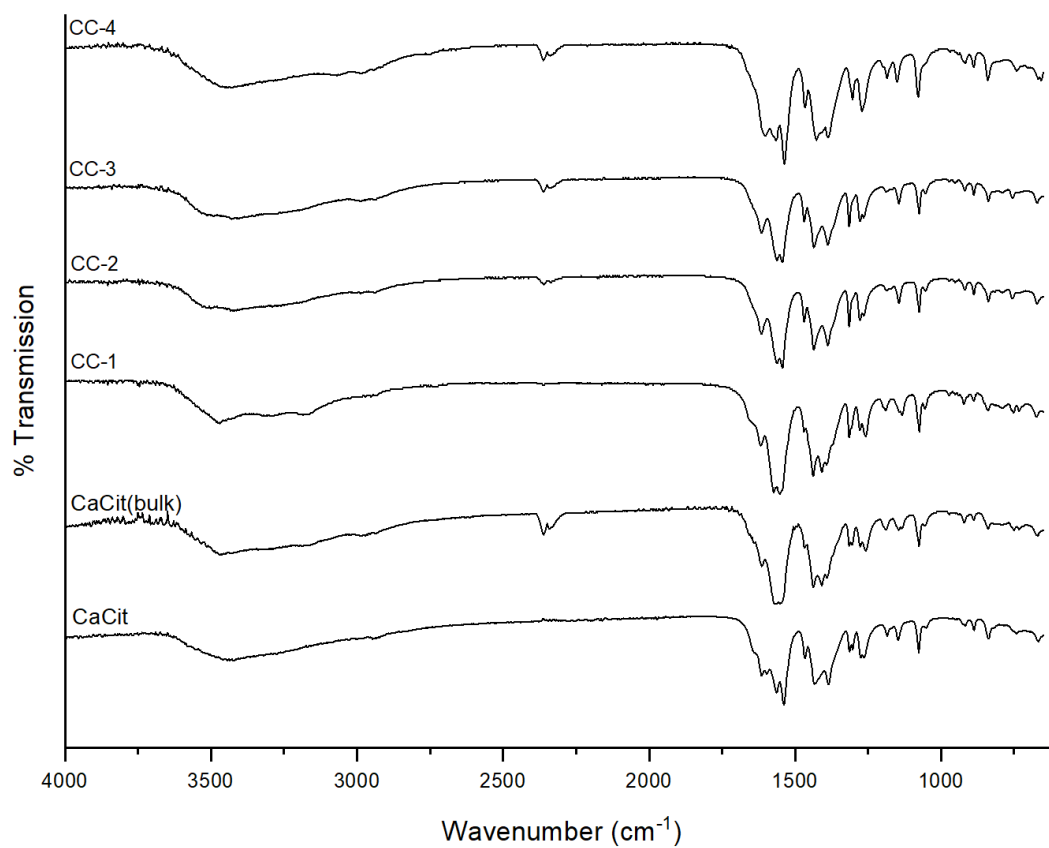


Figure B-6. FTIR spectra of calcium citrate (condition 9-1 to 9-4)

VITA

NAME Monnaya Chalermnon

DATE OF BIRTH 02 April 1997

PLACE OF BIRTH Bangkok

INSTITUTIONS ATTENDED Bachelor of Science in Applied Chemistry, Faculty of Science, Chulalongkorn University, Thailand

HOME ADDRESS 37/3 Soi Suntisuk Nakhonchaisri Road
Dusit 10300 Bangkok

PUBLICATION Chalermnon, M.; Cherdchom, S.; Sereemasapun, A.; Rojanathanes, R.; Khotavivattana, T. Biguanide-Based Synthesis of 1,3,5-Triazine Derivatives with Anticancer Activity and 1,3,5-Triazine Incorporated Calcium Citrate Nanoparticles. *Molecules* 2021, 26, 1028.
<https://doi.org/10.3390/molecules26041028>